LOW-PRESSURE PLASMA FUNCTIONALISATION OF FLUOROPOLYMERS

Dane Lojen

Doctoral Dissertation
Jožef Stefan International Postgraduate School
Ljubljana, Slovenia

Supervisor: Asst. Prof. Dr. Rok Zaplotnik, Jožef Stefan Institute, Ljubljana, Slovenia
Co-Supervisor: Prof. Dr. Alenka Vesel, Jožef Stefan Institute, Ljubljana, Slovenia

Evaluation Board:
Prof. Dr. Miran Mozetič, Chair, Jožef Stefan Institute, Ljubljana, Slovenia
Asst. Prof. Dr. Gregor Primc, Member, Jožef Stefan Institute, Ljubljana, Slovenia
Prof. RNDr. Petr Špatenka, Member, Czech Technical University in Prague, Prague, Czech Republic

MEDNARODNA PODIPLOMSKA ŠOLA JOŽEFA STEFANA
JOŽEF STEFAN INTERNATIONAL POSTGRADUATE SCHOOL

Dane Lojen

LOW-PRESSURE PLASMA FUNCTIONALISATION OF FLUOROPOLYMERS

Doctoral Dissertation

FUNKCIONALIZACIJA FLUORIRANIH POLIMEROV Z NIZKOTLAČNIMI PLAZMAMI

Doktorska disertacija

Supervisor: Asst. Prof. Dr. Rok Zaplotnik

Co-Supervisor: Prof. Dr. Alenka Vesel

Ljubljana, Slovenia, August 2022

Acknowledgments

In the first place, I would like to express my special gratitude to my mentor Asst. Prof. Dr. Rok Zaplotnik and co-mentor Prof. Dr. Alenka Vesel. Asst. Prof. Dr. Rok Zaplotnik is a great mentor, who gave me deep insight into plasma science and practical lab work, always giving helpful advice while leaving me freedom in the search for unique technical solutions to scientific problems. Prof. Dr. Alenka Vesel helped me a lot regarding the art of writing scientific reports and scientific articles with her unbiased view and honesty. She also performed XPS analyses of my plasma-treated samples. I would also like to thank Prof. Dr. Miran Mozetič, who was always accessible despite acting as the head of our Department until recently, and was always willing to share his ideas about possible solutions to the scientific challenges I was facing during my research. I would also like to thank him for all his help with discussing the results of experimental work within our research group and for helping with writing articles. Many thanks also to Asst. Prof. Dr. Gregor Primc for good advice regarding plasma and construction of the new plasma system (and also for 3D-printing some custom-made parts needed for our new plasma system at home) and to Jernej Ekar, who performed SIMS analyses of my plasma-treated samples and shared his honest opinion about the research. Many thanks also to our technician Janez Trtnik for his patience with the repair of broken catalytical probes (that were broken due to plain clumsiness) and manufacturing unique custom-made parts for the new plasma system from technically imperfect drawings. I want to thank the glazier Zvonko Drobnič for his patience and dedication in finding the right solutions for the manufacture of dielectric cups for our new plasma system. Thanks also to other members of our Department for being kind and supportive. I would also like to thank my family for all the support they have given. I am thankful to the Slovenian Research Agency who funded this research under Young Researcher grant P2-0082, Thin-film structures and plasma surface engineering.

Abstract

In the present thesis, the problem of the functionalisation of fluoropolymers was addressed. As chemical methods for the functionalisation of fluoropolymers apply environmentally harmful chemicals, the research was directed to low-pressure non-equilibrium radiofrequency (RF) inductively coupled plasmas of environmentally friendly gasses. The research was focused on polytetrafluoroethylene (PTFE), the most representative fluoropolymer. The interactions between low-pressure cold hydrogen plasma and the PTFE surface were studied using X-ray photoelectron spectroscopy (XPS), Secondary Ion Mass Spectrometry (SIMS), and goniometry (water contact angle - WCA). After optimising the PTFE surface functionalisation with hydrogen plasma, we studied the interaction of pre-treated samples with low-pressure cold oxygen plasmas. A cobalt catalytic probe was used for O-atom density measurements. The subsequent treatment of PTFE with low-pressure hydrogen and oxygen plasmas enabled us to obtain a superhydrophilic PTFE surface with a water contact angle of about 5°. By selective exposure of PTFE to vacuum ultraviolet (VUV) radiation in hydrogen plasma, we discovered that VUV is the main cause of C—F bond breakage in the PTFE surface layer, resulting in the formation of dangling bonds. We found H-atoms of great importance for terminating the dangling bonds and binding the released fluorine into HF molecules. Hydrogen plasma treatment resulted in nearly instant formation (after 1 s) of a few nm thick polyolefin-like layer containing almost no fluorine. The surface of samples treated with hydrogen plasma exhibited a WCA of about 95°. The PTFE with polyolefin-like surface layer was then treated in the afterglow of oxygen plasma. We found that superhydrophilicity (WCA of 5°) of the pre-treated PTFE surface occurred instantly within 0.2 to 0.3 s with an O-atom fluence of about 1×10^{23} m^{-2}. The oxygen content in the treated surface as determined by XPS was about 20 at.% and remained constant over a broad range of O-atom fluences. Oxygen was bound in hydrophilic and hydroneutral functional groups such as hydroxyl, carboxyl or carbonyl. The WCA dependence on the O-atom fluence exhibited a minimum, followed by a dramatic hydrophobic recovery. Ultimately, after prolonged treatment with oxygen plasma, the F/C ratio of the untreated polymer was achieved. The complete hydrophobic recovery indicates that there are simultaneous competitive processes of functionalisation and etching. From the constant oxygen content over a broad range of atom fluences around the WCA minimum, it was concluded that the WCA did not depend only on the chemical composition of the surface, but also on the surface roughness controlled by etching. The method for hydrophilisation of PTFE samples was proved in a small experimental plasma system. To bring our research closer to industrialisation, an industrial size reactor sustaining plasma with four coils coupled in parallel to the same RF generator was developed. Such a reactor can be used for the treatment of polymers of almost arbitrary shape and size. The specialty of this system is the ability to equalise the impedances of leads for each coil separately using sliders. We mounted RF coils into the reactor, and constructed innovative dielectric cups submerged into the reactor, which enabled positioning of the coils in a space sustained at atmospheric pressure, thus preventing arcing and the interference of electromagnetic fields with metallic parts of the reactor. The

innovative solution enabled high atom density in the metallic chamber due to minimised recombination of neutral atoms. We managed to achieve an almost perfect equalisation of the power distribution among coils and thus steady transitions of plasma modes in all coils at elevated RF power. Transitions between plasma modes refer to the number of coils sustaining plasma in a specific mode. The even distribution of power among coils enabled a transition from E- to H-mode for all four coils at reasonable power. The proper operation of the newly constructed plasma system was proved by systematic measurements of O-atom densities within the reactor vessel. We observed tangible gradients close to the plasma exhausts of the dielectric cups, but 21 cm below the dielectric cups we found homogeneous distribution of neutral oxygen atom density of about 1.2×10^{21} m^{-3}.

Povzetek

V doktoratu smo obravnavali problematiko funkcionalizacije fluoriranih polimerov. Ker pri kemijskih metodah funkcionalizacije fluoriranih polimerov uporabljajo okolju nevarne kemikalije, smo se pri naših raziskavah posvetili uporabi nizkotlačnih neravnovesnih radiofrekvenčno (RF) induktivno sklopljenih plazem okolju prijaznih plinov. Osredotočili smo se na politetrafluoroetilen (PTFE), ki je najbolj reprezentativen fluoriran polimer. Z uporabo XPS-a, SIMS-a in goniometrije (kontaktni kot vodne kapljice) smo proučevali interakcije med nizkotlačno hladno vodikovo plazmo in površino PTFE. Po optimizaciji funkcionalizacije površine PTFE z vodikovo plazmo smo proučevali interakcije med predhodno obdelanimi vzorci z vodikovo plazmo in nizkotlačno hladno kisikovo plazmo. Gostote O-atomov smo merili s kobaltovo katalitično sondo. Zaporedna obdelava PTFE z nizkotlačno vodikovo in kisikovo plazmo nam je omogočila superhidrofilizacijo površine PTFE, na kateri smo dosegli kontaktni kot vodne kapljice približno 5°. S selektivno izpostavitvijo PTFE vakuumskemu ultravijoličnemu (VUV) sevanju v vodikovi plazmi smo odkrili, da je VUV glavni vzrok za cepljenje vezi C—F v površinski plasti PTFE, kar povzroča nastanek prostih vezi. Ugotovili smo, da so H-atomi zelo pomembni, ker se vežejo na proste vezi in vežejo sproščen fluor v molekule HF. Obdelava z vodikovo plazmo je povzročila takojšen nastanek (po 1 s) nekaj nm debele poliolefinske plasti, ki skoraj ni vsebovala fluora. Na površini vzorcev, obdelanih z vodikovo plazmo, je bil kontaktni kot vodne kapljice okoli 95°. PTFE s poliolefinom podobno površinsko plastjo smo nato obdelovali v postrazelektritvenem območju kisikove plazme. Ugotovili smo, da je bila pri dozi O-atomov približno 1×10^{23} m^{-2}, superhidrofilnost (kontaktni kot okoli 5°) predhodno obdelane površine PTFE dosežena takoj oziroma po 0,2 do 0,3 s. Vsebnost kisika na obdelani površini, ki smo jo določili z XPS-om, je bila približno 20 at.% in je ostala konstantna v širšem območju doz O-atomov. Kisik se je vezal v hidrofilne oziroma hidronevtralne funkcionalne skupine, kot so hidroksilna, karboksilna in karbonilna. Kontaktni kot je ob večanju doze O-atomov dosegel minimum, čemur je sledila povrnitev površine v hidrofobno stanje. Po dolgotrajni obdelavi s kisikovo plazmo smo na površini dosegli F/C razmerje neobdelanega polimera. Popolna povrnitev v hidrofobno stanje nakazuje, da obstajata sočasna kompetitivna procesa funkcionalizacije in jedkanja. Na podlagi konstantne vsebnosti kisika v širokem razponu doz O-atomov okoli minimuma kontaktnega kota smo ugotovili, da kontaktni kot ni odvisen le od kemične sestave površine, ampak tudi od površinske hrapavosti, na katero vpliva jedkanje. Metodo hidrofilizacije vzorcev PTFE smo dokazali v majhnem eksperimentalnem plazemskem sistemu. Da bi naše raziskave približali industriji, smo razvili reaktor industrijske velikosti, ki generira plazmo s štirimi tuljavami, vezanimi vzporedno z istim RF generatorjem. Takšen reaktor lahko uporabljamo za obdelavo polimerov skoraj poljubnih oblik in velikosti. Posebnost tega sistema je možnost izenačevanja impedanc vodnikov za vsako tuljavo posebej s pomočjo drsnikov. RF tuljave smo namestili v reaktor. Skonstruirali smo inovativne dielektrične razelektritvene cevi potopljene v reaktor, ki so omogočale namestitev tuljav v prostoru, kjer je bil zrak pri atmosferskem tlaku, s čimer smo preprečili nastanek obločne plazme in kakršnih koli interferenc elektromagnetnih polj s kovinskimi

deli reaktorja. Inovativna rešitev je omogočila visoko gostoto atomov v kovinski komori zaradi zmanjšane rekombinacije nevtralnih atomov. Uspelo nam je doseči skoraj popolno izenačitev porazdelitve moči med tuljavami in s tem enakomerne prehode med načinoma plazme v vseh tuljavah pri povišanju RF moči. Prehoda med plazemskima načinoma se nanašata na število tuljav, ki generirajo plazmo v določenem načinu. Enakomerna porazdelitev moči med vsemi tuljavami je omogočila prehode iz E- v H-način za vse štiri tuljave pri zmernih močeh. Pravilno delovanje na novo skonstruiranega plazemskega sistema smo dokazali s sistematičnimi meritvami gostote O-atomov v reaktorski posodi. V bližini izstopov plazme iz razelektritvenih cevi smo opazili znatne gradiente, vendar smo 21 cm pod dielektričnimi cevmi izmerili homogeno porazdelitev gostote nevtralnih atomov kisika približno $1{,}2\times10^{21}$ m^{-3}.

Contents

List of Figures **xiii**

Abbreviations **xv**

1 Introduction **1**
1.1 Thesis Structure 2
1.2 Properties of Polytetrafluoroethylene (PTFE) 3
1.3 Surface Wettability 5
1.4 Plasma PTFE Functionalisation Methods 8
1.5 Thesis Objectives 11
1.6 Hypotheses 12
1.7 Methodology 12

2 Defluorination of the Polytetrafluoroethylene Surface by Hydrogen Plasma **13**

3 Effect of VUV Radiation and Reactive Hydrogen Atoms on Depletion of Fluorine from the Polytetrafluoroethylene Surface **31**

4 Optimisation of Surface Wettability of Polytetrafluoroethylene (PTFE) by Precise Dosing of Oxygen Atoms **43**

5 Power Characteristics of Multiple Inductively Coupled RF Discharges Inside a Metallic Chamber **53**

6 Oxygen Atom Density in a Large Reactor Powered by Four Inductively Coupled Plasma Sources **65**

7 Conclusions **75**

References **79**

Bibliography **83**

Biography **85**

List of Figures

Figure 1: Problems regarding traditional approaches to PTFE functionalisation.....2
Figure 2: Representation of the forces on individual molecules (Yuan & Lee, 2013).....6
Figure 3: Schematic representation of a droplet sitting on the solid/liquid interface (Bico et al., 2002). 7
Figure 4: Schematic representation of a droplet on a model surface consisting of holes and spikes (Bico et al., 2002).....7
Figure 5: Experimental inductively coupled plasma system. 13
Figure 6: PTFE sample enclosed in the holder covered with a MgF_2 window inserted into the plasma system (left) and during H-mode hydrogen plasma treatment (right). 32
Figure 7: Schematic representation of PTFE functionalisation achieved by successive treatments of the PTFE surface with hydrogen and oxygen plasmas.....45
Figure 8: Superhydrophilic PTFE. 45
Figure 9: The innovative plasma reactor (upper left), the flange of the reactor (upper right), the power divider (lower left), and a detail of the impedance regulation slider (lower right). 54
Figure 10: Catalytic probe at the exhaust of the discharge tube. The probe is visible as a bright disc just below the rightmost discharge tube.....66

Abbreviations

1D	... One-dimensional
2D	... Two-dimensional
3D	... Three-dimensional
3D CAD modelling	... Three-dimensional Computer-aided Design modelling
ABS	... Acrylonitrile butadiene styrene
AR-XPS	... Angular resolved X-ray photoelectron spectroscopy
ATR IR	... Attenuated total reflectance infrared spectroscopy
C-DB	... Carbon dangling bonds
DBD	... Dielectric barrier discharge
DC bias	... Direct current bias
ECR	... Electron cyclotron resonance
ESR	... Electron spin resonance
F/C ratio	... Fluorine to carbon ratio
FR4	... Flame retardant4
FTIR	... Fourier-transform infrared spectroscopy
H- content	... Hydrogen content
H-atom	... Neutral hydrogen atom
H-plasma	... Hydrogen plasma
ICP	... Inductively coupled plasma
ICP RF	... Inductively coupled radiofrequency plasma
ICPS	... Inductively coupled plasma source
MAF	... Mobile amorphous fraction
MW	... Microwave
O- content	... Oxygen content
O-atom	... Neutral oxygen atom
OES	... Optical emission spectroscopy
O-plasma	... Oxygen plasma
PET	... Polyethylene terephthalate
PTFE	... Polytetrafluoroethylene
RAF	... Rigid amorphous fraction
RF	... Radiofrequency
RF- generator	... Radiofrequency generator
RMS roughness	... Root mean square surface roughness
SIMS	... Secondary Ion Mass Spectrometry
TFA-XPS	... Thin film analysis X-ray photoelectron spectroscopy
TFE	... Tetrafluoroethylene
TGA	... Thermo-gravimetric analysis
TIG-welded	... Tungsten inert gas-welded
TOA	... Photo-electron take-off angle
ToF-SIMS	... Time-of-flight Secondary Ion Mass Spectrometry
UV	... Ultraviolet radiation

VUV	. . . Vacuum ultraviolet radiation
WCA	. . . Water contact angle
XPS	. . . X-ray photoelectron spectroscopy

Chapter 1

Introduction

Fluorinated polymers consist of fluorine, carbon and many of them contain other elements too. Typical for them are C–F bonds. The most known fluoropolymer is polytetrafluoroethylene (PTFE), commercially named Teflon. PTFE is chemically and biologically inert, has high-temperature resistance and good mechanical properties. Therefore, it is commonly used in technics and medicine (Ebnesajjad, 2000; Okazaki, 2017; Olabisi & Adewale, 2015). The problem connected with its use for some purposes is its low surface energy, strongly aggravating its possibility of adhering to other materials (Takata, Iwao, & Yumoto, 2016), which causes problems related to the deposition of thin layers of various materials, printing and bonding of biological macromolecules and cells on to its surface (Bikerman, 1967; Kwon et al., 2020; Ma et al., 2020; Schonhorn & Hansen, 1967; Takata et al., 2016). Traditional methods for defluorination of the PTFE surface and binding of hydrophilic functional groups include chemical methods such as surface treatment with Na-naphthalenide in tetrahydrofuran followed by BH_3 and H_2O_2 /NaOH treatment (Gabriel, Dahm, & Vahl, 2011), treatment with sodium solution in anhydrous ammonia (Ebnesajjad, 2000), surface reduction with benzoin-di-anion and direct electrochemical reduction of the surface (Mathieson, Brewis, Sutherland, & Cayless, 1994). Because these chemical treatments include toxic, aggressive and environmentally harmful chemical compounds, scientists are searching for environmentally friendly alternatives (Marchesi, Ha, Garton, Swei, & Kristal, 1991; Ohkubo, Endo, & Yamamura, 2018; Ohkubo et al., 2017). The traditional solution to the PTFE adherence problem is depicted in Figure 1. Other options are ion irradiation (Takata et al., 2016), corona treatment (Ebnesajjad, 2011) and plasma treatment. Currently, the most promising alternative is treatment of the PTEF surface with low-pressure cold plasma. However, established plasma treatment methods do not deliver adequate results in the case of PTFE surface treatment (Primc, 2020). Therefore, this doctoral dissertation was dedicated to the study of mechanisms of interaction between different radicals and radiation originating from plasmas with fluorinated polymers. Deep insight into these interactions enabled us to develop a new method for the functionalisation of fluorinated polymer surfaces. Due to the need for upscaling of the presented plasma functionalisation method, a new innovative plasma reactor was developed to sustain plasma with multiple inductors coupled in parallel to a single radiofrequency generator, equipped with an advanced impedance tuning system.

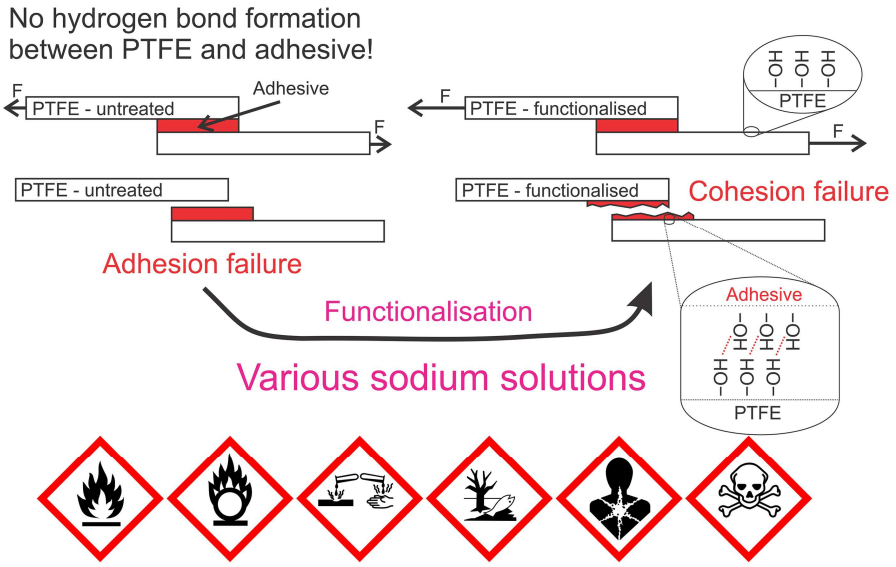

Figure 1: Problems regarding traditional approaches to PTFE functionalisation.

1.1 Thesis Structure

The thesis starts with an explanation of the physical and chemical properties of PTFE, followed by an explanation of the principles of surface wettability, setting the basis for development of plasma functionalisation methods of PTFE. It is followed by a short review of existing research regarding the functionalisation of PTFE, which clearly points out that the established plasma treatments of PTFE are still inferior to traditional chemical functionalisation methods, as they are too slow for industrial use, or plasmas of environmentally harmful gasses are employed. Then follows a description of the thesis objective, and the stated hypothesis and methodology used in the research. The main body of the thesis consists of five scientific papers. Dane Lojen, the author of the thesis, is the first author of three. The articles were published in eminent journals dedicated to surface science, polymer science, vacuum technologies and plasma science: Applied Surface Science, Polymers, Vacuum and Plasma Science and Technology. Dane Lojen, with the help of co-workers, performed plasma treatments, neutral atom density measurements, OES measurements, water contact angle measurements, engineered a new innovative plasma system, performed selections and interpretations of experimental results, and wrote drafts of the papers. X-ray photoelectron spectroscopy (XPS) analyses were performed by the co-mentor, Prof. Dr. Alenka Vesel. Time-of-flight secondary ion mass spectrometry (ToF-SIMS) analyses were performed by Jernej Ekar. The co-authors helped with scientific ideas, experimental advice, assembly of the new plasma system, and the writing of manuscripts. The thesis closes with joined conclusions of all the key findings of all five included articles followed by references, a bibliography, and a short biography about the author.

1.2 Properties of Polytetrafluoroethylene (PTFE)

PTFE was accidentally discovered by Dr. Roy Plunket in 1938, while working at DuPont during development of the synthesis of refrigerant ($CClF_2$–CHF_2) from tetrafluoroethylene (TFE) (Ebnesajjad, 2000).

Nowadays, fluorinated polymers such as PTFE are widely used for various applications in aeronautics, microelectronics, engineering, the chemical industry, optics, textile finishing, the automotive industry, houseware, chemical processing, medical devices, architectural fabrics and wiring insulation (Calleja, Jourdan, Ameduri, & Habas, 2013).

Fluoride compounds, especially PTFE, are used as biomedical materials for artificial blood vessels, artificial lung membranes, catheters, sutures, applications in reconstructive and cosmetic facial surgery and in guided tissue regeneration (GTR scaffolds) (Okazaki, 2017).

PTFE is a chain polymer consisting of repeating units of $–(CF_2)_n–$ (Clark, 1999) with a very high molecular weight (Okazaki, 2017). It is highly chemically resistant and exhibits the highest chemical stability among organic polymers (Ebnesajjad, 2000). It is chemically inert and thus resistant to oxidation, organic solvents, oils, water, acids, and bases (Calleja et al., 2013). PTFE is also biologically inert and non-biodegradable (Okazaki, 2017).

PTFE can be polymerised to extremely high molecular masses in the order of $M_{PTFE} = 10^6$–10^7 Da or perhaps even 10^8 Da, and cannot be dissolved in common solvents (Olabisi & Adewale, 2015).

PTFE has a linear structure with a backbone of carbon-carbon and carbon-fluorine bonds, both of which are extremely strong (C–C = 607 kJ/mol and C–F = 552 kJ/mol) (Ebnesajjad, 2000). In C–F bonding, fluorine has a higher electron density than carbon because it pulls the shared electron pair closer to itself relative to the centre point of the C–F bond. The fluorine atom is larger than the hydrogen atom and it's unshared electron pair is easily converted to F^-. The size of fluorine atoms and the length of C–F bonds are just right to provide a uniform and continuous sheath that entirely blankets the carbon backbone (carbon-carbon bonds), protecting it from chemical attack. The F-atom abstraction mechanism in the C–F bond is ruled out by its polarity and strength, so there is no chain branching in PTFE (Ebnesajjad, 2000).

In general, PTFE is not susceptible to nucleophilic attack because it has no double bonds. However, it can lose fluorine by an electrophilic attack of alkali metals under long-term exposure to heat. Fluorine can be abstracted from PTFE by highly reactive alkali metals such as caesium, potassium, sodium, lithium and highly etching activated magnesium. With the loss of fluorine, the structure of PTFE is destabilised. When the fluorine-to-carbon ratio is decreased, the colour changes to brown and finally black (the black layer is normally comprised of carbon, some oxygen and small content of other elements) (Ebnesajjad, 2000).

At high temperatures, thermal degradation of PTFE may appear. PTFE's weight loss is 1 %/hr at 465°C as measured by thermo-gravimetric analysis (TGA) (Ebnesajjad, 2000). However, thermal degradation of PTFE is not of great concern, as maximum operational temperatures do not often exceed 260 °C (Olabisi & Adewale, 2015).

Pure PTFE does not absorb electromagnetic radiation in visible and UV spectra. Therefore, light does not induce photochemical reactions or degradation reactions (Olabisi & Adewale, 2015).

Electron, X-ray, or γ-ray irradiation leads to the formation of primary and secondary radicals through cleavage of C–C and C–F bonds (Drobny, 2009; Olabisi & Adewale, 2015).

PTFE has a high melting point (more than double of polyethylenes - PE) (Ebnesajjad, 2000), an extremely low friction coefficient (Nunes, Dias, & da Costa Mattos, 2011) and

excellent slipperiness (Okazaki, 2017). However, its resistance to abrasion and wear is poor (Calleja et al., 2013), especially at higher sliding velocities (Olabisi & Adewale, 2015).

Hydrogen bonding of PTFE is ruled out by its neutral electronic state and its symmetrical geometry. Consequently, PTFE is very soft and easily abraded (molecules slip and slide against each other). There is no steric hindrance due to the absence of branches and side chains which results in unconstrained slipping of PTFE molecules against each other (Ebnesajjad, 2000).

In general, the density of PTFE is in a range from 2.1×10^3 to 2.3×10^3 kg/m^3 (the upper limit is for nearly perfect crystalline PTFE) depending on its crystallinity, porosity, and void content. The crystallinity of PTFE upon polymerisation can be as high as 98 %. The crystallinity of processed PTFE may vary from less than 40 % to 70 %, depending on processing conditions. (Olabisi & Adewale, 2015).

For example, the melting point of commercially available PTFE from DuPont - Teflon® is around 327 °C, and its density is 2.18×10^3 kg/m^3 (Nunes et al., 2011). When PTFE melts, it is transformed from a white solid to a transparent gel that is not truly liquefied because of its extremely high molecular mass (the shape is stable due to low molecular movement) (Olabisi & Adewale, 2015).

Steric repulsion between fluorine atoms, due to their size, prevents the formation of the polyethylene-like planar zig-zag conformation in PTFE, though it can be forced into planar zig-zag conformation under extreme pressure (Ebnesajjad, 2000). Generally, the conformation of PTFE is helical, by which steric repulsion is minimised. PTFE is also very hydrophobic (Ebnesajjad, 2000).

In general, fluoropolymers exhibit very low surface energy and critical surface tension. The fluorine sheath is responsible for PTFE having a low surface energy of 1.8×10^{-2} J/m^2 the lowest among organic polymers (its non-branched structure also contributes to the low surface energy). The surface tension value of PTFE is 2.25×10^{-2} J/m^2. This can be explained by intermolecular forces, also called Van der Waals forces (Ebnesajjad, 2000).

PTFE molecules have no permanent dipoles, have low polarisability, and exhibit low ionisation propensity, resulting in the minimisation of polar energy and force, dipole-induced dipole energy and nonpolar energy or forces between PTFE molecules as well as between PTFE and other molecules. The electron balance and neutrality result in high chemical resistance, low polarisability, low dielectric constant, low dissipation factor, and high volume and surface resistance (Ebnesajjad, 2000).

It is generally accepted that PTFE has a semi-crystalline structure (Calleja et al., 2013). The crystal structure of PTFE is not typical because it can have a number of crystal forms and there is also substantial molecular motion present within the crystal well below the melting point. All structural conformations of PTFE are nearly cylindrical with nearly hexagonal packing (Clark, 1999). Due to the helical conformation of the linear PTFE molecules, chains are rigid and fully extended, resembling rod-like cylinders (Ebnesajjad, 2000).

The polymerisation process and unbranched chain structure of PTFE allow for a high crystallisation level despite the chain's high molecular weight. The crystallinity level of virgin PTFE (never melted) is in the range of 92 to 98 %. The crystallisation of PTFE molecules occurs as a banding structure. The length of the bands is in the range of 10 to 100 µm, while the range of band width is 0.2 to 1 µm depending on the rate of cooling. Crystalline slices are created by folding over or stacking crystalline segments that are separated by the amorphous polymer, forming a striating structure. The thickness of the crystalline slices is 20 to 30 nm. (Ebnesajjad, 2000).

According to temperature, PTFE can have a mobile amorphous fraction (MAF), a rigid amorphous fraction (RAF), and a crystalline phase (Calleja et al., 2013).

The main inadequately solved problems regarding adherence of the PTFE surface and printing on its surface are its low surface energy and weak boundary layer (Bikerman, 1967; Schonhorn & Hansen, 1967). PTFE's water contact angle (WCA) values vary between 80 (Hong, Kim, & Choi, 2019) and 140° (Dumée et al., 2016), depending on the manufacturing process, which determines surface roughness and cleanness. Conventional methods for PTFE surface functionalisation and improvement of adhesion properties are etching with sodium-containing corrosive solutions such as Na-napthalenide (Gabriel et al., 2011; Marchesi et al., 1991), ion bombardment (Lee, Lee, Chang, & An, 2014) and flame treatment (Wypych, 2018). However, the disadvantages of chemical etching are toxicity to humans, high environmental load, malodour, and PTFE surface colouration (Ohkubo et al., 2018, 2017).

1.3 Surface Wettability

The surface wettability of PTFE can be evaluated in terms of water contact angle (Liu et al., 2004), measured with a goniometer (Xu, Hu, Wu, & Chen, 2003). The hydrophilic and hydrophobic properties of solids depend on their surface energy. The surface energy of solids (γ^{s}) consists of contributions of the polar component (γ^{p}) and the disperse component (γ^{d}). It can be determined by use of liquids with known γ^{p} and γ^{d} values such as water and di-iodomethane, by measurement of the contact angles of both liquids, through the Owens-Wendt model. (Huang, Ma, Tsai, Hou, & Juang, 2013). Optical systems such as CAM 2000, with a monochromatic light-emitting diode, can be used for imaging liquid droplets (Liu et al., 2004). The static contact angle can be measured with video contact angle systems enabling automatic droplet profile projection of a sessile droplet resting on the sample's surface and its contact angle measurement (Huang et al., 2013). It is preferable to perform multiple measurements on each sample (for example, 5 measurements) and calculate the average value and standard variation (Liu et al., 2004).

The contact angle is defined by the intersection of the liquid-solid interface and the liquid-vapour interface. It is geometrically determined from the droplet side profile by applying a tangent line to the droplet at the triple-phase intersection point (liquid, solid, and gas) along the liquid-vapour interface crossing the line determined by the solid-liquid interface. The interphase where liquid, solid, and vapour coexist is called the "triple point contact line" (Yuan & Lee, 2013).

The wettability of surfaces is usually evaluated by the measurement of contact angles of small liquid droplets. Materials on which droplets form small contact angles (<90°) are considered hydrophilic (surface wetting is favourable, so fluid is spread over a large surface area), while surfaces with high contact angles (>90°) are considered hydrophobic (surface wetting is unfavourable, so the fluid contact surface area is minimised, resulting in a compact-shaped droplet) (Yuan & Lee, 2013).

In ideal cases, the liquid droplet shape is determined by the liquid's surface tension. Within the volume of the liquid, each molecule is pulled equally in every direction by neighbouring molecules resulting in the net force of zero to every molecule, as shown in Figure 2. However, the molecules at the phase boundaries do not have interactions with neighbouring molecules of the same kind in all directions, resulting in the imbalance of the net force per molecule, causing them to be pulled inward by the neighbouring molecules, creating internal pressure. The sum of intermolecular forces that contracts the surface area is called surface tension. As a result, the liquid surface area is contracted to the minimum surface area per fixed volume, so that the lowest surface free energy is maintained (surface per unit of volume is minimised in the shape of a sphere) (Yuan & Lee, 2013).

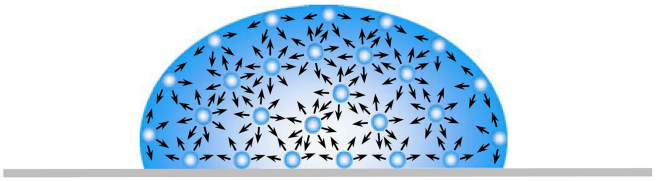

Figure 2: Representation of the forces on individual molecules (Yuan & Lee, 2013).

In practice, the shape of the droplet is determined by the surface tension and by external forces such as gravity. Gravity deforms sessile droplets by flattening and pedant droplets by elongation. In general, the larger the droplet, the greater the effect of gravity on its shape (Yuan & Lee, 2013). In practice, we use droplets with a volume of about 1 µl or less, so the gravitational flattening is negligible for all liquids, including those of small surface tension.

In 1805, Thomas Young described the relation between the contact angle of a liquid droplet on an ideally smooth solid surface in mechanical equilibrium and liquid vapour interfacial tension, solid vapour interfacial tension, and solid-liquid interfacial tension in the equation written below (equation 1) (Yuan & Lee, 2013).

$$\gamma_{lv} = \cos\theta_Y = \gamma_{sv} - \gamma_{sl} \qquad (1),$$

where γ_{lv} is the liquid-vapour interfacial tension, γ_{sv} the solid-vapour interfacial tension, γ_{sl} the solid-liquid interfacial tension and θ_Y the contact angle. (Yuan & Lee, 2013).

Wetting is favoured when interfacial free energy and liquid surface free energies are low and solid surface free energy is high. (Owens & Wendt, 1969).

At this point, it should be highlighted that contact angles measured on rough or/and heterogeneous surfaces are not Young contact angles because Young's model does not include factors accounting for surface roughens or/and inhomogeneity of the solid surface (Yuan & Lee, 2013).

In the case of surface roughness, the slope variations of the surface represent barriers that pin the liquids' front motion when it is moving in one or another direction, resulting in alteration of the contact angle (Yuan & Lee, 2013).

Surface topography exhibits hydrophilic properties, if the droplet follows the topography, which generates an efficient decrease in the contact angle, or it spreads inside the solid textures (solid and liquid). The liquid contact angle is decreased in case of partial wetting when islands of solid emerge. (Bico, Thiele, & Quéré, 2002). The surface is considered to be superhydrophilic when the fluid contact angle is immeasurably low (materials exhibiting very low, but measurable, contact angle values are considered to be superhydrophilic), meaning the droplet transforms into a flat puddle (Yuan & Lee, 2013).

There are also cases in which the film of liquid spreads within the texture and the droplet is sited over a mixture of liquid and solid, as shown in Figure 3. In such cases, the contact angle is between zero and the contact angle found on the flat homogeneous surface (Bico et al., 2002).

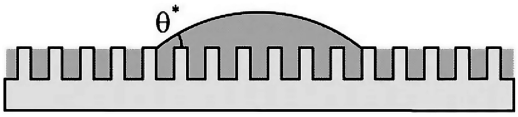

Figure 3: Schematic representation of a droplet sitting on the solid/liquid interface (Bico et al., 2002).

Superhydrophobic surfaces are usually considered to have contact angles higher than 150° meaning that small droplets have a very low contact surface area (Yuan & Lee, 2013). The surface exhibits superhydrophobic properties if there are, for example, sharp corners, and pinning contact lines on the texture. In such a case, the droplet is not stickled to the surface and can be easily removed. If the contact angle is higher than 90°, air is trapped beneath the liquid. Liquid on a model surface consisting of holes and spikes is shown in Figure 4. (Bico et al., 2002).

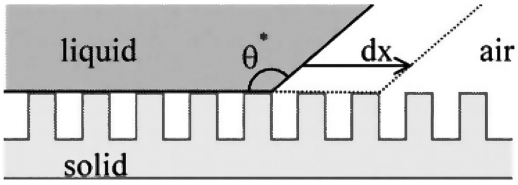

Figure 4: Schematic representation of a droplet on a model surface consisting of holes and spikes (Bico et al., 2002).

The wetting properties of the surface can be simply described by the two dimensionless parameters: the surface roughness and the surface fraction that describes the ratio between the two levels of the surface. These two parameters, together with the Young contact angle (which depends on the chemical nature of the liquid), enable the calculation of the contact angles of certain liquids on a certain surface. (Bico et al., 2002).

The hydrophilicity of the surface generally depends on its chemical composition, namely on functional groups bound onto the surface.

The hydrophilicity of functional groups is quantitatively determined by their hydration number. According to their hydration numbers, functional groups are classified as hydroneutral and hydrophilic. Hydration numbers are also temperature-dependent. Low molecular mass compounds with hydroneutral functional groups are usually well soluble in water. However, there are no hydrated water molecules attached to hydroneutral functional groups. Hydroneutral groups have the hydration number $n_H = 0$, while hydrophilic functional groups have hydration numbers above 0. There are certain functional groups that are polar and have high dipole moments. Therefore, they should be classified as hydrophilic, but they are actually hydroneutral. Hydroneutral groups are, for example $-CN$, $-NO_2$, $-C(O)O-$ and $-CO-$ groups. All hydroneutral groups are aprotic, and thus proton acceptors (Shikata & Okuzono, 2013).

According to their hydration numbers, hydrophilic polar groups are $-CH_2OCH_2-$, $-OH$ and $-C(O)NH_2$ with hydration numbers of 4, 5 and 6, respectively. They are more easily protonated and have slightly lower p_{Ka} than hydroneutral groups. p_{Ka} between -6 and -4 is the value range dividing hydroneutral and hydropilic functional groups (Shikata & Okuzono, 2013).

1.4 Plasma PTFE Functionalisation Methods

Plasma treatment technology is widely used for surface modification of PTFE, due to the fact that surface modifications are possible without alteration of material bulk properties (Hai, Hi, Shimizu, & Yajima, 2015a). Plasma modification techniques have an advantage over other methods because plasma sheaths can follow the work-piece profiles of objects with complex geometries. PTFE surfaces can be modified with radio frequency (RF) plasmas (Hai et al., 2015a), microwave (MW) plasmas (Xu et al., 2003), and atmospheric plasmas such as dielectric barrier discharge (DBD) plasma (Liu et al., 2004). RF plasmas are commonly used for polymer processing in diverse applications. However, their limitation is the need for a vacuum to achieve adequate plasma conditions. (Liu et al., 2004).

Plasma functionalisation mainly depends on the kinetic energy of the energetic species in plasma and vacuum ultra violet (VUV) radiation emitted by energetic species in plasma (Primc, 2020). Since the mid-1990s authors have used argon (Hong et al., 2019; Wilson, Williams, & Pond, 2001), hydrogen (Badey et al., 1996; Inagaki, Tasaka, & Umehara, 1999; Ryan & Badyal, 1995; Yamada, Yamada, Tasaka, & Inagaki, 1996), oxygen (Vandencasteele et al., 2008; Wilson et al., 2001), nitrogen (Hong et al. 2019; Wilson et al. 2001), ammonia (Badey et al., 1996), water (Dumée et al., 2016) and methane plasmas (Jie-Rong & Wakida, 1997), but WCA improvements were incomparably worse than those of chemical treatments. The best results, as reviewed by (Primc 2020), were in the range of water contact angles between 50 and 45°, with PTFE surface oxygen concentration as probed by XPS between 10 and 30 at.% (Primc, 2020).

It was found that PTFE surface hydrophilicity increases with bound oxygen content at the surface, but bound oxygen content tends to be reversely proportional to the oxygen content in plasma. Conventionally, there have been two types of PTFE plasma treatment. The first type of treatment with plasmas rich in oxygen typically results in a low level of functionalisation and, especially at high power, etching process is prevalent (Primc, 2020). Due to defluorination the carbon backbone becomes directly exposed to energetic oxygen species and the breaking of C−C bonds occurs, resulting in the formation of volatile $C_xF_yO_z$ fragments that are desorbed from the surface (Carbone, Verhoeven, Keuning, & van der Mullen, 2016).

Vandencasteele N. et al. treated the PTFE surface in afterglow low-pressure RF oxygen plasma. At low DC bias, WCA of 75°, surface oxygen content of 5 at.% and a decrease in RMS surface roughness was obtained. At higher DC bias, no oxygen was bound to the surface and the surface roughness increased (alveolar structures appeared) (Vandencasteele et al., 2008).

In the second type of PTFE plasma treatment with plasmas containing no or little oxygen (for example, hydrogen plasma), defluorination occurs due to VUV radiation and energetic radicals forming dangling bonds. Oxygen is bound to dangling bonds from residual water vapour within the discharge tube or/and after the treatment when samples are exposed to air (Primc, 2020). In low-pressure RF hydrogen plasmas, around 20 % of power is spent on radiation in the VUV range, in particular between 117 and 280 nm (Fantz, Briefi, Rauner, & Wünderlich, 2016).

Inagaki et al, (1998) performed a comparison of hydrogen plasma treatment of PTFE inside the coil and in the remote zone of 800 mm away from the centre of the coil. Inside the coil in the hydrogen plasma, the prevailing species are VUV photons, electrons, hydrogen ions and neutral hydrogen atoms. On the contrary, in the afterglow, hydrogen atoms are the predominant species. Plasma was sustained by a 13.56 MHz RF generator coupled with a copper coil with 9 turns in a Pyrex tube with a diameter of 45 mm. The pressure of hydrogen in the system was 13.3 Pa.

The best results in the afterglow (remote zone) were achieved with a treatment time of 120 s, and a water contact angle of 78° before rinsing and 77° after rinsing with acetone. In the centre of the coil, at the treatment time of 120 s, the contact angle value was 67° before rinsing and 88° after rinsing. Interestingly optimal results in the centre of the coil were achieved at a treatment time of 60 s with a contact angle 64° before rinsing and 84° after rinsing (Inagaki et al., 1999).

It could be concluded that PTFE hydrophilisation occurs in both zones and that the difference in the water contact angle arises from the removal of degradation products that are formed during direct plasma treatment where extensive etching occurs, but not in the afterglow, where etching is less pronounced. (Inagaki et al., 1999).

It was found that PTFE hydrophilisation in the afterglow, without etching, greatly improves adhesion between PTFE and copper. Failure of the PTFE/copper adhesive joint, therefore, is cohesive rather than adhesive (Inagaki et al., 1999).

Yamada Y. et al. treated the PTFE surface in the afterglow of hydrogen low pressure capacitively coupled RF plasma and obtained a WCA of 57 °and F/C and O/C ratios of 0.41 and 0.12, respectively. Angular resolved X-ray photoelectron spectroscopy (AR-XPS) with the use of extrapolation showed an F/C ratio of zero within the surface layer of 1 nm, indicating that there was complete defluorination within the surface layer (Yamada et al., 1996).

Ishikawa K. et al. showed that afterglow microwave low-pressure H-plasma is causing defluorination and formation of carbon dangling bonds by in situ spin resonance (ESR). Selective exposure to hydrogen radicals (U-shaped tube and light shade), only to VUV radiation and to a combination of VUV radiation and hydrogen radicals (sample holder with MgF_2 filter and a slit allowing the entry of H-atoms positioned in late afterglow) showed that the formation rate of dangling bonds was much higher with simultaneous exposure to hydrogen radicals and VUV than with exposure only to VUV, while no dangling bonds were detected when the PTFE surface was exposed only to neutral atoms (Ishikawa et al., 2011).

Badey et al. (1996) performed PTFE treatment with MW generated (2.45 GHz microwave generator) hydrogen plasma in a quartz tube with a diameter of 16 mm. Samples were located 30 cm from the centre of the discharge tube. Treatment at the H_2 flow of 50 sccm, effective power of 350 W, and treatment time of 60 s led to defluorination and creation of C–C and C–H groups, resulting in the decrease of water contact angle to the value of 83° and the F/C ratio at the surface of 0.90.

Badey et al. (1996) also performed PTFE treatment with ammonia-plasma in the same system. Treatment with an ammonia flow of 30 sccm, effective power of 350 W and treatment time of 120 s led to defluorination and synthesis of C–C, C–H and nitrogen-containing groups, resulting in the contact angle of 53° and F/C ratio of 0.6. They found that both hydrogen and ammonia plasma caused crosslinking in the PTFE (Badey et al., 1996).

Ryan & Badyal (1995) studied the effects of different non-equilibrium glow discharge treatments with plasmas of hydrogen, nitrogen, noble gas and CF_4 on the PTFE surface. It was found that hydrogen plasma caused the greatest decline in fluorine content on the surface. Nitrogen and noble gas plasma treatments resulted in the formation of fibrillary microstructures. CF_4 plasma treatment resulted in the breakage of polymer chains, followed by fluorine atom capping and yielding of $–CF_3$ groups (Ryan & Badyal, 1995).

From the literature, it is evident that functionalisation levels with oxygen or hydrogen plasmas alone are inadequate.

There are two good reasons to use the plasma sustained in a mixture of H_2O/Ar for the treatment of PTFE. Firstly, such plasmas contain many active species which can react

with the surface, and secondly, Ar helps to maintain a steady plasma at low temperatures and pressures (Xu et al., 2003).

Xu H. et al. (2003) treated PTFE samples in MW plasma consisting of H_2O and Ar. PTFE samples were first washed with a solution of methylbenzene, acetone and water to remove possible contaminants, which could affect untreated material surface properties and the plasma treatment process. Samples were processed in plasma MW-powered plasma systems using the mixture of Ar and H_2O. The system consisted of a 2.45 GHz MW generator that was coupled with a quartz tube with a diameter of 30 mm. Argon with a flow rate of 5.0 – 10 sccm was introduced into the quartz tube through a water bubbler held at 20 °C resulting in the gas pressures in the discharge chamber between 27 and 50 Pa (Xu et al., 2003).

Under optimal experimental conditions (400 W, 2.8 cm from the centre of the plasma zone and the time of 120 s), PTFEs surface contact angles decreased from 110° to 23.6°. Bulk properties of the material remained unchanged. Xu H. et al. (2003) also discovered that the WCA decreased with increasing power and treatment time. Prolongation of the treatment time, however, decreased the WCA only to a certain point, after which the effect was less pronounced. They also observed that the optimal processing time to obtain the lowest WCA with a certain processing power increased in tandem with increments of processing power. According to Xu H. et al. (2003), this could be explained by the fact that plasma under a given condition affects only to a certain depth, and when the processing depth is reached, there are no further changes. The fact that the processing time to reach the stable contact angle increases with increasing processing power supports the assumption that plasmas at higher processing powers can modify thicker surface layers (Xu et al., 2003).

Xu H. et al. (2003) also found that the distance between the centre of the plasma zone and the sample greatly influenced the surface modification, probably because of the spatial distribution of active species and the temperature (Xu et al., 2003). Further, Xu H. et al. (2003) found that the WCA reached a constant value of 60° after 5 days (at room temperature, exposed to the atmosphere). It is interesting that the contact angle markedly increased in the first ten hours. Surface recovery originates from the changing fluorine and oxygen contents due to oxidative reactions. Other reasons are the migration of hydrophilic groups under the surface and the migration of chains from the bulk to the surface (Xu et al., 2003).

Xu H. et al. (2003) performed XPS analyses and found that they were able to achieve a decrease in F/C ratio from 1.68 (the theoretical F/C ratio of PTFE 2.0) to the value of 0.41, while the O/C ratio reached the value of 0.55. This indicates that MW plasma treatment with H_2O/Ar plasma introduced high amounts of oxygen and resulted in substantial surface defluorination. With treated samples, they found a peak at 292.4 eV, which was assigned mainly to CF_2 species underneath the surface, and a broader peak at around 285.2 eV to which multiple peaks were fitted. They were assigned to: C=O (288.5 eV), C–O (286.2 eV), and C=C together with CH_2 at 284.6 eV (Xu et al., 2003).

Additionally, Xu H. et al. (2003) examined treated PTFE samples with ATR FTIR in a vacuum in the range of 1 mbar (100 Pa). Untreated PTFE samples had no absorption bands at wavelengths of 2800–4000 cm^{-1}. The spectra of treated samples exhibited absorption peaks at 2882.8 cm^{-1} and 2931.9 cm^{-1}, assigned to sp^3 –C–H, the absorption peak at 3031.1 cm^{-1} assigned to sp^2 –CH, and the absorption peak at 3554.4 cm^{-1} assigned to –OH. It is obvious from ATR FTIR results that many hydrophilic groups were formed in the thickness of PTFE surface film probed by FTIR (Xu et al., 2003).

Huang C. et al. (2013) performed hydrophylisation of the porous and crystalline PTFE membrane surface with RF (13.56 MHz) generated plasma consisting of a mixture of methane (CH_4) and nitrogen (N_2) in a Pyrex discharge tube with the internal diameter of

53 mm and length of 450 mm. A copper coil was located 100 mm from the gas inlet. Flow rates of CH_4 and N_2 were 8 sccm (1:1 methane - nitrogen gas mixture) and the pressure in the discharge tube was 120 mTorr (1.6 Pa). The RF powers used were between 10 and 50 W (Huang et al., 2013). The water contact angle at the PTFE surface decreased with increasing power from the initial 131° to ∼52° at RF power of 50 W, and the contact angle of di-iodomethane was ∼29° at the same RF power. Surface energy increased from an initial 3.7×10^{-3} J/m^2 to 3.79×10^{-2} J/m^2 at 10 W and to 6.01×10^{-2} J/m^2 at 50 W. (Huang et al., 2013). With untreated PTFE only FTIR peaks at 1200 and 1148 cm^{-1} were detected. New absorption peaks at 1930 and 1460 cm^{-1} representing C–H stretching vibrations were found with treated samples. New peaks also appeared at 1380 and 2200 cm^{-1}, which were assigned to both C–N and C≡N bonds. The new peak at 1640 cm^{-1} and the band at 3200–3600 cm^{-1} were assigned to the N–H bond (primary amine) (Huang et al., 2013).

Recently, Nyugen T. H. and Yajima treated PTFE foils in low-pressure non-equilibrium ICP RF plasmas in a gas mixture containing ammonia, argon and water. The WCA value of 4° at the PTFE surface was achieved, rendering superhydrophilic PTFE (Nguyen & Yajima, 2017). The treatment time was several minutes.

Hai W. et al. treated PTFE for 15 min with a plasma consisting of Ar-H_2O-NH_3 with a similar experimental setup and achieved the WCA value of 4° after a 15 min treatment. F/C, N/C and O/C ratios were 0.31, 0.21 and 0.10, respectively. C*–C, C*=C, C*–H, C*–N, C*–O and –(CH_2–C*F_2)n– functional groups were determined by XPS. Additionally, morphological changes at the scale of a hundred nm were found by scanning electron microscopy (Hai, Hi, Shimizu, & Yajima, 2015b).

Although Ar-H_2O-NH_3 low-pressure plasma provides very good PTFE functionalisation capabilities, its major drawback is the content of ammonia, which can corrode vacuum equipment (alkaline water solution), causes lung irritation and has an unpleasant odour, has a large greenhouse effect, causes the formation of particulate matter in the atmosphere and causes surface water eutrophication (Behera, Sharma, Aneja, & Balasubramanian, 2013). Therefore, despite the use of liquid nitrogen ice traps (used by Nyugen T. H. and Yajima and also Hai W. et al.), acceptable in a lab environment, it makes the industrial use of NH_3-containing plasmas very inconvenient. Additionally, Hai W. et al. needed a treatment time of 15 min to achieve the WCA of 4°, which is also inconvenient for industry.

1.5 Thesis Objectives

The purpose of this doctoral thesis is to study the interactions of plasma radicals and radiation with fluorinated polymers.

The research focused on the mechanisms of interaction of hydrogen and oxygen plasmas with the PTFE surface, which affect the different courses of reactions on the surface. Therefore, it was presumed that the functionalisation of PTFE could be achieved by a suitable combination of the effects of both plasmas. The effects of hydrogen ions, neutral hydrogen atoms and vacuum ultraviolet radiation on the alterations of the chemical structure of PTFE were investigated. The influences of the density and the fluence of neutral oxygen atoms on the hydrophilisation of the pre-treated PTFE surface with hydrogen plasma were studied. The ultimate goal of this research was the development of alternative methods of functionalisation (hydrophilisation) of the surface of fluoropolymers using low-pressure plasmas. The scientific results enabled the development of a new process for PTFE functionalisation with successive treatments of the PTFE surface in low-pressure hydrogen and oxygen plasmas. Additionally, the possibilities of upscaling our technology for industrial use were studied.

1.6 Hypotheses

The following hypotheses were stated:

- Low-pressure non-equilibrium hydrogen plasma causes the breakage of C—F bonds in PTFE due to the absorption of VUV radiation resulting in the formation of dangling bonds. Hydrogen atoms are bound to the dangling bonds forming polyolefin-like structures on the surface.
- If PTFE with a previously synthesised polyolefin-like layer is treated with low-pressure non-equilibrium oxygen plasma, oxygen atoms are bound to the surface, forming hydrophilic and hydroneutral functional groups such as hydroxyl, carbonyl and carboxyl groups. The process should be similar to polyethylene functionalisation with oxygen plasma (polyethylene has a polyolefin structure).
- The innovative industrial size plasma system sustaining plasma by four parallelly coupled inductors with the ability of precise impedance tunning enables the functionalisation of polymers of arbitrary sizes and shapes.

1.7 Methodology

Hydrogen and oxygen plasmas were sustained in an experimental inductively coupled reactor consisting of a borosilicate discharge tube, a radiofrequency generator, an impedance matching network, a six-loop water-cooled coil, a flow controller and a two-stage rotary vacuum pump. Low-pressure non-equilibrium hydrogen plasma consists mostly of ions, neutral atoms, electrons, and hydrogen molecules and is a source of extensive vacuum ultraviolet (VUV) radiation. Oxygen plasma is a rich source of neutral O-atoms in the ground state.

Plasmas were characterised by the following methods. Neutral oxygen and hydrogen atom densities in plasmas were measured with cobalt catalytic probes. Measurements of radiation arising from excited plasma species were performed by optical emission spectroscopy (OES). Reflected powers of the plasma system were measured by the power meters built into the RF generator.

The properties of treated PTFE samples were measured using goniometry to determine the water contact angles (WCA) of the surfaces, X-ray photoelectron spectroscopy (XPS), and time-of-flight secondary ion mass spectrometry (ToF-SIMS).

The innovative plasma system with four inductors coupled in parallel to a single RF generator, featuring impedance tunning of the leads of each coil, was designed using 3D CAD modelling (AutoCAD software).

Chapter 2

Defluorination of the Polytetrafluoroethylene Surface by Hydrogen Plasma

This chapter explains the interactions of H-atoms produced in non-equilibrium low-pressure hydrogen plasma with the PTFE surface, and their involvement in PTFE surface defluorination. From literature research, it is clear that H-atoms have an important role in the defluorination process of the PTFE surface in H-plasma, but it remains unclear whether they can cause sufficient defluorination by themselves. In this chapter, the ability of H-atoms to defluorinate the PTFE surface was investigated under different plasma parameters and compared with the defluorination efficiency of hydrogen plasma itself.

To sustain the hydrogen plasma, an RF inductively coupled discharge consisting of a borosilicate glass discharge tube with an internal diameter of 36 mm, a six-loop water-cooled coil, an impedance matching network, an RF generator, a flow controller and a vacuum pump were used. The plasma system is shown in Figure 5.

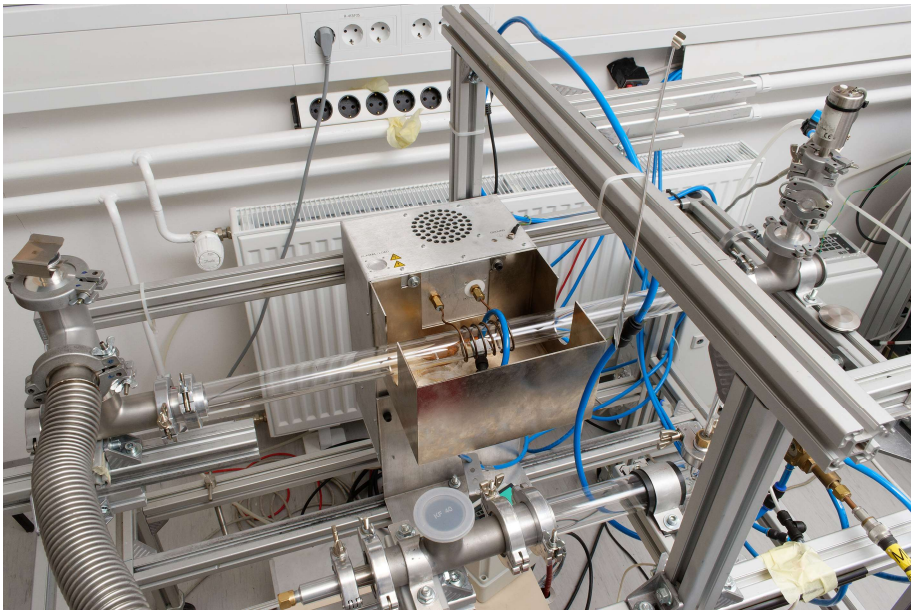

Figure 5: Experimental inductively coupled plasma system.

The PTFE samples were treated in a low-pressure hydrogen plasma at various systematically chosen plasma parameters, including the variation of plasma modes (E-mode, H-mode), generator power, treatment time, and pressure. The location of the samples was also varied with different treatments.

The elemental composition of the treated samples was evaluated by X-ray photoelectron spectroscopy (XPS) – analysed by Alenka Vesel, the chemical composition of the treated surface was evaluated by Time-of-flight secondary ion mass spectrometry (ToF-SIMS) – analysed by Jernej Ekar and the wettability of the treated surface was evaluated by goniometry (contact angle of the water droplet applied to the surface). XPS analyses were performed at different photoelectron take of angles (TOA) in order to obtain depth profiles of the elemental composition of the PTFE surface.

At the discharge power of 400 W, treatment time of 1 s and H_2 pressure of 25 Pa, several samples were inserted into the discharge tube individually and treated with H-mode hydrogen plasma. Within the coil area, WCA was about 83° after the treatment (about the typical value of polyolefins). Within the few centimetres into the early afterglow, the WCA slightly increased to a value close to 100°, and further into the late afterglow, WCA increased linearly with increasing distance from the coil, thus approaching the value of untreated PTFE (115°). The results were explained by weak capacitive coupling between the coil and metallic pump duct.

At the discharge power of 400 W and H_2 pressure of 25 Pa, the treatment time was varied, resulting in the initial decrease of WCA down to about 90° followed by a minimal rise to about 95° where it remained for the treatment time of 9 s. The constant value is explained by the saturated defluorination of the surface.

When the PTFE samples were treated in plasma for 1 s at H_2 pressure of 25 Pa, and the discharge power was varied between 100 and 900 W, the WCA initially dropped to the value of around 90° and stayed approximately constant toward the power of 900 W.

When PTFE samples were treated at the discharge power of 400 W, treatment time of 1 s and the pressure was varied between 10 and 60 Pa, a constant WCA value of approximately 90° was achieved.

As the WCA depends only on the surface energy and surface morphology it cannot provide specific information on the elemental composition, chemistry and morphology of the surface. Therefore, XPS and SIMS analyses were performed.

Untreated PTFE has an F/C ratio of 2.2. The F/C ratio of the PTFE surface treated by H-plasma obtained by XPS analysis at the discharge power of 400 W, H_2 pressure of 25 Pa dropped to about 0.3 after 0.2 s and reached its minimum of about 0.2 after 1 s. After 10 s, the F/C ratio raised to about 0.4.

Using angular XPS at TOA of 15°, the F/C ratio of the PTFE surface, treated at the discharge power of 400 W for 1 s at H_2 pressure of 25 Pa, was about 0.1. From the extrapolation of F/C ratios obtained from several XPS measurements of the same sample taken at TOA values between 15 and 75°, it was found that the F/C ratio at the TOA value of 0° would be practically 0, meaning that the surface was practically fluorine-free.

In the case of E-mode PTFE surface treatment at 25 Pa and the discharge power of 100 W (real power well below 100 W due to the matching network optimisation for the H-mode plasma), there was a gradual decrease in the F/C ratio during treatment reaching a value of about 1.25 after 1 s and approaching the value of 0.6 after several seconds.

The difference between the F/C ratios achieved on the PTFE surface with E- and H-mode plasmas is explained by different mechanisms. E-mode plasma has 3 to 4 orders of magnitude weaker radiation than H-mode plasma, and H-atoms do not penetrate into the subsurface film as VUV photons do. Nevertheless, there is a possibility that H-atoms also attack the surface and are bound to dangling bonds (Yamada et al., 1996). After a treatment of 1 s at 100W, and H_2 pressure of 25 Pa, measured at the TOA of 15° the F/C

ratio was about 0.9, which is significantly lower than the 1.25 measured with the sample surface treated under the same conditions at the standard TOA value of 45°, probably due to a much thinner functionalised layer.

If one is about to confirm the formation of a fluorine-free polyolefin-like layer consisting of −CH− structures, XPS is not the ideal instrument of choice because hydrogen atoms cannot be detected. An advantage of the SIMS is that it has better surface sensitivity compared to XPS, rendering it ideal for analysing very thin surface layers (a few monolayers). Therefore, ToF-SIMS was used for analyses of the H-plasma treated PTFE surfaces. With a treatment time of 1 s and H_2 pressure of 25 Pa, the discharge power was varied. A nearly linear increase of C_xH_y ions signals was observed between the discharge powers of 200 and 400 W and a decrease of C_xF_y ions signals down practically zero in the same power range. However, it is interesting that a substantial decrease of the C_xF_y ions signals happened in the discharge power range of 50 and 200 W, while the strong increase in C_xH_y ions signals intensity occurred only above the discharge power of 150 W. SIMS analysis confirmed the formation of polyolefin-like −CH− structures at the PTFE surface upon treatment with H_2 plasma.

polymers

MDPI

Article

Defluorination of Polytetrafluoroethylene Surface by Hydrogen Plasma

Alenka Vesel [1,*], Dane Lojen [1,2], Rok Zaplotnik [1], Gregor Primc [1], Miran Mozetič [1], Jernej Ekar [1,2], Janez Kovač [1], Marija Gorjanc [3], Manja Kurečič [4] and Karin Stana-Kleinschek [5]

1 Department of Surface Engineering, Jozef Stefan Institute, Jamova cesta 39, 1000 Ljubljana, Slovenia; dane.lojen@ijs.si (D.L.); rok.zaplotnik@ijs.si (R.Z.); gregor.primc@ijs.si (G.P.); miran.mozetic@ijs.si (M.M.); jernej.ekar@ijs.si (J.E.); janez.kovac@ijs.si (J.K.)
2 Jozef Stefan International Postgraduate School, Jamova cesta 39, 1000 Ljubljana, Slovenia
3 Faculty of Natural Sciences and Engineering, University of Ljubljana, Aškerčeva cesta 12, 1000 Ljubljana, Slovenia; marija.gorjanc@ntf.uni-lj.si
4 Faculty of Mechanical Engineering, University of Maribor, Smetanova 17, 2000 Maribor, Slovenia; manja.kurecic@um.si
5 Institute of Chemistry and Technology of Biobased Systems, Graz University of Technology, Rechbauerstraße 12, 8010 Graz, Austria; karin.stanakleinschek@tugraz.at
* Correspondence: alenka.vesel@guest.arnes.si

Received: 6 November 2020; Accepted: 27 November 2020; Published: 29 November 2020

Abstract: Defluorination of polytetrafluoroethylene (PTFE) surface film is a suitable technique for tailoring its surface properties. The influence of discharge parameters on the surface chemistry was investigated systematically using radio-frequency inductively coupled H_2 plasma sustained in the E- and H-modes at various powers, pressures and treatment times. The surface finish was probed by X-ray photoelectron spectroscopy (XPS) and time-of-flight secondary ion mass spectrometry (ToF-SIMS). The measurements of water contact angles (WCA) showed increased wettability of the pristine PTFE; however, they did not reveal remarkable modification in the surface chemistry of the samples treated at various discharge parameters. By contrast, the combination of XPS and ToF-SIMS, however, revealed important differences in the surface chemistry between the E- and H-modes. A well-expressed minimum in the fluorine to carbon ratio F/C as low as 0.2 was observed at the treatment time as short as 1 s when plasma was in the H-mode. More gradual surface chemistry was observed when plasma was in the E-mode, and the minimal achievable F/C ratio was about 0.6. The results were explained by the synergistic effects of hydrogen atoms and vacuum ultraviolet radiation.

Keywords: polytetrafluoroethylene; fluorine depletion; hydrogen plasma; VUV radiation; surface modification; hydrophilic

1. Introduction

Fluorinated polymers are used in various applications [1]. They are renowned for their chemical inertness and thermal stability [2]. The chemical inertness does not allow for reasonable adhesion of any coating deposited by numerous techniques [3,4]. Whatever material is deposited, the surface energy of the coating is much larger than the energy of the substrate; therefore, thin films tend to form 3D particles spontaneously rather than a uniform film. Coatings from liquid solutions also do not adhere well on the surface, especially when the liquid is polar, i.e., water. In order to improve the adhesion of coatings, methods for increasing the surface energy of fluorinated polymers have been invented [5–10]. Fluorinated polymers are usually treated with aggressive chemicals which

cause modification of the surface chemistry. Such techniques were invented in the 1960s, and some are still used nowadays. Common techniques include the application of sodium naphthalide [11], tetraalkylammonium radical anion salt, alkali metal vapours and amalgams [12], and electrochemical methods [13,14]. All these techniques represent an ecological hazard; therefore, researchers have been working on alternative techniques. A straightforward solution is irradiation of fluorinated polymers with beams of photons, electrons, or ions [15,16]. The insulating properties of fluorinated polymers make the techniques employing charged particles rather difficult, however.

A medium that contains both electrons, positively charged ions, and photons is gaseous plasma. Gaseous plasma is a state of gas also consisting of neutral particles (thereafter: radicals), which are chemically extremely reactive. For example, diatomic molecules are partially dissociated upon plasma conditions, and the atoms typically interact with most of the polymers even at room temperature. The atoms may bind to the surface of a polymer, thus forming functional groups of different polarity than those presented in fluorinated polymers. For example, oxygen plasma of a high density of oxygen atoms will cause functionalization of most polymers with various oxygen-containing functional groups [17]. While such treatments with oxygen plasma perform well for most types of polymers, they fail in the case of polytetrafluoroethylene (PTFE) for one simple reason: the binding energy of fluorine to carbon atoms is much larger than those of oxygen; therefore, a simple substitution of fluorine atoms on the surface of PTFE with oxygen atoms is energetically unfavourable. Treatment of fluorinated polymers by oxygen plasma will cause gradual etching of the polymer material rather than surface activation, as shown recently by Primc et al. [18].

Because classical plasma techniques fail in the case of PTFE, researchers have invented a variety of alternative methods. As early as 1987, Clark et al. [14] used a high vacuum plasma reactor to treat PTFE samples with hydrogen plasma. A radiofrequency (RF) generator coupled in a capacity mode was used for plasma generation. The maximum power was 10 W, and the treatment times were up to approximately 250 s. Upon such conditions, the surface film of PTFE was depleted of fluorine, which was proven by X-ray photoelectron spectroscopy (XPS). The water contact angle (WCA) showed moderate hydrophilicity of the treated samples after prolonged treatment. The minimum WCA was 50°. The authors explained the fluorine depletion by the interaction between hydrogen atoms and PTFE, causing the formation of HF molecules that were pumped away from the system.

About a decade later, Badey et al. [19] performed similar experiments, except that they used a powerful microwave (MW) generator for sustaining a dense plasma in a narrow quartz tube. PTFE samples were placed downstream from the centre of the discharge. The best results were observed at large gas flows and moderate discharge powers. The F/C ratio dropped from an original 2.45 to about 0.8. The WCA of water dropped from 115° to approximately 85° and diiodomethane from 84° to approximately 50°. The surface modifications were also monitored by secondary ion mass spectrometry (SIMS), and the authors found numerous C_xH_y peaks after accomplishing the remote plasma treatment. As by Clark et al. [14], Badey et al. [19] also explained the observed results by the interaction between the polymer surface and neutral hydrogen atoms, causing the formation of HF molecules. In the same year, Yamada et al. [20] also applied remote H_2 plasma treatment for the modification of PTFE samples. The plasma source was inductively coupled RF discharge. As by Badey et al. [19], the authors used a quartz tube for the discharge chamber and placed samples in the afterglow region. The authors reported similar results as Badey at large discharge powers. They also performed XPS characterization and found similar functional groups as Badey. The same group also used remote hydrogen plasma treatment to study the adhesion of Cu film on PTFE samples [21]. They obtained the minimum WCA of approximately 75° at the treatment time of approximately 2 min. In another paper, Inagaki et al. [22], used pulsed plasma treatment. An capacitiveRF discharge in the power range between 75 and 100 W was applied at the pressure of 13 Pa. The results and WCAs were slightly larger than in the case of using continuous plasma treatment. The same applied to the F/C ratio.

König et al. [23] used plasmas sustained in various gases for modification of a plasma-deposited fluorocarbon polymer with the structure close to PTFE. Plasma was sustained by a MW discharge in the

electron cyclotron resonance (ECR) mode. The working pressure was as low as 0.2 Pa. The maximum discharge power was 800 W. Samples were additionally biased using a capacitively coupled RF generator. The F/C ratio as deduced from the XPS survey spectra was 1.9 for the untreated material and dropped to 0.72 for plasma-treated samples. Simultaneously, the oxygen to carbon ratio O/C increased from 0.02 to 0.09. Such a surface finish enabled a slight decrease of WCA from the original 106° down to about 86°.

Tanaka et al. [24] investigated defluorination of PTFE by a combination of atmospheric pressure glow plasma treatment and a chemical transport method. Plasma was sustained in a mixture of He and H_2. The lowest F/C ratio reported for such plasma treatment was 0.4. The addition of oxygen in the gas mixture caused a further drop of the F/C concentration and appearance of a few atomic % of oxygen. More recently, Hunke et al. [25] performed direct treatment of PTFE powders in a low-pressure hydrogen plasma. They used a MW discharge and obtained a moderate decrease in the F/C ratio. The authors adopted the explanation provided previously by Inagaki et al. [22].

The review of the early work can be summarized as follows: the defluorination of PTFE surface occurs upon treatment with hydrogen plasma or its flowing afterglow and is explained by the interaction of hydrogen atoms with pristine material causing the formation of a dangling bond on one C atom. The dangling bond is quickly occupied with another H atom, forming the CHF group. This group may decompose by desorption of the HF molecule, and the result is the formation of the CF=CF group. The abundance of H atoms causes the gradual transformation of the polymer surface. A typical treatment time needed for observing a rather low F/C ratio is of the order of a minute.

In the present paper, we disclose experiments with hydrogen plasma performed in the same reactor at different conditions. Gaseous plasma was created in different discharge modes; therefore, some plasma parameters depended enormously on discharge conditions.

2. Materials and Methods

PTFE foils were purchased from Goodfellow Ltd. (Huntingdon, UK). The foils with a thickness of 0.5 mm were cut to pieces of 10 × 10 mm^2 and cleaned with ethanol, followed by drying at ambient conditions.

PTFE was treated in a glass discharge chamber using an electrodeless radio-frequency (RF) discharge. A schematic of the discharge chamber is shown in Figure 1. The discharge chamber was a long glass tube with a diameter of 4 cm. It was pumped on one side, and on the other side, H_2 gas was introduced through the flow controller. The vacuum system was sealed with rubber gaskets. It was pumped with a two-stage rotary pump of a nominal pumping speed of 80 m^3/h. The experimental conditions, therefore, enabled achieving the ultimate pressure just below 1 Pa after pumping for a reasonable time. Optical emission spectroscopy (OES) was used to check any gaseous impurities in the discharge chamber. Spectral features of any trace gases were below the detection limit of the spectrometer; therefore, the system was hermetically tight, and the residual atmosphere contained water vapour only. Plasma was sustained within the coil, as shown in Figure 1 and diffusing plasma expanded far away from the coil. The coil was connected to the RF generator via a matching network. The matching network allowed for coupling optimization to run the plasma mostly in the H-mode, depending on the power. The generator operated at the standard frequency of 13.56 MHz and adjustable output power up to 1000 W. The samples were treated at various conditions, i.e., various powers from 100 to 1000 W, hydrogen pressures from 10 to 60 Pa, and treatment times from 0.5 to 12 s.

The surface wettability of samples was measured using a Drop Shape Analyser DSA-100 (Krüss GmbH, Hamburg, Germany). A static contact angle was measured using a sessile drop method. The volume of a drop was 1 μL. MiliQ water was used for determination of the wettability.

Surface modifications were probed by XPS and time-of-flight secondary ion mass spectrometry (ToF-SIMS). The XPS characterization was performed using an XPS instrument (model TFA XPS from Physical Electronics, Münich, Germany). The samples were irradiated with monochromatic Al $K\alpha_{1,2}$ radiation with the photon energy of 1486.6 eV. Spectra were measured at an electron take-off angle

(TOA) of 45°. Selected samples were also measured at various TOAs to manipulate the detection depth of XPS. Survey spectra were acquired at a pass-energy of 187 eV using an energy step of 0.4 eV. High-resolution carbon C1s spectra were measured at a pass-energy of 23.5 eV using an energy step of 0.1 eV. An additional electron gun was used for compensation of the surface charge. Spectra were calibrated by adjusting the C1s peak corresponding to CF_2 groups to 292 eV. The measured spectra were analyzed using MultiPak v8.1c software (Ulvac-Phi Inc., Kanagawa, Japan, 2006) from Physical Electronics, which was supplied with the spectrometer. Linear background subtraction was used.

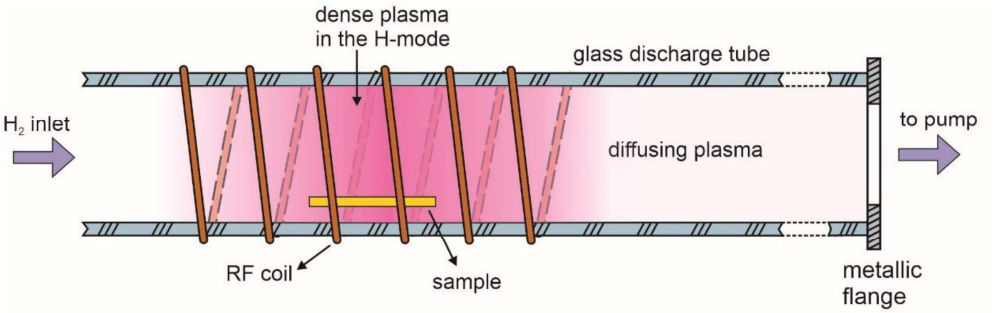

Figure 1. Schematic of the plasma set-up.

ToF-SIMS analyses were performed using a ToF-SIMS 5 instrument (ION-TOF, Münster, Germany) equipped with a bismuth liquid metal ion gun with a kinetic energy of 30 keV. The analyses were performed in an ultra-high vacuum of approximately 10^{-7} Pa. The ToF-SIMS spectra were measured by scanning a Bi^{3+} cluster ion beam over the surface spot of approximately 100×100 μm^2. An electron gun was used to allow for charge compensation on the sample surfaces during the analysis. Positive and negative ion spectra were measured

3. Results and Discussion

3.1. Modification of the Surface Wettability

Samples were placed at different positions along the discharge tube to measure the gradient in the surface wettability. Some of them were placed inside the RF coil, and many were placed away from the coil, in the direction of the pump duct. The water contact angle was measured for all these samples, and the result is presented in Figure 2. Plasma treatment time in all cases was 1 s, the hydrogen pressure was 25 Pa, and the discharge power was 400 W. The WCA for the untreated sample was approximately 110°. One can observe a gradual increase in the WCA with the increasing distance from the RF coil. The samples treated within the coil assume the WCA of approximately 83°, which is the value already reported by previously cited authors. This value is typical for oxygen-free polymers such as polyolefins. Such a rather low WCA extends a few cm away from the coil, which is explained by the simple fact that a dense plasma in the H-mode was not limited to the coil only, but also stretched outside of the coil as shown schematically in Figure 1. Away from the coil, the WCA increases to approximately 100° within a distance of several cm. Thereafter, the WCA increases rather linearly with increasing distance, and at large distances approaches the value typical for the untreated sample. The measured points scatter somehow, but the trend is obvious and is presented by straight lines. The results summarized in Figure 2, therefore, suggest almost complete defluorination of the PTFE samples upon treatment with a dense, glowing hydrogen plasma, and a more gradual activation upon treatment with a diffusing plasma, which in our case is a result of a weak capacitive coupling between the coil and the metallic pump duct.

Polymers **2020**, *12*, 2855

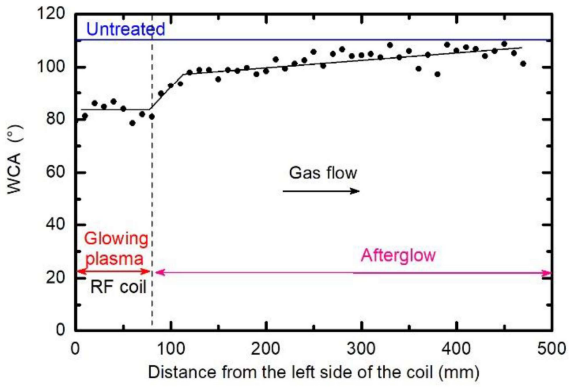

Figure 2. Variation of water contact angle (WCA) on the polytetrafluoroethylene (PTFE) surface of the samples arranged along the discharge tube. The treatment time was 1 s, the hydrogen pressure was 25 Pa, and the discharge power was 400 W.

As already reported by numerous authors, the WCA depends on numerous treatment parameters, including the treatment time, the pressure, and the power absorbed by the gaseous plasma [20–22,26,27]. To get additional information about the evolution of the surface wettability, we treated several samples inside the RF coil at various conditions. Figure 3 represents the WCA versus plasma treatment time. We adopted the same parameters as in Figure 2, i.e., the pressure of 25 Pa and the power of 400 W. It seems that the WCA in Figure 3 does not really depend on treatment time at these particular discharge conditions. All values lay at approximately 90°, with the exception of the first measurement corresponding to the lowest treatment time of 0.5 s where the standard deviation is rather large. The almost constant WCA, as revealed from Figure 3, is explained by the saturated defluorination of the surface. This effect will be further discussed later. Figure 4 is a plot of the WCA versus the discharge power for the treatment time of 1 s and the pressure of 25 Pa. Again, one can observe a rather constant WCA, except for the measurement performed at the lowest power of 100 W. The WCA also does not depend much on the H_2 pressure in the discharge tube, as shown in Figure 5. Figures 3–5, therefore indicate that the surface activation is accomplished within the second of plasma treatment providing the discharge power is reasonably large, and the pressure is in the range between 10 and 60 Pa.

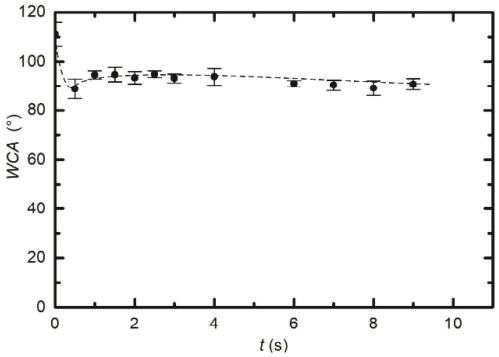

Figure 3. Variation of surface wettability with treatment time. The samples were inside the radiofrequency (RF) coil. Discharge power and hydrogen pressure were constant at 400 W and 25 Pa, respectively.

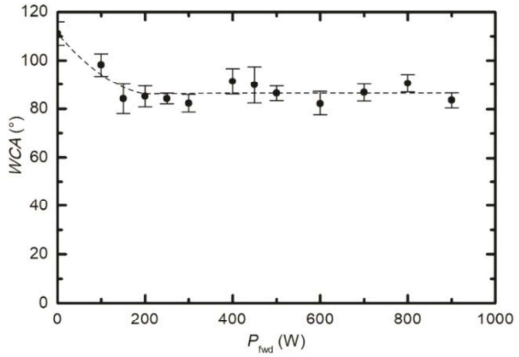

Figure 4. Variation of surface wettability with the forward discharge power. Treatment time and hydrogen pressure were constant at 1 s and 25 Pa, respectively.

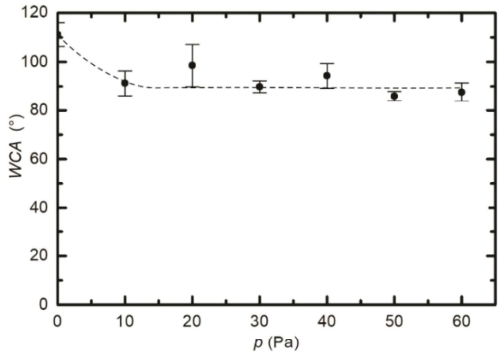

Figure 5. Variation of surface wettability with hydrogen pressure. Treatment time and discharge power were constant at 1 s and 400 W, respectively.

The water contact angles, as observed from Figures 2–5, indicate a rather marginal increase of the PTFE wettability, i.e., the WCA remained above 80°. Such a WCA was reported already by Badey at al. [4] and Konig at al. [8]. Somehow lower WCA of 75° was reported by Yamada et al. [5], and the WCA of about 50° was found by Clark et al. [2]. The discrepancy was explained recently by Primc [3] who showed that the WCA on the surface of fluorinated polymers depends on the concentration of other elements. Even a small concentration of oxygen, for example, caused a decrease of the WCA below the values typical for polyolefins (about 80°).

The results of the surface wettability as probed by the WCA do not show any obvious trend. Because this technique does not reveal the chemical modifications taking place on the sample surface upon plasma treatment, we additionally performed research on the composition and structure of the surface film as probed by XPS and ToF-SIMS to further elaborate details about the surface chemistry.

3.2. Chemical Modifications as Determined by X-ray Photoelectron Spectroscopy (XPS)

Figure 6 shows the XPS F/C ratio versus the treatment time when plasma was sustained at a large power of 400 W (lower curve) and at low power of 100 W (upper curve). See also supplementary Figures S1 and S2 showing individual survey spectra and elemental composition versus treatment time. The upper curve of Figure 6 corresponds to the same experimental conditions as the WCA measurement at the discharge power of 100 W in Figure 4, which reveals incomplete activation of the surface at 100 W after the treatment for 1 s. Examining Figure 6, it is obvious that incomplete surface activation is a consequence of the insufficient removal of fluorine from the surface of PTFE, because the F/C concentration after the treatment for 1 is still about 1.25, thus far from complete defluorination.

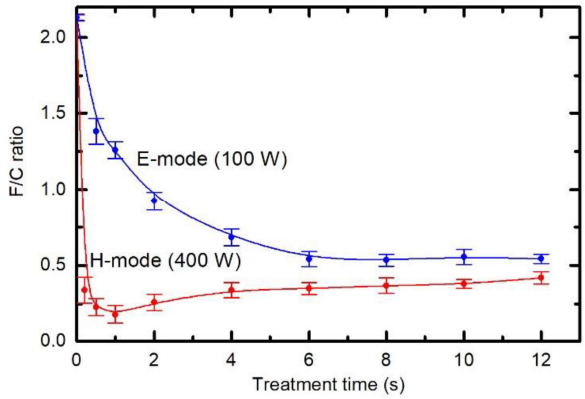

Figure 6. Variation of the X-ray photoelectron spectroscopy (XPS) F/C ratio versus treatment time for two different powers. Hydrogen pressure was constant at 25 Pa.

The upper curve in Figure 6 shows a gradual decrease of the F/C ratio with increasing treatment time. Gaseous plasma at the pressure of 25 Pa and RF power of 100 W is sustained in the E-mode. Because the matching network was optimized for coupling in the H-mode, a significant fraction of the RF power was reflected and thus not absorbed by the gaseous plasma. The power absorbed in plasma for the case of the upper curve of Figure 6 is, therefore, well below 100 W. Still, the surface film as probed by XPS is depleted of fluorine even after several seconds of plasma treatment and approaches a value of approximately 0.6. It seems that such a concentration of fluorine is about all one can achieve upon treatment of PTFE in hydrogen plasma sustained in the E-mode.

The mechanism is completely different when plasma is sustained in the H-mode (lower curve). In this case, the surface film is depleted of fluorine even after approximately 0.2 s of plasma treatment. The F/C ratio further decreases with increasing treatment time until a minimum at approximately 1 s appears. Thereafter, a gradual but slow increase in the F/C ratio is observed. After approximately 10 s, the F/C ratio assumes a value of approximately 0.4. This value is lower than what is achievable in the E-mode.

A huge difference in the surface composition between the E- and H-modes, as evident from Figure 6, should be explained by different mechanisms. Gaseous plasma in the H-mode is an extensive source of vacuum ultraviolet (VUV) radiation [28]. Recently, Fantz et al. investigated the details regarding the radiation arising from H_2 plasma sustained by an inductively coupled RF discharge in the H-mode [29]. The discharge configuration was almost identical to the one shown in Figure 1. Fantz et al. showed that approximately 10% of the available discharge power is transformed into radiation in the VUV range. This radiation causes bond scission in the surface film of a thickness of the order of a penetration depth for VUV photons. The penetration depth depends on the wavelength (i.e., photon energy) but is definitely larger than the escape depth of photoelectrons. By considering this fact, one can assume a rather homogenous treatment of the surface film with the VUV. The bond scission enables further reactions, including the interaction with H atoms. The H atoms attack the dangling bonds as already reported by Badey et al. [19]. Furthermore, they interact with F atoms forming HF molecules, which are desorbed upon vacuum conditions and pumped away. The combination of bond scission caused by absorption of VUV radiation and chemical interaction with H atoms should, therefore, ensure an F-free surface. Such an effect cannot be confirmed from XPS measurements because of the final escape depth of photoelectrons. It will be shown later in this paper that the best technique to prove the F-free surface is ToF-SIMS.

After prolonged treatment of PTFE samples in the H-mode, the F/C ratio does not remain constant but increases slowly with increasing treatment time. Such an increase may be explained by a different thickness of the F-depleted surface film rather than by incomplete defluorination. This effect will be explained later by using angular-resolved XPS characterization (AR-XPS).

When plasma is in the E-mode, the minimum in the F/C ratio is not observed, which may be a consequence of the fact that such plasma is not a significant source of VUV radiation. The luminosity of plasma in the E-mode is typically 3–4 orders of magnitude lower than in the H-mode at this pressure, i.e., 25 Pa. The difference in plasma luminosities between the E- and H-modes normally increases with increasing pressure, as shown by Fantz et al. [29]. The F/C ratio, however, does not deviate for orders of magnitude but is comparable for long treatment times. The comparison of the two curves in Figure 6, therefore, indicate that the intensive VUV radiation only accelerates defluorination of the surface film. A rather low F/C ratio observed after the treatment in the E-mode should be because of other mechanisms. It was already mentioned that H atoms attack the polymer surface and dangling bonds, causing the formation of the volatile HF molecule. Badey et al. [19], as well as Yamada et al. [20], investigated the evolution of the F/C ratio in the flowing afterglow where VUV radiation is negligible, but the density of H atoms is still significant. They found moderate F/C ratios of approximately 0.8. Somehow, lower F/C ratio was also reported by König et al. [23]. Unlike VUV radiation, the H atoms do not penetrate into the solid polymer; therefore, the chemical modification should be limited to a thinner film in the E-mode as compared to the H-mode. Such a difference in the thickness of the well-affected film can explain the fact that the achievable F/C ratio in the E-mode is lower than in the H-mode. A confirmation for the statement about the F-free surface for the H-mode is provided in Figure 7, which shows the F/C ratios as deduced from AR-XPS. The lower curve is for the sample treated for 1 s in the H-mode, whereas the upper for the sample treated for the same time in the E-mode. The F/C ratio in the H-mode gradually increases with increasing take-off angle θ (TOA). Detection depth (d) is given by the following relation, $d = 3\lambda \cdot \sin(\theta)$, where λ is the inelastic mean free path of photoelectrons. The detection depth thus increases with increasing TOA. The gradual increase in the F/C ratio is explained by the formation of the almost F-free surface as well as a subsurface layer with a thickness close to the detection depth of XPS. Extrapolation of the lower curve to the TOA $\theta = 0°$ reveals the F/C ratio is practically zero on the surface. Unfortunately, measurements at extremely low TOA are not feasible.

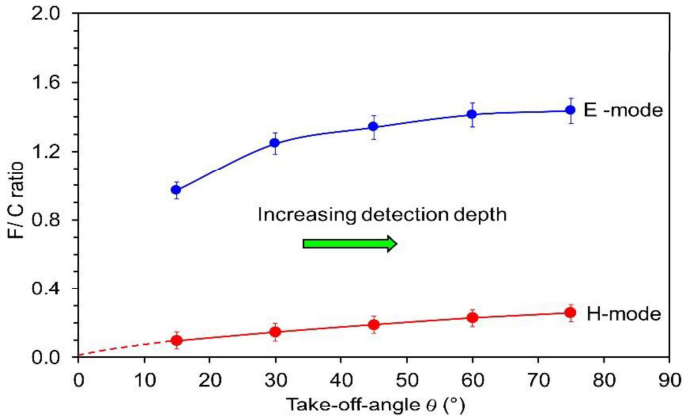

Figure 7. Variation of the AR-XPS F/C ratio versus the photoelectron take-off angle for two different powers and the same pressures of 25 Pa and treatment times of 1 s.

As shown before in Figure 6, a defluorination is incomplete when plasma is in the E-mode for 1 s. The upper curve in Figure 7 confirms this. However, it is interesting that the F/C ratio in Figure 7 increases by a factor of approximately 1.5 when the TOA is increased from $\theta = 15$ to 75°. Obviously, the surface film contains much less fluorine than the subsurface one, and there is a significant gradient in F concentration. Any extrapolation of the curve towards the TOA $\theta = 0°$ would be speculation; therefore, it is not shown in Figure 7.

Figures 6 and 7 indicate large differences in surface chemistry, depending on the type of discharge. The differences can be further elaborated by performing measurements at a fixed treatment time and

pressure, but different RF powers. The result is plotted in Figure 8. Here, the F/C ratio reaches the minimum at 400 W. At larger powers, the F/C is somehow slightly larger. The behaviour of the curve for powers between 400 and 900 W is similar to the lower curve in Figure 6. In both cases, the fluence of VUV radiation increases with increasing value at the abscissa. More interesting is the behaviour at lower powers. One can observe a gradual and rather linear decrease of the F/C ratio with increasing power. The discharge power of 300 W results in the F/C ratio of approximately 0.5, similar to what is observed in Figure 6 for the upper curve after prolonged plasma treatment. Comparison of Figures 6 and 8, therefore, indicates that the key parameter governing the surface chemistry is the fluence of reactive species and/or VUV radiation rather than discharge power or treatment times. Nonetheless, it is important that the surface finish in the E-mode as deduced from XPS is different to that in the H-mode. In addition to Figure 8, see also supplementary Figures S3 and S4 showing individual survey spectra and elemental composition versus the discharge power.

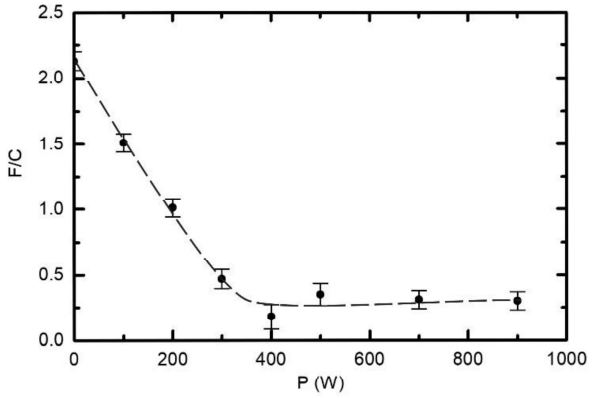

Figure 8. Variation of the F/C ratio versus the discharge power. Treatment time and H_2 pressure were constant at 1 s and 25 Pa, respectively.

The variation of the F/C ratio versus the discharge power (Figure 8) is different to the behaviour of WCA (Figure 4). Comparison of Figures 4 and 8 indicates that even an incomplete defluorination causes the drop of the water contact angle to values typical for polyolefins.

Figure 9 reveals the high-resolution C1s spectra for the untreated sample and samples treated in the H-mode for 1 and 12 s. There is a huge difference between the untreated and treated samples. The untreated sample contains only carbon bonded in CF_2 groups. The C1s peak, therefore, appears at a binding energy of approximately 292 eV. There is also a small peak at approximately 285 eV, which corresponds to surface impurities. The treated samples exhibit the opposite behaviour—the major peak is at about 285 eV, whereas some features also persist at higher binding energies up to approximately 294 eV. Taking into account Figure 7, and the discussion thereafter, it can be concluded that the features correspond to degraded PTFE-like film, whereas the main peak at 285 eV corresponds to F-depleted surface film. Therefore, we can conclude that the surface film of samples treated in H_2 plasma in the H-mode contains olefin-like carbon. It is interesting that the intensity in the range of binding energies from about 287 and 294 eV is slightly larger for the case of 12 s than for 1s of plasma treatment. The reasons for this have already been elaborated when explaining the behaviour of the lower curve in Figures 6 and 7.

By considering the upper discussion, the C1s peak of samples treated in the E-mode should differ from those in the H-mode. Figure 10 represents solid proof of the evolution of the surface chemistry upon treatment of PTFE samples in the E- and H-modes. The behaviour of the two curves at 400 and 800 W was already explained. Interesting, and sound with the previous discussion, is the behaviour of the curves acquired after the treatment at discharge powers of 100 and 200 W. In both cases, plasma was in the E-mode. The curve at 100 W indicates that the rather intact PTFE still persists, but a fraction is

already modified enough to form various carbon chemistries including intermediate ones, as already reported by Badey et al. [19]. A well-expressed peak is observed at approximately 292 eV, as well as a broad feature between 292 and 285 eV. This indicates that CH groups have already appeared on the surface, but the thin surface film also contains other groups with binding energies between 292 and 285 eV. The spectrum corresponding to treatment at 200 W shows a gradual deviation from the untreated PTFE to a surface film of polyolefin-like structure. As discussed above and in keeping with the observations in Figures 6 and 7, the thickness of the F-free surface film in the E-mode is much lower than the escape depth of photoelectrons, so the significant contribution of photoelectrons with binding energies of 292 eV still persists. In between the two well-defined peaks at 292 and 285 eV, there is a rich structure, which could be deconvoluted almost arbitrarily taking into account a variety of functional groups as well as peculiarities of XPS regarding the interpretation of F-containing functional groups [30]. For this reason, we made no attempt to deconvolute C1s peaks shown in Figure 10.

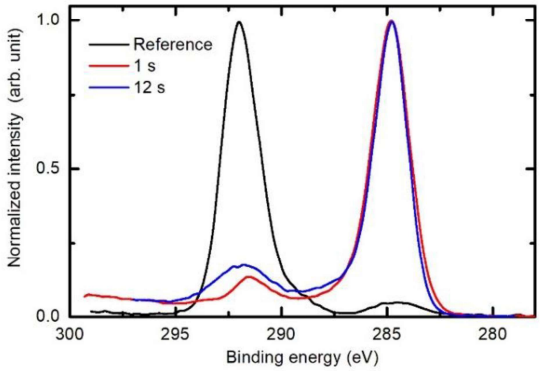

Figure 9. Comparison of XPS high-resolution C1s spectra of the untreated PTFE, and PTFE exposed to H_2 plasma for 1 and 12 s. The discharge power and the pressure were constant at 400 W and 25 Pa, respectively.

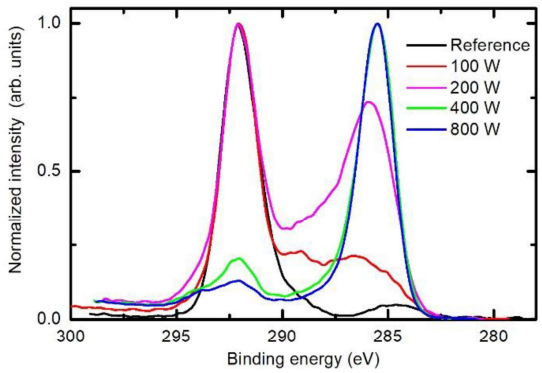

Figure 10. Comparison of the selected XPS high-resolution C1s spectra of the PTFE samples treated for various powers. The treatment time and the pressure were constant at 1 s and 25 Pa, respectively.

3.3. Chemical Modifications as Determined by Time-of-Flight Secondary Ion Mass Spectrometry (ToF-SIMS)

Deconvolution of C1s XPS spectra of fluorinated samples definitely represents a scientific challenge. Therefore, it is useful to characterize selected samples also with an alternative technique, such as ToF-SIMS. The evolution of the ToF-SIMS spectral features was investigated systematically for the treatment time of 1 s and hydrogen pressure of 25 Pa. We varied the discharge power to obtain further insight into the surface chemistry. Some examples of the selected positive in negative ion spectra of the samples are shown in Supplementary Figures S5–S8. Figure 11 shows the selective negative ion

intensities and Figure 12 positive ion intensities. One can observe a gradual decreasing of the F^{2-} intensity versus the discharge power. This behaviour indicates depletion of the surface film as probed by ToF-SIMS. It should be noted that the surface sensitivity of ToF-SIMS is superior in comparison to XPS. Simultaneous to decreasing of the F^{2-} intensity, a number of fluorine-free ions appear in the ToF-SIMS negative ion spectra. All of them keep increasing with increasing discharge power up to the power of 400 W. Thereafter, the intensity of fluorine-free ions in ToF-SIMS spectra remains constant. This observation is in keeping with results presented in Figure 11, where exactly the same effect was observed. Unfortunately, ToF-SIMS does not allow for reliable quantification of the measured spectra. The drop of the intensity of F^{2-} for more than a factor of 50 indicates practically F-free surface.

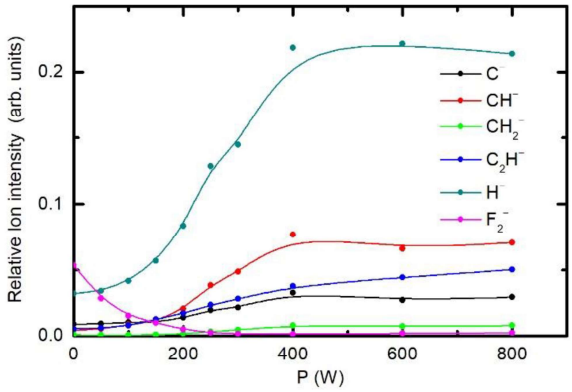

Figure 11. Variation of time-of-flight secondary ion mass spectrometry (ToF-SIMS) intensities of selected negative ions. The pressure was 25 Pa and treatment time 1 s.

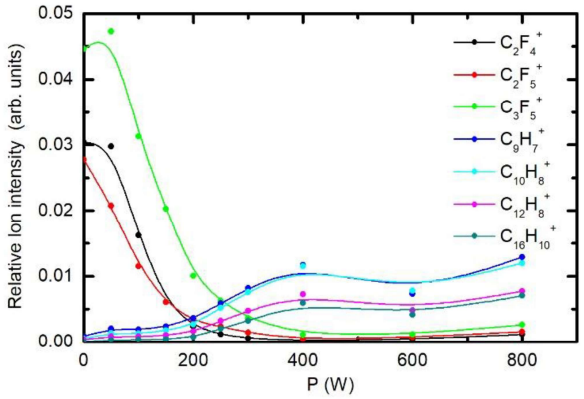

Figure 12. Variation of ToF-SIMS intensities of selected positive ions. The pressure was 25 Pa and treatment time 1 s.

Figure 12 shows the behaviour of positive ion fragments. The intensities of F-containing ions decreases monotonously with increasing discharge power, and the minimum is observed at the power of 400 W. By contrast, the ions containing hydrogen increase gradually up to the power of 400 W and remain fairly intact thereafter. The ToF-SIMS results are, therefore, in keeping with those obtained by XPS.

4. Conclusions

Systematic characterization of PTFE was performed to reveal the kinetics of fluorine depletion of the surface film of this polymer upon treatment with hydrogen plasma at various conditions. Unlike previous authors, we concentrated on rather short treatment times of the order of a second.

Such short times are attractive for any application of gaseous plasma technology for surface processing of products made from fluorinated polymers. A broad range of parameters was found useful for the depletion of the surface film. Nominal discharge powers of the RF generator of as low as 100 W are capable of depletion of the surface film within several seconds of plasma treatment. The intensity of surface chemical reactions increases with increasing discharge power, and the reactions become almost instant once the discharge is in the H-mode. A significant difference in the surface finish between the discharge modes was observed. In the case the discharge is in the E-mode, the F concentration decreases monotonously with increasing treatment time, and the minimal achievable F/C ratio is just above 0.5. By contrast, when the plasma is in the H-mode, a well-defined minimum in the F concentration occurs at rather short treatment times. The minimal F/C ratio as deduced from the XPS spectra acquired at standard take-off angle is about 0.2. The surface layer of the polymer, however, is almost free from fluorine, which is proved by ARXPS as well as by the behaviour of specific ion fragments acquired by ToF-SIMS. Experiments performed at different discharge conditions qualitatively indicate that the key parameter governing the surface finish is the fluence of reactive plasma species. Unfortunately, our experimental set-up did not allow for reliable determination of the radiation in the VUV range. The surface finish versus the fluence of VUV radiation upon treatment of fluorinated polymers with hydrogen plasma, therefore, remains a scientific challenge.

Supplementary Materials: The following are available online at http://www.mdpi.com/2073-4360/12/12/2855/s1, Figure S1: XPS survey spectra of PTFE treated in hydrogen plasma for various treatment times. Hydrogen pressure was constant at 25 Pa and the discharge power was: (a) 100 W and (b) 400 W., Figure S2: XPS surface composition of PTFE treated in hydrogen plasma at various treatment times: (a) for discharge power of 100 W and (b) for discharge power of 400 W. Hydrogen pressure was 25 Pa., Figure S3: XPS survey spectra of PTFE treated in hydrogen plasma at various forward powers. Hydrogen pressure was constant at 25 Pa and treatment time was 1 s., Figure S4: XPS surface composition of PTFE treated in hydrogen plasma at various forward powers. Hydrogen pressure was 25 Pa and treatment time was 1 s., Figure S5: ToF-SIMS spectra of the untreated PTFE: (a) positive ion spectra and (b) negative ion spectra. Figure S6: ToF-SIMS spectra of the PTFE treated in H_2 plasma at the power of 150 W: (a) positive ion spectra and (b) negative ion spectra. The pressure was 25 Pa and treatment time was 1 s., Figure S7: ToF-SIMS spectra of the PTFE treated in H_2 plasma at the power of 400 W: (a) positive ion spectra and (b) negative ion spectra. The pressure was 25 Pa and treatment time was 1 s., Figure S8: ToF-SIMS spectra of the PTFE treated in H_2 plasma at the power of 800 W: (a) positive ion spectra and (b) negative ion spectra. The pressure was 25 Pa and treatment time was 1 s.

Author Contributions: Conceptualization, A.V. and R.Z.; methodology, A.V. and R.Z.; validation, A.V., D.L. and R.Z.; formal analysis, D.L., A.V., J.E. and M.G.; investigation, D.L., A.V. and R.Z.; resources, G.P.; data curation, D.L., A.V., J.E. and J.K.; writing—original draft preparation, A.V.; writing—review and editing, M.M.; supervision, R.Z. and A.V.; project administration, M.K. and G.P.; funding acquisition, M.K. and K.S.-K. All authors have read and agreed to the published version of the manuscript.

Funding: The authors acknowledge the financial support from the Slovenian Research Agency—project No. J2-1728 (Initial stages in surface functionalization of polymers by plasma radicals) and P2-0082 (Thin-film structures and plasma surface engineering).

Conflicts of Interest: The authors declare no conflict of interest. The funders had no role in the design of the study; in the collection, analyses, or interpretation of data; in the writing of the manuscript, or in the decision to publish the results.

References

1. Améduri, B. The promising future of fluoropolymers. *Macromol. Chem. Phys.* **2020**, *221*, 1900573. [CrossRef]
2. McKeen, L.W. Chapter 11—Fluoropolymers. In *Fatigue and Tribological Properties of Plastics and Elastomers*, 2nd ed.; McKeen, L.W., Ed.; William Andrew Publishing: Oxford, UK, 2010; pp. 249–264. [CrossRef]
3. Ohkubo, Y.; Shibahara, M.; Nagatani, A.; Honda, K.; Endo, K.; Yamamura, K. Comparison between adhesion properties of adhesive bonding and adhesive-free adhesion for heat-assisted plasma-treated polytetrafluoroethylene (PTFE). *J. Adhes.* **2020**, *96*, 776–796. [CrossRef]
4. Badey, J.P.; Espuche, E.; Jugnet, Y.; Chabert, B.; Duct, T.M. Influence of chemical and plasma treatments on the adhesive properties of PTFE with an epoxy resin. *Int. J. Adhes. Adhes.* **1996**, *16*, 173–178. [CrossRef]

5. Lee, S.W.; Hong, J.W.; Wye, M.Y.; Kim, J.H.; Kang, H.J.; Lee, Y.S. Surface modification and adhesion improvement of PTFE film by ion beam irradiation. *Nucl. Instrum. Methods Phys. Res. B* **2004**, *219*, 963–967. [CrossRef]
6. Baumgärtner, K.M.; Schneider, J.; Schulz, A.; Feichtinger, J.; Walker, M. Short-time plasma pre-treatment of polytetrafluoroethylene for improved adhesion. *Surf. Coat. Technol.* **2001**, *142*, 501–506. [CrossRef]
7. Koh, S.-K.; Park, S.-C.; Kim, S.-R.; Choi, W.-K.; Jung, H.-J.; Pae, K.D. Surface modification of polytetrafluoroethylene by Ar+ irradiation for improved adhesion to other materials. *J. Appl. Polym. Sci.* **1997**, *64*, 1913–1921. [CrossRef]
8. Hopp, B.; Kresz, N.; Kokavecz, J.; Smausz, T.; Schieferdecker, H.; Döring, A.; Marti, O.; Bor, Z. Adhesive and morphological characteristics of surface chemically modified polytetrafluoroethylene films. *Appl. Surf. Sci.* **2004**, *221*, 437–443. [CrossRef]
9. Ohkubo, Y.; Ishihara, K.; Shibahara, M.; Nagatani, A.; Honda, K.; Endo, K.; Yamamura, K. Drastic improvement in adhesion property of polytetrafluoroethylene (PTFE) via heat-assisted plasma treatment using a heater. *Sci. Rep.* **2017**, *7*, 9476. [CrossRef]
10. Gilman, A.; Piskarev, M.; Yablokov, M.; Kechek'Yan, A.; Kuznetsov, A.A. Adhesive properties of PTFE modified by DC discharge. *J. Phys. Conf. Ser.* **2014**, *516*, 012012. [CrossRef]
11. Marchesi, J.T.; Ha, K.; Garton, A.; Swei, G.S.; Kristal, K.W. Adhesion to sodium naphthalenide treated fluoropolymers. Part II. Effects of treatment conditions and fluoropolymer structure. *J. Adhes.* **1991**, *36*, 55–69. [CrossRef]
12. Kavan, L.; Dousek, F.P.; Janda, P.; Weber, J. Carbonization of highly oriented poly(tetrafluoroethylene). *Chem. Mater.* **1999**, *11*, 329–335. [CrossRef]
13. Ha, K.; McClain, S.; Suib, S.L.; Garton, A. Adhesion to sodium naphthalenide treated fluoropolymers Part I-Analytical methodology. *J. Adhes.* **1991**, *33*, 169–184. [CrossRef]
14. Clark, D.T.; Hutton, D.R. Surface modification by plasma techniques. 1. The interactions of a hydrogen plasma with fluoropolymer surfaces. *J. Polym. Sci. Part A Polym. Chem.* **1987**, *25*, 2643–2664. [CrossRef]
15. Wang, L.; Angert, N.; Trautmann, C.; Vetter, J. Effect of ion irradiation and heat treatment on adhesion in the Cu / Teflon system. *J. Adhes. Sci. Technol.* **1995**, *9*, 1523–1529. [CrossRef]
16. Takata, R.; Iwao, T.; Yumoto, M. Surface modification of PTFE using low-energy nitrogen ion irradiation: Improvement in adhesive strength on modification of deep modifying layer. *Electron. Commun. Jpn.* **2016**, *99*, 93–99. [CrossRef]
17. Vesel, A.; Mozetic, M. New developments in surface functionalization of polymers using controlled plasma treatments. *J. Phys. D Appl. Phys.* **2017**, *50*, 293001. [CrossRef]
18. Primc, G. Recent advances in surface activation of polytetrafluoroethylene (PTFE) by gaseous plasma treatments. *Polymers* **2020**, *12*, 2295. [CrossRef]
19. Badey, J.P.; Espuche, E.; Sage, D.; Chabert, B.; Jugnet, Y.; Batier, C.; Duc, T.M. A comparative study of the effects of ammonia and hydrogen plasma downstream treatment on the surface modification of polytetrafluoroethylene. *Polymer* **1996**, *37*, 1377–1386. [CrossRef]
20. Yamada, Y.; Yamada, T.; Tasaka, S.; Inagaki, N. Surface modification of poly(tetrafluoroethylene) by remote hydrogen plasma. *Macromolecules* **1996**, *29*, 4331–4339. [CrossRef]
21. Inagaki, N.; Tasaka, S.; Umehara, T. Effects of surface modification by remote hydrogen plasma on adhesion in poly(tetrafluoroethylene)/copper composites. *J. Appl. Polym. Sci.* **1999**, *71*, 2191–2200. [CrossRef]
22. Inagaki, N.; Tasaka, S.; Narushima, K.; Teranishi, K. Surface modification of poly(tetrafluoroethylene) with pulsed hydrogen plasma. *J. Appl. Polym. Sci.* **2002**, *83*, 340–348. [CrossRef]
23. König, U.; Nitschke, M.; Pilz, M.; Simon, F.; Arnhold, C.; Werner, C. Stability and ageing of plasma treated poly(tetrafluoroethylene) surfaces. *Colloid. Surf. B* **2002**, *25*, 313–324. [CrossRef]
24. Tanaka, K.; Takahashi, K.; Kogoma, M. Defluorination of polytetrafluoroethylene by combination of atmospheric pressure glow plasma treatment and chemical transport method. In Proceedings of the 20th International Symposium on Plasma Chemistry, Philadelphia, PA, USA, 24–29 July 2011.
25. Hunke, H.; Soin, N.; Shah, T.; Kramer, E.; Pascual, A.; Karuna, M.; Siores, E. Low-pressure H_2, NH_3 microwave plasma treatment of polytetrafluoroethylene (PTFE) powders: Chemical, thermal and wettability analysis. *Materials* **2015**, *8*, 2258–2275. [CrossRef]

26. Zanini, S.; Barni, R.; Pergola, R.D.; Riccardi, C. Modification of the PTFE wettability by oxygen plasma treatments: Influence of the operating parameters and investigation of the ageing behaviour. *J. Phys. D Appl. Phys.* **2014**, *47*, 325202. [CrossRef]
27. Abourayana, H.M.; Dowling, D.P. Plasma Processing for Tailoring the Surface Properties of Polymers. In *Surface Energy*; Aliofkhazraei, M., Ed.; Intech Open: Rijeka, Croatia, 2015.
28. Wilken, R.; Holländer, A.; Behnisch, J. Quantitative comparison between vacuum-ultraviolet irradiation and remote hydrogen plasma treatment of hydrocarbon polymers. *Plasmas Polym.* **1998**, *3*, 165–175. [CrossRef]
29. Fantz, U.; Briefi, S.; Rauner, D.; Wünderlich, D. Quantification of the VUV radiation in low pressure hydrogen and nitrogen plasmas. *Plasma Sources Sci. Technol.* **2016**, *25*, 045006. [CrossRef]
30. Ferraria, A.M.; Lopes da Silva, J.D.; Botelho do Rego, A.M. XPS studies of directly fluorinated HDPE: Problems and solutions. *Polymer* **2003**, *44*, 7241–7249. [CrossRef]

Chapter 3

Effect of VUV Radiation and Reactive Hydrogen Atoms on Depletion of Fluorine from the Polytetrafluoroethylene Surface

This chapter reveals the interactions of individual species of hydrogen plasma with the surface of PTFE during the pre-functionalisation step prior to functionalisation with O-atoms. Understanding the effects of species formed in hydrogen plasma on the functionalisation of the PTFE surface is of great importance for the potential upscaling of the experimental process of PTFE pre-functionalisation with hydrogen plasma to an industrial scale.

The same experimental plasma system was used as for the experiments presented in chapter 2. Initially, the emitted spectra of H-plasma were measured by optical emission spectroscopy (OES). H_α, H_β, H_γ, H_δ lines and Fulcher molecular band were monitored along the discharge tube to obtain an axial radiation profile. The wavelengths were chosen because they are indicative of the VUV radiation distinctive for the Lyman series (transition to the ground state). Lyman series are typically an order of magnitude larger than the Balmer series (H_α, H_β, H_γ, H_δ), and are known for their ability to break C—F bonds. We measured the Balmer series because our OES instrument was not suitable for the measurement of VUV wavelengths. The axial profile of hydrogen neutral atom density was measured using a cobalt catalytic probe.

The PTFE surface was exposed either directly to glowing hydrogen plasma, either to only VUV and UV radiation, to only UV radiation, or to VUV radiation and neutral hydrogen atoms. PTFE samples were treated in the glow, early afterglow, and late afterglow plasmas. During exposure of the PTFE surface to only VUV radiation, samples were placed into a borosilicate glass enclosure covered with a MgF_2 (good transmittance above 115 nm) window. During exposure of the PTFE surface to VUV radiation and neutral hydrogen atoms simultaneously, a similar borosilicate glass enclosure was used as for the exposure of PTFE to only VUV radiation. The difference was that there was a narrow slit in the wall of the enclosure to enable the diffusion of H-atoms and thus their interaction with the surface of the sample. A 10 mm opening was made on the side of the glass chamber to allow hydrogen atoms to enter the space inside the glass chamber by diffusion – in this case, the sample was exposed to atoms and radiation, but not to ions (plasma generation was not possible due to the small size of the chamber).

The elemental compositions within the surface layers of untreated and treated PTFE samples were measured by X-ray photoelectron spectroscopy (XPS) by Prof. Dr. Alenka Vesel. The discharge power for sustaining hydrogen plasma was 500 W and the hydrogen pressure 25 Pa. The results showed that the intensities of typical spectral features arising from hydrogen plasma are about three orders of magnitude smaller in the early afterglow than in the glow region, and the radiation intensity is negligible in late afterglow. Neutral H-atom densities were about 3×10^{21} in the glowing plasma region, about 1×10^{21} m^{-3} in the early afterglow and about 4×10^{18} m^{-3} in late afterglow.

The F/C ratio of untreated PTFE was 2.2. The PTFE surface that was directly exposed to glowing plasma was efficiently defluorinated as the F/C ratio was decreased to about 0.4 after 1 s, but after prolonged treatment, it increased to about 1. The sample exposed to only VUV radiation was defluorinated, but the defluorination rate was somewhat slower as after 1 s, the F/C ratio decreased to approximately 0.9 and after 6 s to approximately 0.5. The F/C ratio of the surface exposed to VUV radiation and H-atoms also decreased to 0.5, but the decrease was slightly faster (after 3 s of treatment). In the case that MgF_2 glass was replaced with quartz glass, when using a close configuration in the glow region, the F/C ratio of the PTFE surface decreased to only 1.5, which is much higher than the 0.8, achieved with the MgF_2 window. In the early afterglow the F/C ratio of the directly exposed sample decreased to 0.6 after 5 s, the sample exposed to only VUV radiation obtained an F/C of 1.9, and the sample exposed to H-atoms and VUV radiation reached the F/C ratio of 2.1. In the late afterglow, the F/C ratio of the directly exposed sample was 2.2.

The PTFE sample enclosed in the holder covered with a MgF_2 window and its treatment in hydrogen plasma are shown in the photographs in Figure 6.

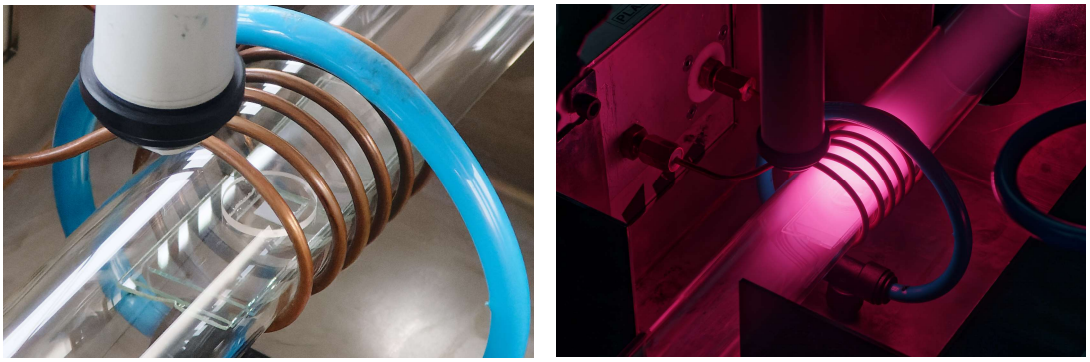

Figure 6: PTFE sample enclosed in the holder covered with a MgF_2 window inserted into the plasma system (left) and during H-mode hydrogen plasma treatment (right).

The minimum F/C ratio resulting from direct exposure of the PTFE surface to plasma and further increase of the F/C ratio with treatment time was explained by thermal effects causing desorption of light C-rich fragments. The efficiency of VUV radiation for PTFE defluorination (breakage of C−F bonds causing the formation of dangling bonds) was proved. The slightly faster defluorination of the PTFE surface with the combination of VUV radiation and H-atoms was explained by their synergistic effects. It was hypothesised that VUV radiation breaks C−F bonds and causes the formation of dangling bonds that are terminated by the bonding of H-atoms, and H-atoms also capture the released F-atoms by the formation of HF molecules. If the sample is exposed only to VUV, F-atoms might be bound back onto the dangling bonds. It was also found that UV radiation from Lyman

B – X band and continuum (transition a to b) of neutral hydrogen molecules above 155 nm has sufficient energy to break C−F bonds. However, the defluorination efficiency is lower than that of VUV radiation because of the higher penetration depth (penetration depth decreases with shorter wavelengths). It was found that the combination of weak radiation and high concentrations of H-atoms also causes F depletion as the F/C ratio decreased to 0.6 in the early afterglow while the PTFE surface was directly exposed to plasma. It was found that the H-atoms in such a case are of great importance because both radiation and the amount of charged particles are much lower in early afterglow than in glow plasma. This was further confirmed by the fact that the sample enclosed within the glass encloser covered with the MgF_2 window treated in the early afterglow for 5 s exhibited the F/C ratio of only 1.9. The F/C ratio of 2.1 achieved with the treatment of the PTFE surface within early afterglow in the open glass encloser covered with the MgF_2 window could be explained by the fact that H-atom concentration is greatly reduced due to the recombination process at the walls of the enclosure, while diffusion delivering new H-atoms within the enclosure through the narrow slit, is a slow process. However, it was found that only H-atoms in the late afterglow, where there was no significant radiation and where the density of ions was negligible, did not cause defluorination on the PTFE surface within the 5 s treatment time interval.

Applied Surface Science 533 (2020) 147356

Contents lists available at ScienceDirect

Applied Surface Science

journal homepage: www.elsevier.com/locate/apsusc

Effect of VUV radiation and reactive hydrogen atoms on depletion of fluorine from polytetrafluoroethylene surface

Dane Lojen[a,b], Rok Zaplotnik[a], Gregor Primc[a], Miran Mozetič[a], Alenka Vesel[a,*]

[a] Jozef Stefan Institute, Jamova cesta 39, 1000 Ljubljana, Slovenia
[b] Jozef Stefan International Postgraduate School, Jamova cesta 39, 1000 Ljubljana, Slovenia

ARTICLE INFO

Keywords:
polytetrafluoroethylene (PTFE)
Surface modification
VUV radiation
Hydrogen plasma
Optical windows
Plasma-surface interactions

ABSTRACT

Modification of polytetrafluoroethylene (PTFE) surface upon treatment with reactive species from hydrogen plasma (ions, neutral atoms, and UV/VUV) as well as synergistic effects are presented and explained. PTFE samples were either directly exposed to hydrogen plasma or separately to UV/VUV radiation or atomic hydrogen, and the resulting evolution of the surface composition was determined by X-ray photoelectron spectroscopy. High-density plasma was created by an inductively-coupled radiofrequency discharge in the H-mode. Samples placed in specially designed holders were covered with various optical windows (magnesium fluoride, quartz glass, or borosilicate glass), to allow for separate treatments with either VUV, UV or visible radiation. Rapid fluorine depletion was observed either at a direct exposure to plasma or to VUV; however, the best results were observed at a combined treatment with VUV/UV and atomic hydrogen. For direct treatment, a minimum in the F/C ratio was observed at the shortest time of 1 s. The F/C dropped from 2.2 to 0.4, whereas at longer times it increased to 1. For treatment with UV/VUV and for the combined treatment with UV/VUV and atoms, the F/C decreased with treatment time and stabilized at 0.6 and 0.4, respectively. Exposure to the afterglow did not result in significant modification.

1. Introduction

Plasmas are often used for improving surface wettability of polymeric materials [1]. Reactive species formed in plasma such as ions, neutral atoms, metastables, electrons, and UV/VUV radiation play an important role in polymer surface modification [2–4]. By choosing a different configuration of the discharge system and different discharge parameters, it is possible to manipulate the type and density of plasma radicals and ions to which polymer is exposed, and consequently, influence the degree of a polymer surface modification. In some studies, it was found that a single type of plasma species (often atoms in the ground state) already causes modification of a polymer surface, but many authors agree that synergistic effects are often much more important [5–8].

The wettability of most polymers is increased by a brief treatment with oxygen plasma [9]. Although the exact mechanisms on the atomic scale are still unclear, it is generally accepted that the reactive oxygen plasma species interact chemically with the polymer surface causing functionalization with polar functional groups [10]. Such a treatment, however, is rather insufficient in the case of fluorinated polymers because the treatment with oxygen plasma often leads to etching rather than functionalization [11–13].

Nevertheless, it has been shown by several authors that the PTFE surface layer can be modified significantly using plasmas containing hydrogen that causes depletion of fluorine from the surface of PTFE [14–16]. In a previous paper, we have treated PTFE with H_2S plasma and found significant depletion of fluorine from the polymer surface, which was explained by photolysis, which appeared as a consequence of irradiation with VUV photons and simultaneous interaction with hydrogen atoms [17]. As shown by Skuratet et al., VUV photolysis of PTFE can cause the formation of free radicals [18]:

$$-CF_2-CF_2-CF_2-CF_2-+h\nu \rightarrow -CF_2-\dot{C}F-CF_2-CF_2-+\dot{F} \quad (1)$$

$$-CF_2-CF_2-CF_2-CF_2-+h\nu \rightarrow -CF_2-CF_2\bullet + \bullet CF_2-CF_2- \quad (2)$$

These free radicals can react with hydrogen atoms from plasma. However, it is still unclear whether solely individual species such as only VUV or only hydrogen atoms alone can cause significant surface modification, or whether a necessary condition to cause surface depletion of fluorine is a synergy between VUV and hydrogen atoms.

Tajima et al. [19] investigated the crosslinking of polyethylene (PE)

* Corresponding author.
E-mail address: alenka.vesel@guest.arnes.si (A. Vesel).

https://doi.org/10.1016/j.apsusc.2020.147356
Received 21 February 2020; Received in revised form 22 July 2020; Accepted 23 July 2020
Available online 01 August 2020

surface exposed to ions, neutrals, and photons from inductively coupled Ar plasma. To de-convolute the effects of the various plasma species, Tajima used various optical windows with different transmissivities such as LiF, CaF_2, Al_2O_3, and SiO_2. The extent of surface crosslinking was determined by measuring the coefficient of friction. They found that surface modification occurred primarily because of the simultaneous effects of uncharged particles and VUV radiation, and secondarily due to ions and VUV radiation. Especially the VUV radiation at 137.7 nm was found to be important for chain-induced crosslinking.

Cho et al. investigated the modification of polyethylene terephthalate (PET) films exposed to the Ar–O_2 mixture [20] and to pure Ar plasma [3]. For both types of plasma, PET samples were either directly exposed to plasma or were covered with MgF_2 or quartz optical windows, transmitting only UV/VUV or UV radiation, respectively. They found that UV/VUV photons did not cause any changes in the surface roughness. Moreover, in the case of pure Ar plasma, UV/VUV photoirradiation did not cause any significant degradation of oxygen functionalities on the PET surface. However, degradation of C—O and O═C—O and consequential increase in C═O was observed for the sample exposed directly to Ar plasma. In the case of the Ar-O_2 mixture, they found the formation of the oxygen functionalities on the PET surface. Because of the elimination of ion etching, the formation of oxygen functionalities was enhanced for the sample covered with both optical windows in comparison to the sample that was directly exposed to Ar-O_2 plasma.

The same group also investigated the modification of PET polymer versus the dose of VUV photons emitted from O_2 or H_2 plasma [21]. They found that VUV irradiation caused the cleavage of C—O and O═C—O groups. Their concentration decreased and a carbonized layer that absorbs VUV photons was formed; therefore, reactions induced by VUV photons were limited to only several nanometers below the surface. They also found that VUV irradiation had only a minor effect on the surface roughness because only a slight increase in surface roughness was observed, and the surface remained smooth even after prolonged VUV irradiation. VUV irradiation also caused a decrease in the PET film thickness as a consequence of bond cleavage and formation of volatile products that desorb from the surface upon vacuum conditions [21]. They also proposed a model of modification by VUV photons and atoms from oxygen and hydrogen plasma. After the formation of dangling bonds during photolysis induced by VUV photons acting on C—O and O═C—O groups, hydrogen atoms from H_2 plasma terminated the dangling bonds. Whereas in the case of oxygen plasma, the dangling bonds acted as reaction sites for further reaction with oxygen atoms (either in the ground or metastable states) and molecules leading to an increase of the amount of C—O and O═C—O groups [21].

To further enlighten the role of various species and their synergy, we have investigated the mechanisms of PTFE modification in H_2 plasma and the role of various plasma species, especially the role of UV/VUV radiation and neutral hydrogen atoms.

2. Experimental

2.1. Plasma treatment

PTFE foils with a thickness of 0.5 mm were purchased from Goodfellow Ltd. The foils were cut to rectangular pieces with a size 5 × 5 mm^2 and placed to different positions in a plasma system shown in Fig. 1.

The discharge tube made from borosilicate glass was pumped with a rotary pump of a nominal pumping speed of 80 $m^3\ h^{-1}$, and the final pressure was approximately 1 Pa. Experiments were performed at the hydrogen pressure of 25 Pa (flow rate 85 sccm). Plasma was created using an RF discharge inside the discharge tube with a length of 80 cm and a diameter of 4 cm. A coil with six turns was mounted to the tube, as shown in Fig. 1. The coil was connected to an RF generator via a matching network. The RF generator operated at a frequency of 13.56 MHz, and its forward power was set to 500 W. At these conditions, highly luminous plasma was limited inside the coil, and discharge was sustained in the almost pure inductive mode (H-mode). The dissociation fraction was of the order of 10% and the radiation flux 10^{16} $cm^{-2}\ s^{-1}$. The power density was 25 W cm^{-3}.

PTFE samples were placed at three different positions: (1) in the middle of the coil, where the sample is subjected to various species including atoms, ions, and UV/VUV radiation; (2) to the early afterglow 2 cm away from the coils left edge, where the contribution of ions is negligible; and (3) in the late afterglow 55 cm from the coils left edge, where the sample is exposed to hydrogen atoms only. All three positions are marked in Fig. 1. Furthermore, for the cases of samples being placed in the glow and early afterglow regions, the samples were mounted onto holders with or without an additional top shielding using MgF_2, quartz or borosilicate optical windows to either transmit a specific type of radiation or eliminate the UV/VUV radiation, ions and/or atoms. When using a top-shield window, two configurations were applied; hereinafter called open or closed configuration. In a closed configuration, the sample was placed in a modular borosilicate glass chamber (holder) and covered by one of the above mentioned top-shield windows. In such a configuration, the contributions of atoms and ions were eliminated, and only photons with a particular wavelength were transmitted. Whereas in an open configuration, a 10 mm opening was made on the side of the glass chamber to allow hydrogen atoms enter the space inside the glass chamber by diffusion – in this case, the sample was exposed to atoms and radiation, but not to ions (plasma generation within the sample chamber was not possible due to the small size of the chamber). All three sample mounting configurations are shown in Fig. 2.

MgF_2 window (thickness 2 mm) was purchased from Crystal GmbH. The quartz glass windows of thickness 1.1 mm were purchased from Jinzhou City Success Quartz Glass Factory and the borosilicate windows of thickness 1.1 mm from Deltalab. In Table 1, the characteristics of the top-shield windows are shown. MgF_2 window is transparent for UV and VUV radiation, i.e., wavelengths longer than 115 nm. Quartz window is transparent for UV radiation, i.e., wavelengths longer than 155 nm, whereas borosilicate window effectively absorbs both VUV and a part of UV radiation because it is transparent for wavelengths above ~ 300 nm.

Exposure times of the samples ranged from 1 to 7 s for the experiments where samples were exposed directly to plasma and for experiments with the MgF_2 window. Experiments with quartz and borosilicate windows were performed only at exposure times of 5 s.

2.2. Plasma characterization

Plasma was characterized by optical emission spectroscopy (OES) and catalytic probes (to determine the density of hydrogen atoms). OES measurements were performed using a 16-bit Avantes AvaSpec 3648 fiber optic spectrometer, with a nominal spectral resolution of 0.5 nm in the range of 200 to 1100 nm. The integration time ranged from 0.1 ms to 60 s. A typical OES spectrum is shown in Fig. 3. Here, the H_α, H_β, and H_γ lines were left to saturation to make the Fulcher band of hydrogen molecules clearly distinguishable. The OES spectra were measured along the tube to get a distribution of radiation. Because of the linear response of the sensor, normalization to the lowest integration time was done. The results are shown in Fig. 4.

Hydrogen atom density along the tube was measured with a catalytic probe described elsewhere [22]. The results are shown in Fig. 5.

2.3. Surface characterization

For surface characterization of PTFE samples after various treatments, we used an XPS instrument TFA–XPS from Physical Electronics (Munich, Germany). The samples were excited with monochromatic Al $K\alpha_{1,2}$ radiation at 1486.6 eV over an area of 400 μm^2. Photoelectrons were detected with a hemispherical analyser positioned at an angle of

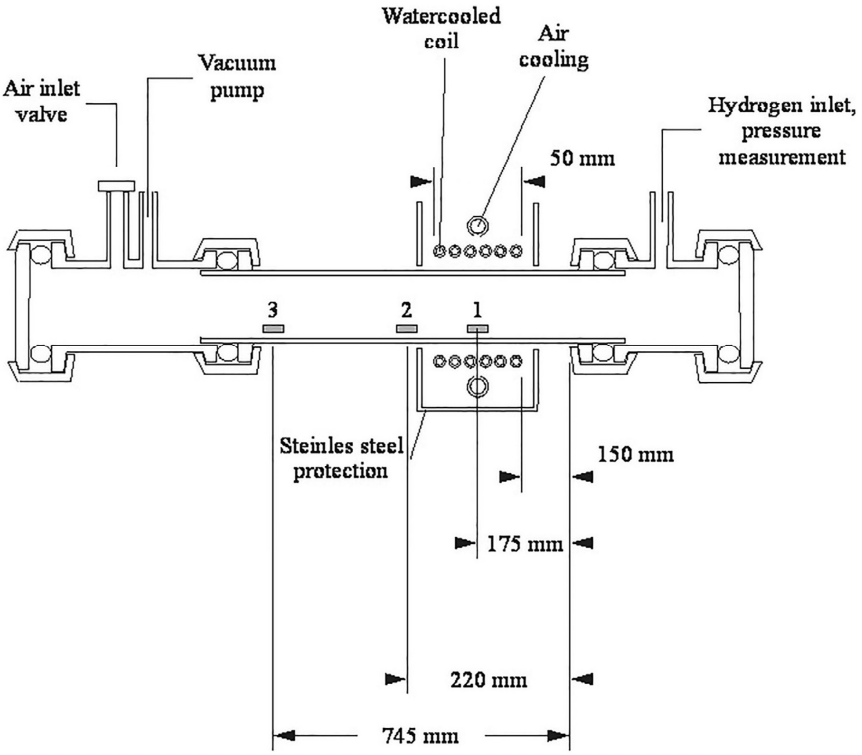

Fig. 1. Experimental plasma system.

45° with respect to the normal of the sample surface. XPS survey spectra were measured at a pass energy of 187 eV using an energy step of 0.4 eV. High-resolution C1s peaks were measured at a pass energy of 29.35 eV using an energy step of 0.125 eV. Individual survey and high-resolution spectra of the samples can be found in Supplementary information. An additional electron gun was used for surface neutralization during XPS measurements. Spectra were calibrated by using adventitious carbon C-C that was assign a value of 284.8 eV. The measured spectra were analysed using MultiPak v8.1c software (supplied by Physical Electronics, Munich Germany).

3. Results and discussion

Samples were treated in the highly luminous plasma when placed at position 1, as marked in Fig. 1. The time evolution of PTFE surface atomic composition for the case of direct plasma treatment (configuration A in Fig. 2), as deduced from XPS survey spectra, is shown in Fig. 6. Individual XPS survey spectra can be found in Supplemental (Fig. S1). As expected, the surface of the untreated PTFE contains only carbon and fluorine. The fluorine concentration is ~ 69 at. %, which is close enough to the theoretical value (i.e., ~ 67 at. %). Even a second of exposure to luminous hydrogen plasma causes a dramatic decrease in the fluorine content, which is also reflected in the shape of C1s peaks showing degradation of CF_2 groups (see Fig. S2 in Supplemental). The original F/C ratio of 2.2 drops to approximately 0.4. Simultaneously, some oxygen appears on the surface. The decrease of the F/C ratio is explained by a bond scission because of VUV radiation, as shown in Eq. (1). The appearance of oxygen may or may not be due to the residual atmosphere in the plasma system. Dangling bonds formed upon treatment of the PTFE may interact with oxygen upon breaking vacuum conditions and before mounting the sample into the XPS instrument. The concentration of oxygen is rather low at up to a few at. %, thus the surface of the sample treated directly with hydrogen plasma is far from being completely oxidized.

Such a quick modification of the PTFE surface, as shown in Fig. 6, and in Supplemental (Figs. S1, S2), is explained by extensive radiation in the UV and VUV range of the OES spectrum. Our spectrometer does not allow measuring the hard UV part of the spectrum, but the intensive Balmer series suggest even more intensive Lyman series of hydrogen atoms. The Balmer series reveal transitions to the first excited state, whereas the Lyman series reveal transitions to the ground state; therefore, the latter is always more intensive. According to Fantz et al. [23] the intensity of Lyman series is over an order of magnitude larger than the Balmer series in the inductively coupled plasma (ICP) in the H-mode sustained in a practically identical reactor as ours. Furthermore, Fantz also measured the molecular bands (both Lyman and Werner) and found their intensity comparable to the Lyman H_α. In fact, they found that the total VUV flux onto a surface facing hydrogen ICP plasma is few times 10^{20} photons $m^{-2}\,s^{-1}$ and the radiant power in the VUV range is approximately 100 W at the forward RF power of 600 W. Such a huge flux of VUV radiation causes significant bond scission in the thin surface film as the penetration depth is only of the order of 10 nm.

The F/C ratio in Fig. 6 does not decrease further for treatment times more than a second. In fact, the opposite effect is clearly visible in Fig. 6: there is a minimum in the F curve. The minimum has been already observed for other plasma/polymer systems and explained by thermal effects [24]. The PTFE sample exposed directly to hydrogen plasma is heated predominantly by surface neutralization of hydrogen ions, absorption of photons, and surface recombination of hydrogen atoms to parent molecules. Furthermore, the ions bombard the surface because they are accelerated in the sheath next to the surface. In our case, the samples were kept at a floating potential; therefore, the kinetic energy of ions is approximately 20 eV. The contribution of different mechanisms for heating the material cannot be calculated because of uncertainties in coefficients, but they can be estimated. The density of plasma sustained in the H-mode at the pressure of a few 10 Pa is often

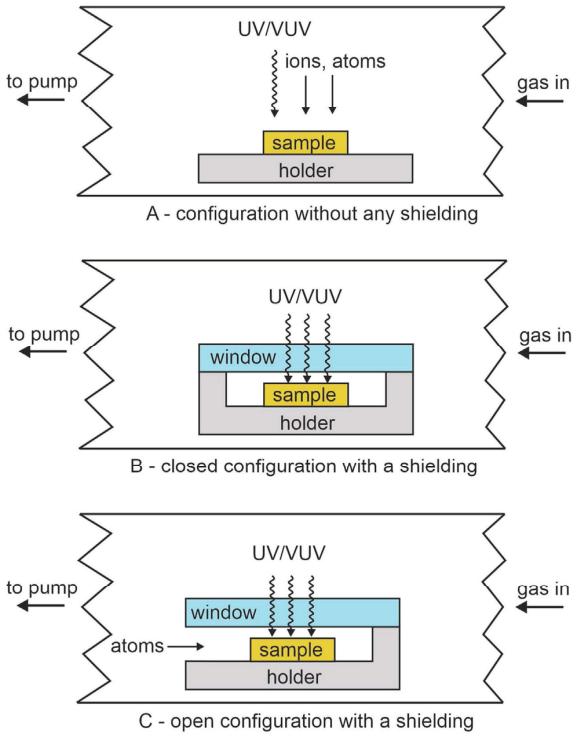

Fig. 2. The sample holders. A) the sample is placed on a microscope slide, B) the sample in modular borosilicate glass sample holder is covered with a window to prevent any interaction with ions or atoms, C) same as B) but there is an opening in the side-wall of the sample holder to allow H-atoms interacting with the sample.

Table 1
Characteristics of different top window shields used in the experiments.

Top windowshield	Transparent for wavelengthslonger than	Cutoff wavelength**	Radiation
MgF_2	115 nm*		VUV + UV
Quartz	155 nm*	164.4 nm	UV
borosilicate	> 300 nm***	330 nm	Above UV

*as measured by OES [3,20].
**corresponding to 20% transmittance [19].
*** measured with our OES.

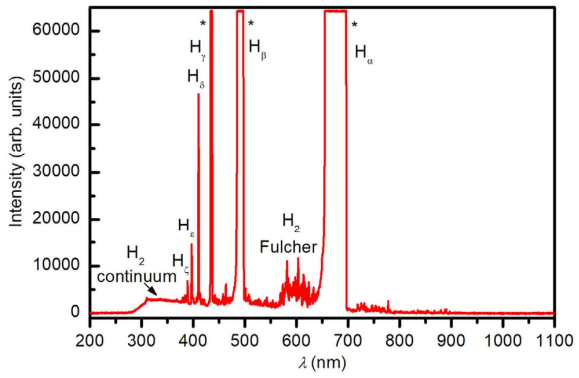

Fig. 3. A typical OES spectrum of hydrogen plasma inside the coil.

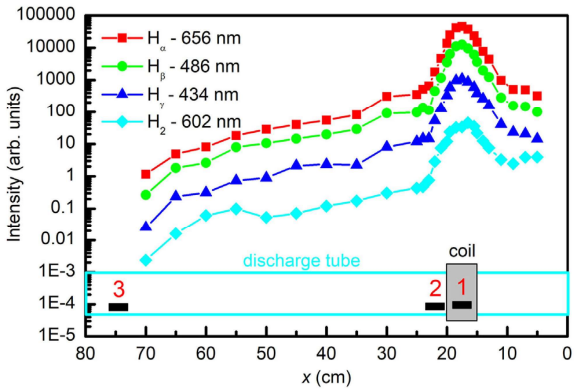

Fig. 4. Variation of the intensity of typical spectral features along the discharge tube. Rectangle indicates the position of the coil. Various positions of the samples are shown with numbers: (1) in glow region, (2) early afterglow, and (3) late afterglow.

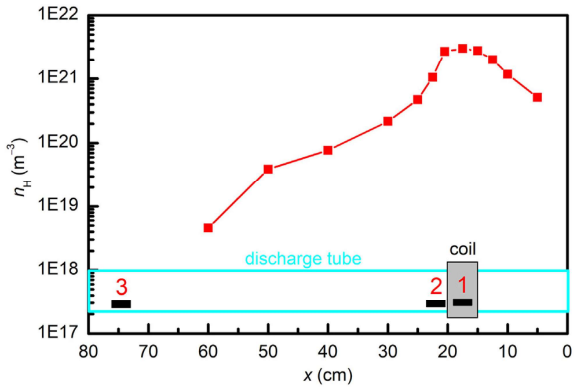

Fig. 5. Variation of the H-atom density along the discharge tube.

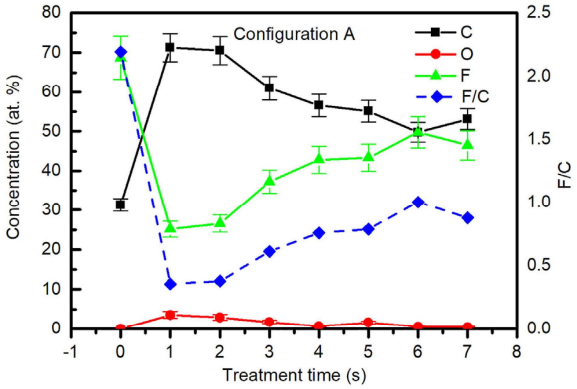

Fig. 6. The time evolution of the surface composition for a direct exposure of PTFE to hydrogen plasma (configuration A in Fig. 2).

few times 10^{18} m^{-3}. The flux of ions onto the surface of a plasma-facing material is a product of an ion density and the Bohm velocity [25], i.e., 4×10^4 W m^{-2} at the ion density of 10^{18} m^{-3}. The power dissipated on the polymer surface by heterogeneous recombination of H atoms to parent molecules can be estimated from a known H-atom density (Fig. 5) and its recombination coefficient (i.e. $(8 \pm 3) \times 10^{-4}$ [26]). At the H-atom density of 3×10^{21} (see Fig. 5) and the average random velocity of H atoms of 3000 m/s, the power dissipated on the PTFE

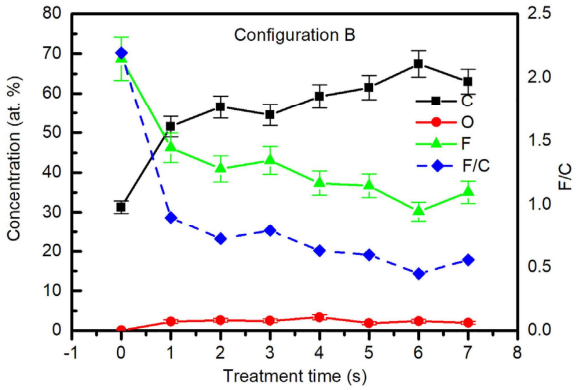

Fig. 7. The time evolution of the surface composition for exposure of PTFE to VUV radiation from hydrogen plasma only (configuration B in Fig. 2).

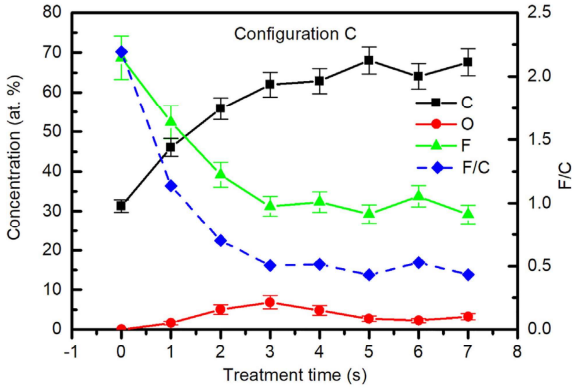

Fig. 8. The time evolution of the surface composition for exposure of PTFE to VUV radiation from hydrogen plasma and H-atoms (configuration C in Fig. 2).

surface because of heterogeneous recombination of H atoms is just below 10^3 W m^{-2}. This is at least an order of magnitude smaller than the power dissipated due to surface neutralization of charged particles and bombardment by ions because of the fact, that the foil was always at the floating potential. The power dissipated by absorption of UV and VUV radiation with the flux 10^{20} m^{-2} s^{-1} [23] is roughly 160 W m^{-2}. There are other heating methods such as accommodation of gaseous molecules and atoms, but their energy is marginal as compared to the potential and kinetic energy of ions. The polymer temperature, therefore, increases rapidly upon direct treatment with gaseous plasma (configuration A in Fig. 2), and much slower in the case of indirect treatments (configurations B and C in Fig. 2). Melting was observed with a naked eye after approximately 10 s of the direct plasma treatment. The increased temperature causes photochemical etching of the PTFE, and thus a loss of F-depleted material. That is why a minimum is observed in the F curve of Fig. 6.

The evolution of surface composition with treatment time is different when the sample is covered with a window (see also Fig. S3 in Supplemental). Fig. 7 reveals the atom concentration on the PTFE surface as deduced from XPS survey spectra for the case of a closed configuration B as shown in Fig. 2. In this configuration, the sample is exposed to the radiation only, because the MgF_2 window prevents ions or atoms to interact with the PTFE surface. Interestingly enough, the F/C ratio decreases significantly even after a second of treatment, but not as much as in the case of direct exposure to hydrogen plasma. The result shown in Fig. 7 indicates that the F/C ratio drops to approximately 0.9 after a second of treatment with the radiation only and keeps decreasing until it becames approximately 0.5, i.e., close to the value observed in Fig. 6 for 1 s treatment. Evidently, the radiation alone can cause the desired modification; however, the required treatment time to obtain a very low F/C ratio is longer. In this case, the thermal effects are less pronounced than in the case of direct exposure to plasma but not negligible taking into account intensive radiation, at least for treatment times up to 7 s. Therefore, no degradation of the F-depleted layer is observed and the CF_2 peak in high-resolution spectra (see Fig. S4 in Suppplemental) keeps decreasing with increasing treatment time.

Because the F/C ratio does not increase for prolonged treatment, and the CF_2 peak does not partially recover as in the case of the configuration A, it is feasible to conclude that the heating is not extensive enough to cause significant desorption of F-depleted material. As already estimated, the major heating mechanism of any plasma-facing material is surface neutralization and bombardment with ions. Because the sample in the configuration B (Fig. 2) is exposed to VUV radiation only, the heating is moderate at about 160 W m^{-2}. Such a power density will cause heating at the rate of the order of 1 K/s providing the thermal capacity of the shield from Fig. 2B is large.

Similar results as in the configuration B of Fig. 2 are also observed in the configuration C. In this case, the PTFE samples were allowed to interact with atomic hydrogen as well as with radiation. The time evolution of the surface composition for configuration C (Fig. 2) at position 1 (Fig. 1) is shown in Fig. 8. Corresponding XPS survey and high-resolution spectra are shown in Figs. S5 and S6 in Supplemental. The curves in Fig. 8 are rather smooth and indicate the asymptotic approach of the surface composition to the value observed for the case of direct exposure to the hydrogen plasma for 1 s. The thermal effects in configuration C should be similar to that of the configuration B, because the H-atom density within the shield should be much smaller than in the unperturbed plasma (Fig. 5).

For comparison, the time evolution of the most important result (i.e., F/C ratio as deduced from XPS survey spectra) for all three configurations is shown in Fig. 9. The measured data points are somewhat scattered, but the trend is obvious: for the case of direct exposure to hydrogen plasma (configuration A) a minimum is observed, whereas for the other two cases (configurations B, C) a gradual approach of the F/C ratio to the value of approximately 0.5 is observed. As mentioned earlier, the minimum in the curve obtained for the case of direct exposure is attributed to thermal effects that in turn cause significant desorption of light C-rich fragments. There is a slight difference between configurations B and C, but it is hardly relevant, taking into account the accuracy of XPS.

In another set of experiments, the MgF_2 window was replaced with quartz glass or a borosilicate glass window using the configuration B (Fig. 2). The experiments were only performed for the treatment time of 5 s where the results presented in Fig. 9 show already good depletion of

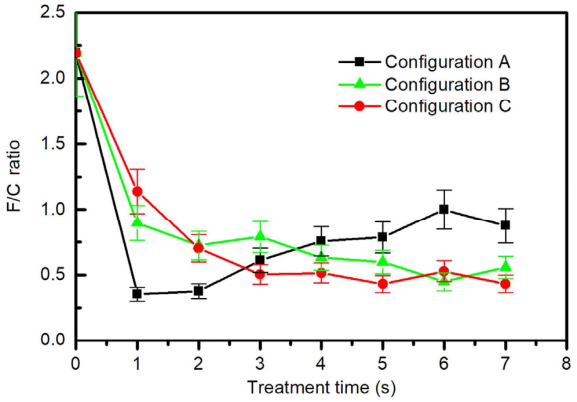

Fig. 9. Variation of the F/C signal versus treatment time for PTFE sample with or without shielding with MgF_2 window.

Table 2
Surface chemical composition of PTFE samples placed in a glow region (position 1) after treatment with various plasma species for 5 s.

Sample position	Configuration – treatment conditions	C (at. %)	O (at. %)	F (at. %)	F/C	Plasma species
	untreated	31.1	0.4	68.5	2.2	
1 - H_2 glow	A - without window	55.1	1.6	43.3	0.8	H, H^+, UV, VUV
	B - MgF_2 closed	61.5	1.8	36.7	0.6	UV, VUV
	C - MgF_2 open	68.0	2.7	29.3	0.4	H, UV, VUV
	B - Quartz closed	39.2	2.4	58.4	1.5	UV
	B - borosilicate closed	32.1	0.6	67.3	2.1	/

F for the configurations B and C. The F/C ratio for all configurations when the samples are treated in the middle of the coil (position 1 of Fig. 1) are summarized in Table 2. The F/C ratio for the case of the sample covered with a quartz window is 1.5. This value is definitely below the value typical for the untreated PTFE, but much higher than for the case of a sample covered with MgF_2 window. As mentioned earlier in this paper, the quartz glass is transparent for UV, but absorbs VUV radiation. The result of Table 2 clearly shows that the UV radiation causes depletion of F from the surface, but the effect is far less pronounced than for VUV radiation. According to Fantz et al. [23], the UV radiation from ICP hydrogen plasma in the H-mode arises partially from the Lyman B – X band as well as the continuum (transition a – b) of neutral hydrogen molecules. The radiation in the range above 155 nm (the cut-off, see Table 1) is comparable to the radiation in the VUV range, but the depletion of the surface (Table 2) is much less efficient, especially when considering the behaviour of curves presented in Figs. 7 and 8. The UV radiation definitely causes bond scission in the surface of PTFE and thus F depletion, but the lower efficiency as compared to VUV could be explained by a larger penetration depth of such radiation in polymers. The penetration depth increases with increasing wavelength in the UV-VUV range so fewer photons are absorbed in the surface film (as probed by XPS); therefore, the depletion of F is much lower in the case of UV than VUV radiation. Still, it is not negligible, as deduced from the result shown in Table 2.

Table 2 also shows the surface composition as measured by XPS in the case when the sample is in configuration B of Fig. 2, but the window is made from borosilicate glass. The F/C ratio for this case is practically the same as for the untreated sample. As shown in Table 1, this material is neither transparent for VUV nor UV, thus the result is highly expected.

The treatment of the PTFE samples in all three configurations (A, B, and C) was also performed away from the region of extensive luminosity. Fig. 4 reveals that the radiation at position 2 is roughly two orders of magnitude less intensive than within the coil. This position is referred to as “early afterglow”. At position 2, the radiation and the flux of ions on the PTFE surface are much less intensive than at position 1 (in the centre of the coil), but the H-atom density is almost comparable, as shown in Fig. 5. The results of XPS characterization using different configurations for the case of exposure to the early afterglow of hydrogen plasma for 5 s are shown in Table 3. The F/C ratio for the case A of direct exposure of PTFE to an early afterglow for 5 s is rather low at 0.6. This value is somehow larger that for the optimal treatments in the glowing plasma itself, but the difference is not significant. Radiation effects cannot explain the result because of the huge differences, as shown in Fig. 4. Furthermore, the density of charged particles at position 2 is negligible as compared to glowing plasma inside the coil. The rather complete depletion of the F in the case of direct exposure to the early afterglow is therefore explained by extensive interaction of PTFE surface with atomic hydrogen. The thermal effects in the early afterglow are considered to be of minor importance for the 5 s treatment; therefore, one can conclude that a large flux of atoms (similar to that in the centre of the coil) together with weak irradiation causes surface modification. This conclusion is supported by the F/C ratio for the samples covered with MgF_2 window (configuration B, C), which is also presented in Table 3. For the case of a covered sample, the F/C ratio hardly differs from the value of an untreated sample. The huge difference in the F/C ratios between the uncovered (marked as “A - without window” in Table 3) and the sample covered with MgF_2 window (marked “B - MgF_2 closed” in Table 3) therefore confirms the key role of atomic hydrogen. Poor depletion in the case of PTFE exposure to the early afterglow was also observed for the case of borosilicate glass and MgF_2 windows in the configuration C of Fig. 2. In the case of borosilicate glass, the measured F/C is even somehow larger than for untreated samples but within the limits of an experimental error.

Few samples were also treated in the late afterglow, at position 3, as marked in Fig. 1. Based on the results summarized in Tables 2 and 3, only direct exposures were performed (configuration A in Fig. 2). As shown in Fig. 4, the radiation in the late afterglow is further reduced and is 4–5 orders of magnitude weaker than inside the coil. Also, the H-atom density is close to the detection limit of the catalytic probe (see Fig. 5). The F/C ratio of a sample exposed to the late afterglow is added to Table 3. It is the same as for the untreated sample indicating a little effect of such treatment on the surface chemistry. Obviously, both the H-atom density and the radiation are too weak at the position 3 of Fig. 1 to cause any measurable effect after 5 s.

The results summarized in Tables 2 and 3, therefore, indicate the synergy between the UV and/or VUV radiation and H atoms. The difference in the F/C ratio for the direct treatment and treatment with the MgF_2 window (Table 3) is significant (0.6 versus about 2). It is not feasible to measure the H-atom flux onto the surface of the PTFE sample in the configuration C, but it is definitely much smaller than in the configuration A. The reason is surface recombination of H atoms within the shield covered with the MgF_2 window. The loss of atoms should be replaced by diffusion of H atoms from the surrounding atmosphere as shown with an arrow in Fig. 2C. The diffusion is a slow process for particle transport, so the H-atom density within the shield of Fig. 2C is much smaller than in the configuration of Fig. 2A. The F/C ratio for the”closed” and “open” configurations in Tables 2 and 3 is similar, and so is in configurations B and C in Fig. 9. This observation indicates that

Table 3
Surface chemical composition of PTFE samples placed in the early or late afterglow (position 2, 3) after treatment with various plasma species for 5 s.

Sample position	Configuration – treatment conditions	C (at. %)	O (at. %)	F (at. %)	F/C	Plasma species
2 - Early afterglow	A - without window	58.5	4.6	36.9	0.6	H, UV, VUV
	B - MgF_2 closed	33.7	0.9	65.5	1.9	UV, VUV
	C - MgF_2 open	32.0	0.5	67.5	2.1	H, UV, VUV
	C - borosilicate open	29.5	0.7	69.8	2.4	H
3 - Late afterglow	A - without window	31.3	0.8	67.9	2.2	H

the required flux of H atoms to benefit from the synergy with VUV radiation is rather small, definitely much smaller than the available H-atom flux in the configuration without the MgF_2 window.

A feasible explanation of the synergy between the H atoms and radiation is as follows: The VUV and even UV radiation causes bond scission. The VUV photons' energies exceed the C-F binding energy, which is approximately 6 eV [27]. The H atoms (if present) terminate the dangling bonds and also interact with F-atoms to form more stable HF molecules. The flux of H atoms on the surface of a sample directly exposed to plasma in the H-mode or in the early afterglow is large. Fig. 5 reveals H-atom densities between approximately 6 and 30 $\times$ 10^{20} m^{-3}, which corresponds to the flux of H atoms onto the surface of between 6 and 30 $\times$ 10^{23} m^{-2} s^{-1} at the neutral gas kinetic temperature of 700 K. This is orders of magnitude larger than the flux of photons (approximately 1 $\times$ 10^{20} m^{-2} s^{-1}). The available flux upon direct exposure is more than enough to terminate the dangling bonds and thus prevent the termination by F atoms. If the flux of H atoms is insufficient, the depletion of the surface layer is a much slower process as revealed from the comparison between the direct and indirect treatment in the early afterglow (Table 3).

4. Conclusions

The experimental results presented in this paper show the rapid depletion of fluorine from the PTFE surface, providing the fluence of VUV radiation is rather significant. Because the penetration depth of VUV in organic material is low, the extensive absorption of such photons causes significant bond scission in the surface layer of PTFE. According to the results summarized in Figs. 7–9, the required VUV fluence for the optimal depletion of fluorine from the PTFE surface is close to 10^{17} cm^{-2}. The atom surface density in solid materials is of the order of 10^{15} cm^{-2}; therefore, the efficiency of VUV radiation is far from 100%, which can be explained by a finite penetration depth of such photons in the PTFE material. The efficiency is further increased by synergistic effects of hydrogen atoms. In the case of direct exposure of PTFE to hydrogen plasma in the H-mode, the required VUV fluence for the optimal depletion is a few times lower than for the case of VUV radiation alone. Nevertheless, the required fluence is not so significantly lower; therefore, it can be concluded that in most practical cases, the exposure of PTFE to VUV radiation alone is effective enough. The direct exposure to plasma causes pronounced heating of the polymer; therefore, the optimal conditions are within a very limited range of treatment times. This effect makes direct exposure less attractive for practical applications where depletion of fluorine from the PTFE surface is desired, i.e., for improved wettability before deposition of the desired coating. The UV radiation itself (without VUV contribution) causes weak depletion of the PTFE surface which is explained by the fact that the photons in the high-energy part of the deep UV radiation have the energy larger than the C-F binding energy, but the penetration depth in organic material for UV is larger than for VUV, so the surface effects are less pronounced. The H atoms alone (without hard UV or VUV radiation) do not cause measurable effects on the surface composition of PTFE.

The work presented in this paper was performed using small samples placed in the experimental plasma device separately. In any practical application, however, the materials to be depleted from fluorine should move through the discharge zone at speed optimized to achieve the appropriate fluences of reactive plasma species and radiation.

CRediT authorship contribution statement

Dane Lojen: Visualization, Investigation, Formal analysis. **Rok Zaplotnik:** Conceptualization, Methodology. **Gregor Primc:** Validation, Data curation. **Miran Mozetič:** Writing - review & editing, Funding acquisition. **Alenka Vesel:** Supervision, Project administration, Writing - original draft.

Declaration of Competing Interest

The authors declare that they have no known competing financial interests or personal relationships that could have appeared to influence the work reported in this paper.

Acknowledgements

The authors acknowledge the financial support from the Slovenian Research Agency - project No. J2-1728 (Initial stages in surface functionalization of polymers by plasma radicals) and P2-0082 (Thin film structures and plasma surface engineering).

Appendix A. Supplementary data

Supplementary data to this article can be found online at https://doi.org/10.1016/j.apsusc.2020.147356.

References

[1] A. Vesel, M. Mozetic, New developments in surface functionalization of polymers using controlled plasma treatments, J. Phys. D: Appl. Phys. 50 (2017) 293001.
[2] T. Dufour, J. Hubert, N. Vandencasteele, P. Viville, R. Lazzaroni, F. Reniers, Competitive and synergistic effects between excimer VUV radiation and O radicals on the etching mechanisms of polyethylene and fluoropolymer surfaces treated by an atmospheric He–O_2 post-discharge, J. Phys. D: Appl. Phys. 46 (2013) 315203.
[3] K. Cho, K. Takenaka, Y. Setsuhara, M. Shiratani, M. Sekine, M. Hori, Effects of irradiation with ions and photons in ultraviolet–vacuum ultraviolet regions on nano-surface properties of polymers exposed to plasmas, Jap. J. Appl. Phys. 51 (2012) 01AJ02.
[4] A.J. Knoll, P. Luan, E.A.J. Bartis, V.S.S.K. Kondeti, P.J. Bruggeman, G.S. Oehrlein, Cold atmospheric pressure plasma VUV interactions with surfaces: effect of local gas environment and source design, Plasma Process. Polym. 13 (2016) 1069–1079.
[5] A. Vesel, M. Kolar, N. Recek, K. Kutasi, K. Stana-Kleinschek, M. Mozetic, Etching of blood proteins in the early and late flowing afterglow of oxygen plasma, Plasma Process. Polym. 11 (2014) 12–23.
[6] W.D. Silva, T. Belmonte, D. Duday, G. Frache, C. Noel, P. Choquet, H.N. Migeon, A.M. Maliska, Interaction mechanisms between Ar-O_2 post-discharge and biphenyl, Plasma Process. Polym. 9 (2012) 207–216.
[7] V. Hody, T. Belmonte, C.D. Pintassilgo, F. Poncin-Epaillard, T. Czerwiec, G. Henrion, Y. Segui, J. Loureiro, Modification of hexatriacontane by O_2–N_2 microwave post-discharges, Plasma Chem. Plasma Process. 26 (2006) 251–266.
[8] E.A. Bernardelli, T. Belmonte, D. Duday, G. Frache, F. Poncin-Epaillard, C. Noël, P. Choquet, H.N. Migeon, A. Maliska, Interaction mechanisms between Ar–O_2 post-discharge and stearic acid I: Behaviour of thin films, Plasma Chem. Plasma Process. 31 (2011) 189–203.
[9] G. Borcia, C.A. Anderson, N.M.D. Brown, Dielectric barrier discharge for surface treatment: application to selected polymers in film and fibre form, Plasma Sources Sci. Technol. 12 (2003) 335–344.
[10] G. Borcia, C.A. Anderson, N.M.D. Brown, The surface oxidation of selected polymers using an atmospheric pressure air dielectric barrier discharge. Part II, Appl. Surf. Sci. 225 (2004) 186–197.
[11] A.J. Knoll, P. Luan, A. Pranda, R.L. Bruce, G.S. Oehrlein, Polymer etching by atmospheric-pressure plasma jet and surface micro-discharge sources: Activation energy analysis and etching directionality, Plasma Process. Polym. 15 (2018) 1700217.
[12] N. Vandencasteele, B. Nisol, P. Viville, R. Lazzaroni, D.G. Castner, F. Reniers, Plasma-Modified PTFE for Biological Applications: Correlation between Protein-Resistant Properties and Surface Characteristics, Plasma Process. Polym. 5 (2008) 661–671.
[13] S. Zanini, R. Barni, R.D. Pergola, C. Riccardi, Modification of the PTFE wettability by oxygen plasma treatments: influence of the operating parameters and investigation of the ageing behaviour, J. Phys. D: Appl. Phys. 47 (2014) 325202.
[14] N. Inagaki, S. Tasaka, K. Narushima, K. Teranishi, Surface modification of poly (tetrafluoroethylene) with pulsed hydrogen plasma, J. Appl. Polym. Sci. 83 (2002) 340–348.
[15] Y. Yamada, T. Yamada, S. Tasaka, N. Inagaki, Surface modification of poly(tetrafluoroethylene) by remote hydrogen plasma, Macromolecules 29 (1996) 4331–4339.
[16] M.E. Ryan, J.P.S. Badyal, Surface texturing of PTFE film using nonequilibrium plasmas, Macromolecules 28 (1995) 1377–1382.
[17] A. Vesel, J. Kovac, R. Zaplotnik, M. Modic, M. Mozetic, Modification of polytetrafluoroethylene surfaces using H_2S plasma treatment, Appl. Surf. Sci. 357 (2015) 1325–1332.
[18] V.E. Skurat, A.C. Samsonov, A.P. Nikiforov, Sources of hyperthermal atomic oxygen as sources of vacuum ultraviolet radiation, in: 9th International Symposium on Materials in a Space Environment proceedings, ESTEC, ESA Noordwijk, the

Netherlands, 2003.
[19] S. Tajima, K. Komvopoulos, Effect of reactive species on surface crosslinking of plasma-treated polymers investigated by surface force microscopy, Appl. Phys. Lett. 89 (2006) 124102.
[20] K. Cho, Y. Setsuhara, K. Takenaka, M. Shiratani, M. Sekine, M. Hori, Effects of photoirradiation in UV and VUV regions during plasma exposure to polymers, Thin Solid Films 519 (2011) 6810–6814.
[21] Y. Zhang, K. Ishikawa, M. Mozetic, T. Tsutsumi, H. Kondo, M. Sekine, M. Hori, Polyethylene terephthalate (PET) surface modification by VUV and neutral active species in remote oxygen or hydrogen plasmas, Plasma Process. Polym. 16 (2019) 1800175.
[22] R. Zaplotnik, A. Vesel, M. Mozetic, A fiber optic catalytic sensor for neutral atom measurements in oxygen plasma, Sensors 12 (2012) 3857–3867.
[23] U. Fantz, S. Briefi, D. Rauner, D. Wünderlich, Quantification of the VUV radiation in low pressure hydrogen and nitrogen plasmas, Plasma Sources Sci. Technol. 25 (2016) 045006.
[24] J. Izdebska, T. Sabu, Printing on Polymers: Fundamentals and Applications, Elsevier Science Publishing Co Inc, Waltham, USA, 2016.
[25] Research Group Reactive Plasmas, Plasma Calculator, https://www.ep2.ruhr-uni-bochum.de/index.php/plasma-calculator, Ruhr-Universität Bochum, Accesed: June 5, 2020.
[26] R. Zaplotnik, A. Vesel, M. Mozetic, Atomic oxygen and hydrogen loss coefficient on functionalized polyethylene terephthalate, polystyrene, and polytetra-fluoroethylene polymers, Plasma Process. Polym. 15 (2018) 1800021.
[27] D.M. Lemal, Perspective on fluorocarbon chemistry, J. Org. Chem. 69 (2004) 1–11.

Chapter 4

Optimisation of Surface Wettability of Polytetrafluoroethylene (PTFE) by Precise Dosing of Oxygen Atoms

This chapter discusses the superhydrophilisation of hydrogen plasma pre-functionalised PTFE with non-equilibrium low-pressure oxygen (O_2) RF inductively coupled plasma. In the previous two chapters, it was demonstrated that hydrogen plasma efficiently defluorinates the PTFE surface, but the WCA of the plasma-treated PTFE surface remains high and surface energy remains low. Therefore, the possibilities of using oxygen plasma for optimal hydrophilisation of the samples were examined. We chose oxygen plasma because we hypothesised that O-atoms will interact chemically with the polyolefin-like surface, thus causing functionalisation with polar functional groups.

We used the same experimental system as in chapters 2 and 3. Each sample was initially pre-treated with hydrogen plasma at optimal conditions. The real power of the hydrogen plasma was 355 W, the H_2 pressure 25 Pa, and flowrate 140 sccm (with pre-treatment conditions chosen according to the research in chapters 2 and 3).

After pre-treatment in hydrogen plasma, the samples were treated in the flowing afterglow of oxygen plasma. The real power of plasma was 465 W, the pressure of O_2 30 Pa, the O_2 flowrate 105 sccm and the treatment time varied between 0.03 and 300 s. Time variation under the given conditions was performed at three different coil-to-sample distances of 150, 300 and 500 mm. O-atom densities were measured with a cobalt catalytic probe at 150, 300 and 500 mm from the coil and were 3.4×10^{21}, 3.2×10^{21} and 2.4×10^{21} m^{-3}, respectively. The dose of received neutral oxygen atoms increases linearly with increased treatment time. Therefore, precise dosing of neutral oxygen atoms was possible by variation of the treatment time. In the experimental series performed at 150, 300 and 500 mm in the afterglow, the hydrophilicity of the surface was determined by measuring the static WCA of treated PTFE surfaces. The elemental composition of the treated PTFE surfaces was determined by XPS analysis.

The WCA of untreated samples was 111 ± 4° and samples pre-treated with hydrogen plasma exhibited a WCA of 94 ± 3°. According to the elemental analysis by XPS (at standard TOA of 45°), the untreated samples consisted of 32 at.% of carbon and 68 at.% of fluorine, while pre-treated samples consisted of 75.4 at.% of carbon, 20.8 at.% of fluorine and 3.8 at.% of oxygen.

Variation of the treatment time at all coil-to-sample distances resulted in the instant decrease of WCA to about 20° after 0.03 s of treatment. Then all three curves exhibited a plateau between 18 and 15°. WCA minima at coil-to-sample distances of 150, 300 and 500 mm were in the range between 5 and 7° appearing at treatment times of 0.20, 0.25 and

0.30 s, respectively. With longer treatment times, the WCA increased toward the value of untreated samples.

All three curves were plotted against the fluence of O-atoms. The initial courses of WCA curves and minima almost overlapped and appeared at 1×10^{23} m^{-2}, 1.3×10^{23} m^{-2} and 3×10^{23} m^{-2} at coil-to-sample distances of 150, 300 and 500 mm. At the coil-to-sample distance of 150 mm, the hydrophobic recovery starts beyond the O-atom fluence of 3×10^{23} m^{-2} and the WCA hydrophobic recovery is faster than at the coil-to-sample distance of 500 mm. The coinciding competitive processes of etching and functionalisation explain the hydrophobic recovery. Because the polyolefin-like layer formed during the hydrogen plasma pre-treatment is very thin, it is important that the dose of received O-atoms is just right to provide the formation of hydrophilic groups but not too high, as large doses cause etching. The increased etching rate at a closer coil-to-sample distance is explained by a higher density of oxygen ions because their concentration is about one order of magnitude greater in early afterglow than in late afterglow. However, the initial functionalisation at close coil-to-sample distances occurs despite etching due to the high initial interaction probability of O-atoms.

XPS analysis of the hydrogen plasma pre-treated PTFE functionalised with reactive species from oxygen plasma at the coil-to-sample distance of 150 mm showed an instant initial rise in oxygen concentration to about 20 at.% after 0.03 s of treatment (O-atom fluence of about 1.5×10^{22} m^{-2}). The amount of oxygen in the surface film remained approximately constant up to the treatment time of 1 s (O-atom fluence of about 5×10^{23} m^{-2}). Beyond 1 s of treatment, O-concentration decreased quickly and after 13 s (O-atom fluence of 6.9×10^{24} m^{-2}) it dropped to about 2.5 at.%. After 1 s of treatment, the F concentration and F/C ratio started to increase and almost reached values that are characteristic of untreated samples after 10 s.

At the coil-to-sample distance of 500 mm, XPS analysis showed very similar trends as at the coil-to-sample distance of 150 mm. The difference was in the O-atom fluences at which the O-concentration in the sample's surface was approximately constant (ranging between 1×10^{22} and 4×10^{24} m^{-2}). The broader range of O-atom fluences in plasma at which O-concentration in the sample's surface film was constant was also accompanied by the broader WCA minimum curve.

The higher fluence value at a coil-to-sample distance of 500 mm rather than at 150 mm, where hydrophobic recovery due to surface etching became apparent, was explained by the marginal density of charged particles 500 mm away from the coil causing slower etching of the functionalised polyolefin-like layer.

The WCA minima appearing at constant O-concentrations and F/C ratios within certain fluence ranges could be explained by the fact that the WCA does not depend solely on the surface composition but also on the morphology of the surface.

Despite neutral oxygen atoms in the ground state appearing to be the most important for surface functionalisation kinetics, positively charged ions also influence the etching rate (an order of magnitude greater O-atom fluence was needed to achieve complete hydrophobic recovery at the coil-to-sample distance of 500 mm than at 150 mm). The importance of ions is supported by the fact that the differences in measured O-atom densities at different surface positions were marginal in comparison to the required fluences for full hydrophobic recovery of the surface.

Functionalisation of the PTFE surface by successive treatments with hydrogen and oxygen plasmas is illustrated in Figure 7.

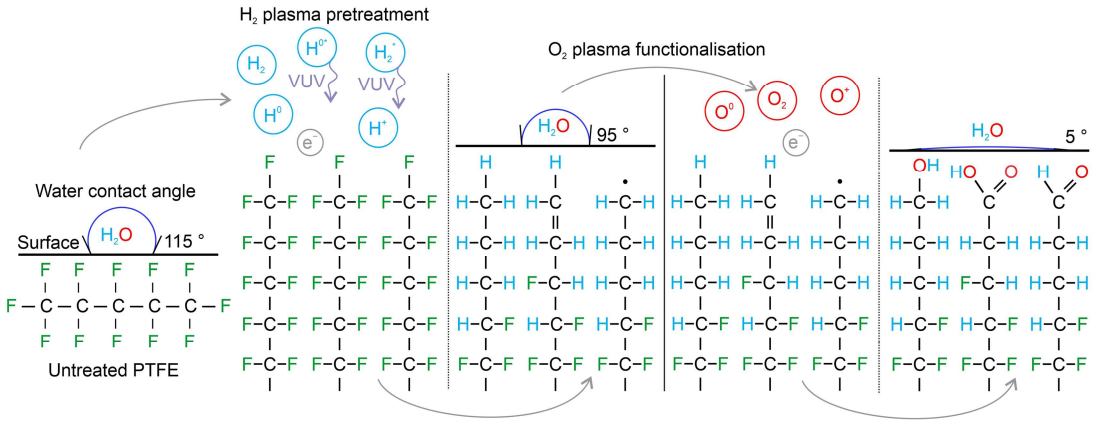

Figure 7: Schematic representation of PTFE functionalisation achieved by successive treatments of the PTFE surface with hydrogen and oxygen plasmas.

Figure 8 shows a water droplet on the surface of plasma-treated PTFE exhibiting the water contact angle of about 5° showing that PTFE was successfully rendered superhydrophilic.

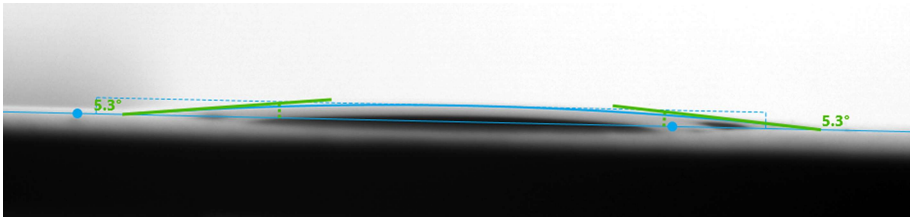

Figure 8: Superhydrophilic PTFE.

Applied Surface Science 598 (2022) 153817

Contents lists available at ScienceDirect

Applied Surface Science

journal homepage: www.elsevier.com/locate/apsusc

Full Length Article

Optimization of surface wettability of polytetrafluoroethylene (PTFE) by precise dosing of oxygen atoms

Dane Lojen [a,b], Rok Zaplotnik [a], Gregor Primc [a], Miran Mozetič [a], Alenka Vesel [a,*]

[a] Jožef Stefan Institute, Department of Surface Engineering, Slovenia
[b] Jozef Stefan International Postgraduate School, Slovenia

ARTICLE INFO

Keywords:
Polytetrafluoroethylene (PTFE)
Surface functionalisation
Surface wettability
Two-step treatment
Defluorination
Hydrogen plasma
Oxygen plasma

ABSTRACT

Fluorinated polymers such as PTFE cannot be functionalized with polar, oxygen-containing functional groups by a one-step treatment with oxygen plasma because the treatment would preferentially lead to surface etching rather than substitution of fluorine with oxygen. A novel method for the functionalization of PTFE is presented. PTFE was initially treated in low-pressure non-equilibrium inductively coupled RF hydrogen plasma in the H-mode to obtain an appropriate surface finish for functionalization with oxygen atoms. The hydrogen-plasma treatment ensured the formation of a polyolefine-like surface film, which was functionalized with polar groups by subsequent exposure to a fluence of O atoms in the range between approximately 1×10^{22} m^{-2} and 1×10^{26} m^{-2}. The evolutions of the surface wettability and composition were studied systematically in this range of O-atom fluences. A deep and rather broad minimum of the water contact angle (WCA) was observed. The minimum of the WCA was correlated to the concentrations of elements in the surface as analysed by X-ray photoelectron spectroscopy. A complete hydrophobic recovery was observed at the largest O-atom fluence, which coincided with the restoration of the surface composition. The surface kinetics upon exposure to O atoms or a weakly ionized oxygen plasma was studied and explained.

1. Introduction

Polytetrafluoroethylene (PTFE) is a non-biodegradable polymer with high chemical and biological resistance and inertness [1]. Because of its physical and chemical properties, PTFE can be used in various applications, from kitchenware to polymeric body implants. Due to its composition, the polymer exhibits low surface energy, large water contact angle (WCA), and thus low wettability, which in turn causes inadequate adhesion of many materials. The consequences include poor printability [2] and glueability [3], as well as the inability for covalent bonding of biomolecules to fluorine-containing materials [4]. These effects were recognized decades ago as limiting factors in the widespread application of such polymers [5,6].

Extensive research has been performed on surface functionalization and improvement of adhesion properties of PTFE. Conventional chemical methods involve etching with sodium-containing corrosive solutions such as Na-naphthalene followed by BH_3 and H_2O_2/NaOH treatments [7,8], immersion in a solution of sodium in anhydrous liquid ammonia [9], solutions of sodium naphtalenide in tetrahydrofuran, direct electrochemical reduction, treatment with an alkali metal amalgam, reduction with benzoin di-anion, deposition of aluminum by evaporation [10]. The latter technique, however, only increases the wettability but not the adhesion since a metal film evaporated on the PTFE surface exhibits a very poor adhesion. The disadvantages of chemical etching include toxicity to humans, ecological hazard, malodor, and PTFE surface coloration [7,11,12]. Other methods for modification of PTFE surface properties are ion irradiation [3], corona treatment [13], and plasma treatment [14].

An environmentally friendlier and safer alternative for the improvement of adhesion and wettability of polymers is treatment with various gaseous plasmas. Gaseous plasma is a medium containing electrons and ions, neutral atoms in the ground and excited states, as well as radiation. Particularly important for surface modification of polymers are photons of energy above the threshold for breaking bonds in polymer materials, i.e. in the UV-C and vacuum ultraviolet (VUV) ranges [15–17]. The VUV radiation is particularly intensive in plasmas sustained by discharges of large power density [18] and often causes significant modifications in surface properties of polymer materials [19]. The surface kinetics upon plasma functionalization also depends on the kinetic energy of positively charged ions and the oxidation potential of

* Corresponding author.
E-mail address: alenka.vesel@guest.arnes.si (A. Vesel).

https://doi.org/10.1016/j.apsusc.2022.153817
Received 28 February 2022; Received in revised form 24 May 2022; Accepted 25 May 2022
Available online 28 May 2022

neutral reactive species [20].

Through decades, authors used different plasmas for the functionalization of PTFE: argon [21,22], hydrogen [23–26], oxygen [22,27], nitrogen [21], ammonia [23], water [28] and methane [29]. However, wettability improvements, as measured by WCA, were inadequate compared to the chemical treatments. The best results obtained with plasmas of single molecular gases were WCAs in the range between 50 and 45° and PTFE surface oxygen contents between 10 and 30 at. % [20]. Carefully designed experiments, however, may provide plasma conditions where a superhydrophilic surface finish of PTFE is obtained. For example, [30] reported very low WCA of about 4° after prolonged treatment with argon plasma at the pressure of 10 Pa. The treatment for almost 10 min at the discharge power of 8 W enabled both nanostructuring and surface oxidation.

The authors reported different types of plasmas used for surface modification of PTFE. The first type is treatment with plasmas rich in oxygen. Reactive oxygen species, however, do not have sufficient potential energy for breaking C – F bonds in PTFE. The consequence is a low level of functionalization when treating PTFE by oxygen plasma. The etching process prevails instead of substituting fluorine with oxygen in the surface film [20]. Treatment with oxygen plasma results in the formation of volatile $C_xF_yO_z$ fragments that are desorbed from the surface [31]. The effect was further elaborated by [27], who found that no oxygen was bound to the PTFE surface upon RF self-biasing during the plasma treatment, and the surface roughness increased by the appearance of alveolar structures.

Some authors used oxygen-free plasmas (for example, hydrogen plasma) for the treatment of PTFE. They reported defluorination of the surface film, which was explained by the formation of dangling bonds due to bond-scission by VUV radiation [19,20,32]. Low-pressure RF hydrogen plasma emits up to 20% of power as VUV radiation [15]. Oxygen from the residual atmosphere (particularly water vapour) in the discharge tube or/and after the treatment, when the sample is exposed to air, is bound to the dangling bonds [20].

In our previous research [19], we exposed PTFE to low-pressure RF inductively coupled (ICP) H_2 plasma. We managed to separate the VUV radiation, the flux of charged particles, and the flux of neutral atoms to selectively treat the samples. The samples exposed to H_2 plasma for 1 s exhibited the F/C ratio 0.4, as analysed by XPS. The same ratio was observed for samples exposed to VUV/UV radiation and H atoms. The exposure to VUV only resulted in an F/C of 0.6. Exposure to H atoms only did not cause considerable defluorination. It was hypothesized that the mechanism of defluorination of PTFE in H_2 plasma is based on synergistic effects of VUV radiation (breaking C – F bonds) and H-atoms binding to the dangling bonds [19]. It was reported by several authors including [33–35] that the treatment of polymers with VUV radiation only (for example from exciplex sources) causes significant modification of surface properties. Some polymers treated by VUV radiation at prolonged treatment times assume the superhydrophilic surface finish. However, the effect may be due to the extensive dissociation of oxygen in the gas phase by VUV radiation. For example, it was clearly demonstrated that the oxygen concentration in the ambient atmosphere upon treatment of polymers contributes significantly to the observed polymer wettability [36].

In another research [37], we exposed PTFE to low-pressure RF ICP H_2 plasma running in different discharge modes. We found that PTFE exposed to H_2 plasma in the H-mode for 1 s resulted in a decrease of F/C ratio to 0.2, but the static WCA remained rather large at 83°. If experiments were repeated in the E-mode, longer times were needed to obtain the minimum – i.e. minimal F/C ratio of 0.6 was obtained after several seconds of plasma treatment. The difference between E- and H-modes was assigned to the lack of VUV radiation in the E-mode. Time-of-Flight Secondary Ion Mass Spectrometry (ToF-SIMS) confirmed the presence of $C_xH_y^+$ and the absence $C_xF_y^+$ ions on the surface film, indicating the formation of a polyolefin-like surface layer. Additionally, the measured WCA value of 80° is typical for polyolefins [37]. This is in accordance with the findings of Yamada et al., who treated PTFE in the afterglow of low-pressure RF ICP H_2 plasma and found the immeasurably low F/C ratio within the surface layer with a thickness of 1 nm using AR-XPS [26].

2. Materials and methods

PTFE foil was purchased from Goodfellow Ltd. (Huntington UK). The foil with a thickness of 0.5 mm was cut to rectangular pieces of 25 × 9 mm. Prior to treatments, the samples were cleaned with ethanol.

The plasma system is schematically shown in Fig. 1. The experimental system consisted of a borosilicate glass discharge tube, a water-cooled copper coil with 6 loops with an additional forced-air cooling and a stainless steel electromagnetic field shielding mounted directly onto the Dressler Hochfrequenz-Technik GmbH impedance matching network, a CESAR Dressler RF generator from Advanced Energy (13.56 MHz), an Aera FC7700 flow controller from Advanced Energy, a MKS baratron and an Edwards E2M80 two-stage vacuum pump.

The PTFE samples were first pretreated in the H_2 plasma. The inductively coupled plasma was sustained in the H-mode. The samples were placed inside the RF coil, as shown in Fig. 1. The treatment time in the H_2 plasma was 1 s. This treatment time enabled defluorination of the surface film [19,37]. The forward power of the RF generator was 385 W, whereas the reflected power was 30 W. The H_2 pressure was set to 25 Pa, and the H_2 flow rate was 140 standard cm^3/min (sccm).

After the hydrogen plasma pretreatment, the samples were treated in the flowing afterglow of oxygen plasma. Oxygen plasma was also sustained in the H-mode. Prior the O_2 plasma treatment, the samples were moved away from the RF coil to the positions marked in Fig. 1. We have chosen the afterglow because the direct exposure of the pretreated samples to a dense plasma in the center of the RF coil would cause immediate etching and thus the loss of the fluorine-depleted surface film. The forward power of the RF generator was set to 465 W, and the reflected power was 100 W. The O_2 flow rate was 105 sccm, whereas the O_2 pressure was 30 Pa. A photo of the O_2 plasma in the discharge tube is shown in Fig. 2. The dense plasma in the H-mode is concentrated in the volume inside the coil, while weak radiation is also observed in the flowing afterglow region, in the direction from the coil towards the pump duct. The samples were treated in the flowing afterglow at various positions, i.e. 150, 300, and 500 mm away from the coil. These positions of the samples are marked in Figs. 1 and 2. Fig. 2 reveals very weak emissivity of the plasma in the flowing afterglow, so a skilled person may conclude that the density of charged particles and/or electron temperature in the afterglow is much smaller than in the plasma within the RF coil. The treatment times of samples exposed to the oxygen plasma afterglow were varied between 0.03 and 100 s.

Neutral oxygen atom densities were measured using a cobalt catalytic probe at the selected coil-to-sample distances. A probe is presented to details elsewhere [38,39]. The O-atom densities at the selected positions are shown in Table 1.

From Table 1, it can be seen that the differences in the O-atom densities and fluxes between all the three coil-to-sample distances are quite small. This means that the recombination of the neutral O atoms along the discharge tube is relatively ineffective. The reasons have been explained elsewhere [16,40].

The samples treated by the flowing afterglow of oxygen plasma were analysed by X-ray photoelectron spectroscopy (XPS) and WCA. WCAs on treated PTFE surface were measured with Krüss DSA-100 drop shape analyzer in conjunction with Krüss Advance 1.10 software (Krüss, Hamburg, Germany). A static water contact angle was measured. A volume of water droplet was 1.5 μL.

The chemical composition of treated PTFE samples was determined by XPS instrument TFA–XPS from Physical Electronics (Munich, Germany) equipped with the hemispherical analyzer and monochromatic X-ray source. The samples were excited with monochromatic Al $K\alpha_{1,2}$ radiation at 1486.6 eV over an area of 400 μm^2. The photoelectron take-off

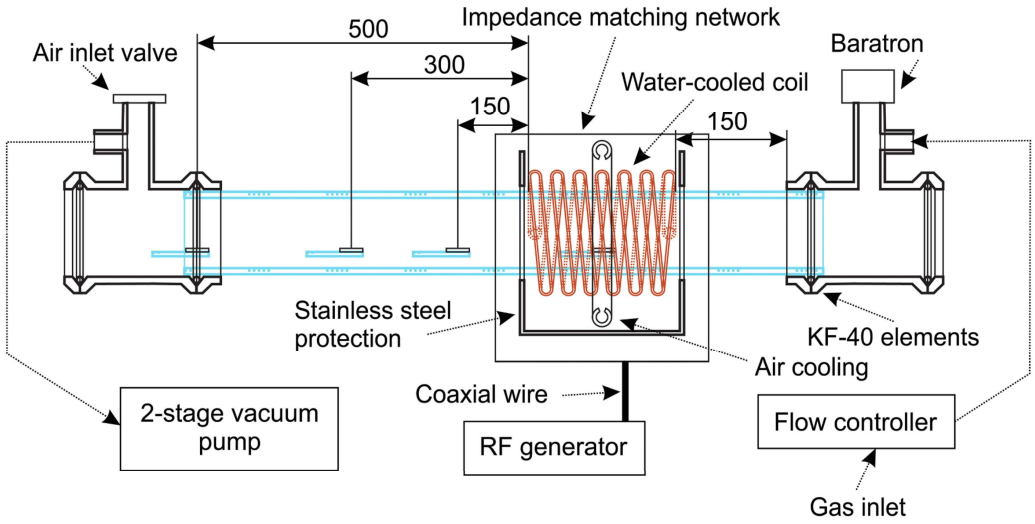

Fig. 1. System configuration for the coil-to-sample distances of 150, 300 and 500 mm.

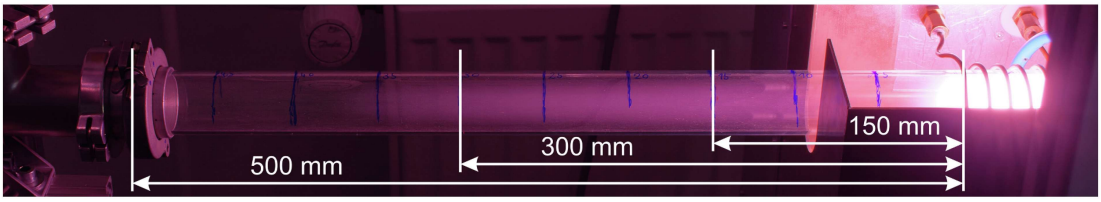

Fig. 2. Oxygen plasma in the discharge tube (positions of samples are marked).

Table 1
Neutral O atom densities and the corresponding fluxes measured with the cobalt catalytic probe at chosen coil-to-sample distances.

Experimental series	Neutral O-atom density [m^{-3}]	Neutral O-atom flux [$m^{-2}\,s^{-1}$]
150 mm coil-to-sample distance	3.4×10^{21}	5.3×10^{23}
300 mm coil-to-sample distance	3.2×10^{21}	5.1×10^{23}
500 mm coil-to-sample distance	2.4×10^{21}	3.7×10^{23}

angle was 45°. During XPS measurements, an electron gun was used for the surface charge neutralization. The measured spectra were referenced to the C–C/C–H peak of the C 1 s at 284.8 eV. The software MultiPak v8.1c (Physical Electronics, Munich, Germany) was used for the evaluation of the measured spectra.

3. Results and discussion

The wettability of the samples was evaluated immediately after treatments. The WCA of original samples was 111 ± 4°. The treatment of PTFE samples in a dense H_2 plasma in the H-mode caused a small increase of the wettability because the WCA dropped to 94 ± 3°. The decrease of the WCA after H_2 plasma treatment is explained by defluorination of the surface film and thus the formation of a very thin film of polyolefin-like structures. The composition of the surface of H_2 plasma-treated samples as deduced from the XPS survey spectra was 75.4 at.% of carbon, 20.8 at.% of fluorine, and 3.8 at.% of oxygen. Here we should note that the composition of the untreated PTFE was 32 at.% of carbon and 68 at.% of fluorine.

Systematic measurements of the surface wettability after the treatment with oxygen atoms were performed for all positions marked in Fig. 2. The evolution of the surface wettability of samples pretreated by H_2 plasma and then treated in the afterglow of O_2 plasma is shown in Fig. 3. The measured value at the treatment time of 0 s corresponds to the sample treated with H_2 plasma only. The evolution of surface wettability, presented in Fig. 3, shows interesting results that are worth discussing. One can observe deep, almost overlapping minima in all curves. As mentioned above, the WCA of the H_2 plasma-treated sample is large at about 94°. Even a very short treatment time in O_2-plasma afterglow causes a dramatic drop in the WCA. The very low WCA is explained by surface activation, i.e. formation of oxygen-functional groups on the surface of H_2 plasma-pretreated samples. After the

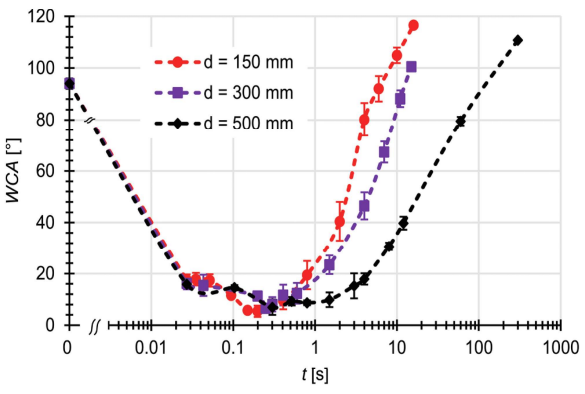

Fig. 3. Dependence of WCA on treatment time for all series of experiments.

shortest treatment time of 0.03 s, the WCA drops to approximately 15° to 18°. Fig. 3 indicates that this initial drop does not depend on the position of the sample in the afterglow. Further treatment in the afterglow of the O_2 plasma causes an additional decrease of the WCA for about 10°. The prolonged treatment, however, causes an increase of the WCA until a complete hydrophobic recovery is observed. The hydrophobic recovery is faster for samples treated closer to the RF coil. The x-axis scale in Fig. 3 has to be logarithmic because the duration of the hydrophobic recovery depends significantly on the position of the sample in the oxygen plasma afterglow upon treatment.

Detailed examination of the Fig. 3. indicates that the WCA minima at coil-to-sample distances of 150, 300, and 500 mm are between 5° and 7°. The minima are achieved at the treatment times between 0.2 and 0.3 s. It is evident from Fig. 3 that functionalization occurs quickly, especially at the closest coil-to-sample distance.

It is generally accepted that the main reactants in O_2 plasma afterglows are atoms in the ground state. The O-atom density in the afterglow is several orders of magnitude higher than the density of other reactants, particularly ionized atoms or molecules [17,41]. Fig. 4 shows the WCA versus the fluence of neutral O-atoms for the samples treated at all three positions in the O_2 afterglow. The distance between the curves is somehow smaller but the effect is not significant. The minima appear at the O-atom fluences of 1×10^{23} m^{-2}, 1.3×10^{23} m^{-2}, and 3×10^{23} m^{-2} for the afterglow distances of 150, 300, and 500 mm, respectively.

The minima on the curves, shown in Figs. 3 and 4 can be explained by two competitive surface reactions: functionalization and etching. The pretreatment of PTFE samples with H_2 plasma results in the depletion of fluorine in the surface layer. The reactive oxygen species readily interact with – CH groups and carbon dangling bonds on the surface layer of the PTFE, which is almost free of fluorine. The O atoms in the afterglow have a kinetic energy of only about 1/25 eV. However, the chemical bonding of the O atoms to the surface is a highly exothermic process and thus likely to occur [42]. Experimental results on the evolution of the functional groups on the surface of a polyolefine confirmed a very high probability for the formation of hydroxyl groups on the surface of pristine polyolefine [43,44]. At optimal, O atoms are chemically bound to the sample surface, thus forming polar functional groups resulting in the WCA decrease. Simultaneously to binding of O atoms to hydrocarbons, etching occurs as well, resulting in thinning of the fluorine-depleted surface layer. The etching rate is very low, but the fluorine-depleted film's thickness is very small, too. At large O-atom fluences, the entire fluorine-depleted film is etched away, and the polymer wettability regains the original value, typical for the untreated PTFE.

Because the WCA minima of the samples treated at various afterglow positions are achieved at very similar O-atom fluences, and the absolute WCA values are very similar, it is reasonable to hypothesize that the initial stage of functionalization depends on the fluence of received O atoms. However, after receiving the O-atom fluences above 3×10^{23} m^{-2}, the WCA of samples treated closer to the coil starts to rise faster than the WCA of samples treated further away from the coil. The differences in the wettability among samples treated at different positions in the oxygen plasma afterglow at the same received O-atom fluence could be explained by different etching rates at the different coil-to-sample distances. Higher etching rates at closer coil-to-sample distances could be a consequence of other reactive oxygen species. Fig. 2 qualitatively shows that the density of charged particles decreases with increasing distance from the RF coil. The presence of higher amounts of ions may well explain the faster etching of samples closer to the coil. The absolute density of ions is, of course, orders of magnitude lower than the density of O atoms, but the etching rate may also be orders of magnitude higher than at the presence of only O atoms. However, the presence of oxygen ions should not influence the initial functionalization because the initial interaction probability is high [42].

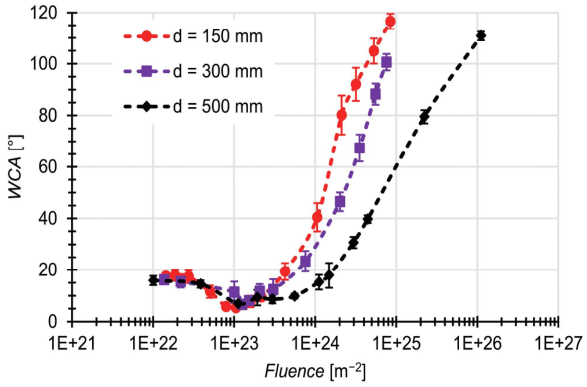

Fig. 4. WCA versus the fluence of neutral-O atoms - parameter is the distance of the sample from the RF coil.

The upper discussion proposes surface kinetics, particularly functionalization and etching upon the treatment of the H_2-plasma pretreated PTFE in the flowing afterglow of O_2 plasma. Both processes shall influence the surface composition. Functionalization shall cause an increase in the oxygen concentration, while etching shall cause the reappearance of the fluorocarbon layer at the surface. We performed a systematic XPS analysis of treated samples to further elaborate on both effects. Fig. 5 and Fig. 6 show the dependences of elemental compositions of the PTFE surfaces on treatment times in O_2 afterglow for the experiments performed at the coil-to-sample distances of 150 and 500 mm, respectively.

Both Figs. 5 and 6 reveal the results that are sound with the upper discussion regarding the evolution of the surface wettability. The oxygen and fluorine concentrations of the sample treated with H_2 plasma only are low (this case is shown at treatment time 0 s in Figs. 5 and 6). The oxygen concentration increases to approximately 20 at.% even at the shortest treatment time in the O_2 plasma afterglows. The pronounced increase in the oxygen concentration, as measured by XPS, corresponds to the significant increase of the surface wettability (decrease in the WCA). The oxygen concentrations remain fairly constant in ranges of treatment times from 0.03 s to about 1 s (at the coil-to-sample distance of 150 mm) or 10 s (at the coil-to-sample distance of 500 mm). This behavior clearly confirms the statement about the saturation of the sample surface with polar oxygen-containing functional groups. The fluorine contents remain relatively intact in these ranges of treatment times and are essentially the same as of the sample treated only with H_2 plasma. After prolonged treatment, however, the F concentration starts increasing and eventually reaches the value typical for the pristine PTFE. The XPS results are, therefore, in agreement with the WCA measurements.

Comparison of Figs. 5 and 6 show that the curves representing the WCA and the elemental compositions are similar at both coil-to-sample distances. A difference appears after prolonged treatment in oxygen plasma afterglow. This difference could be attributed to somewhat higher O-atom density at the coil-to-sample distance of 150 mm (Table 1), but the more feasible explanation is the lack of other reactive species capable of etching polymers at the coil-to-sample distance of 500 mm.

Additionally, Fig. 5 shows the evolutions of elemental composition and WCA on the sample surface versus the fluence of neutral O atoms of the experiments performed at the coil-to-sample distance of 150 mm (see the secondary x-axis at the top of the diagram). Within the fluence range from 1.5×10^{22} to 6×10^{23} m^{-2}, the amount of oxygen in the treated surface layer is approximately 20 at. %. The amount of oxygen at the sample's surface remains constant, while the WCA starts to decrease with increasing O-atom fluence and reaches its minimum of 5° at the O-atom fluence of 1×10^{23} m^{-2}. Interestingly enough, the oxygen content in the surface layer remains constant (at about 20 at. %) up to the fluence of 5×10^{23} m^{-2}, at which WCA reaches the value of 20° again. Within the O-atom fluence range of 1.5×10^{22} to 1×10^{23} m^{-2}, the F

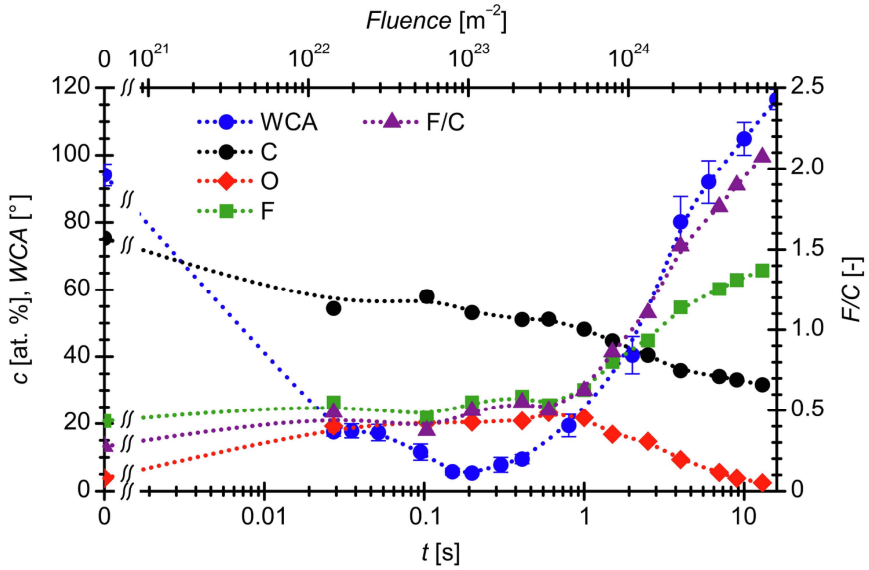

Fig. 5. Dependences of elemental composition and WCA versus: the treatment time and the fluence of neutral O-atoms of samples treated at coil-to-sample distance of 150 mm.

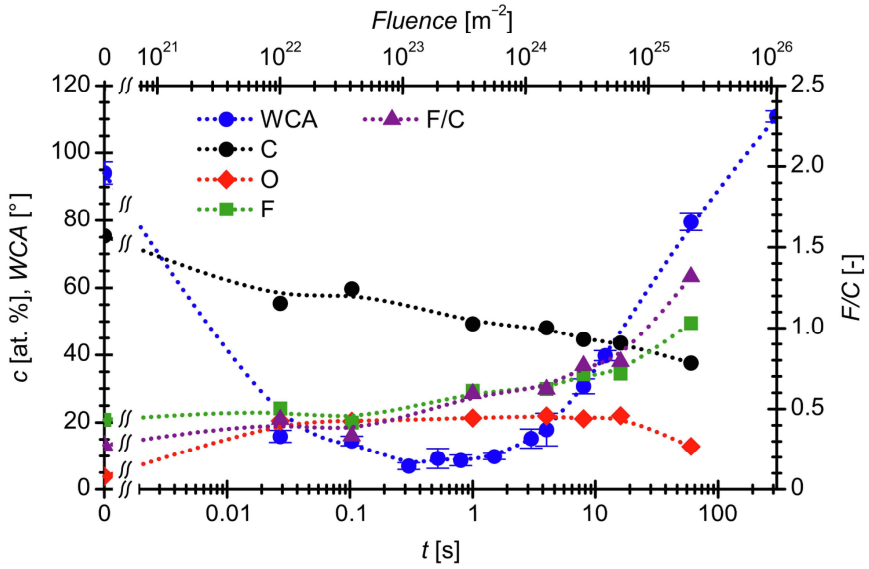

Fig. 6. Dependences of elemental composition and WCA versus: the treatment time and the fluence of neutral O-atoms of samples treated at coil-to-sample distance of 500 mm.

content and the F/C ratio in the surface layer are approximately constant in ranges of 20 to 25° at. % and 0.3 to 0.5, respectively. Above the O-atom fluence of 1×10^{23} m^{-2}, where WCA reaches its minimum, both F content and F/C ratio start to rise moderately. Constant O and F contents and F/C ratio in the surface layer at the O-atom fluences between 1.5×10^{22} and 1×10^{23} m^{-2}, where WCA decreases from 18 to 5°, could be explained by the fact that the WCA of treated PTFE surface does not depend only on its elemental composition, but it also depends on surface roughness, that is known to increase with the increasing O-atom fluence causing continuous etching [27,45]. The discrepancy between the behaviors of WCA and surface composition might also be explained by the etching of initially formed hydroxyl groups and the formation of less hydrophilic groups [46,47].

The diagram of Fig. 6 also shows the dependences of the elemental composition and the WCA of the treated PTFE surface versus the fluence of neutral O atoms (secondary x-axis) at the coil-to-sample distance of 500 mm. The results are similar to those presented in Fig. 5, but there are some differences. At the position of 500 mm, the WCA is rising slower with the increasing O-atom fluence in the range between 1×10^{23} m^{-2} and 6×10^{23} m^{-2} than at position 150 mm. Above the O-atom fluence of 1.5×10^{24} m^{-2}, both WCA and F/C start to rise rapidly.

The slight shift of WCA minimum to somewhat higher O-atom fluence and the extended range of O-atom fluences before WCA starts to rise rapidly, at a coil-to-sample distance of 500 mm, could be explained by slower etching of the surface layer at this position, where the density of other reactive species (charged molecules) is marginal as compared to

the density of neutral O-atoms. Consequently, a somewhat higher O atom fluence is needed to achieve optimal surface roughness at a longer distance from the RF coil.

Plasma-treated polymers usually do not exhibit stable wettability over prolonged ageing. All experiments reported in this manuscript were performed immediately after the plasma treatment (WCA in particular) or in a reasonable time, say about 10 min after the plasma treatment (XPS). The ageing of plasma-activated polymers (or hydrophobic recovery) is explained by different effects including the reorientation of polar groups into the surface layer of polymer or the ablation of molecular fragments from the polymer surfaces [48]. The ageing was not only observed when a polymer was treated with oxygen plasma but also with a plasma sustained in argon at the pressure of 10 Pa and discharge power as low as several W [49]. Interestingly enough, the WCA did not increase monotonously with ageing time for the case a plasma-treated polymer was mixed with graphene nanomaterials [50]. The grafting of hydrophilic polymers on plasma-activated polymer substrates suppresses the hydrophobic recovery, but the ageing phenomenon persists even in such cases [51].

4. Conclusion

A new method was presented for the hydrophilization of fluorine-containing polymers in a highly controllable manner. The method comprises two steps. First, the PTFE samples are exposed to dense H_2 plasma sustained by an inductively coupled RF discharge in the H-mode. Then, the samples are exposed to O_2 plasma afterglow. The treatment with H_2 plasma causes the depletion of fluorine and the binding of hydrogen within the surface film. Reactive oxygen species in the afterglow cause functionalization with polar functional groups. The range of O-atom fluences useful for the optimization of the surface wettability was determined. The fluences of the order of 10^{22} m^{-2} caused significant functionalization, while fluences above approximately 10^{24} m^{-2} caused the loss of hydrophilicity, which was due to the etching of the fluorine-depleted surface film. Excellent wettability of PTFE with the water static contact angle as low as 5° was achieved in a limited range of O-atom fluences peaking at about 1×10^{23} m^{-2}.

The first treatment was performed in a dense H_2 plasma, and the treatment time was 1 s. Such a short treatment caused a drop in the fluorine concentration within the surface film as probed by XPS from 66 as found for the uuntreated PTFE to approximately 20 at.%. Knowing the penetration depth of the photoelectrons, one can conclude that the surface is almost free from fluorine after the hydrogen plasma treatment. The rapid removal of F atoms was explained by the C − F bond scission due to irradiation of the sample surface with VUV radiation arising from resonant states of both H atoms (Lyman series) and H_2 molecules (Lyman and Werner bands). The dangling carbon bonds were most probably occupied with hydrogen atoms, thus forming a very thin surface film resembling polyolefins.

Polyolefins are known to chemically interact with oxygen atoms, even at room temperature, forming polar oxygen-containing functional groups. These functional groups, in turn, cause a significant increase in wettability. The oxidation kinetics was studied systematically versus the fluence of oxygen atoms. Well-defined minima in the WCA, corresponding to the maxima in the oxygen concentrations as measured by XPS, were observed at various experimental conditions. The minima appear after receiving the fluences of approximately 1×10^{23} O-atoms / m^{-2}. Increasing O-atom fluence causes slow etching of the modified surface film. Large fluencies of the order of 10^{25} m^{-2} cause almost complete removal of the surface film depleted of fluorine, and thus the loss of hydrophilicity and the re-establishment of the original surface composition typical for the untreated PTFE materials. An excellent agreement between wettability, as determined by WCA, and surface composition as measured by XPS was observed.

Experiments on the surface functionalization with polar functional groups were performed in flowing O_2 plasma afterglow. The samples were positioned at a few distances from the dense plasma within the RF coil, to study details, in particular the influence of other reactive oxygen plasma species on the surface kinetics. Neutral oxygen atoms in the ground state are by far the most important reactants governing the functionalization kinetics, but the experiments showed rather clearly that other species (probably positively charged ions) also influence the etching rate. Namely, the full restoration of the original surface composition was observed at the O-atom fluence of 1×10^{25} m^{-2}, in the case in which samples were placed 150 mm away from the RF coil, while an order of magnitude higher O-atom fluence was necessary at the distance of 500 mm. The O-atom densities at both afterglow locations were measured with a catalytic probe, and they were approximately 3.4×10^{21} m^{-3} at 150 mm, and 2.4×10^{21} m^{-3} at 500 mm. The difference was, therefore, marginal as compared to the fluences required for complete restoration of the original structure, thus suggesting more complex surface etching kinetics than only interaction with O atoms.

The results reported in this paper can give directions for any upscaling of the treatment procedure. The results clearly show that the decisive parameter is the fluence of O atoms. If such a fluence is feasible to assure in a large system, the technique is useful for ecologically benign surface activation of PTFE or similar materials.

CRediT authorship contribution statement

Dane Lojen: Visualization, Investigation, Formal analysis, Writing – original draft. **Rok Zaplotnik:** Conceptualization, Methodology, Supervision. **Gregor Primc:** Validation, Data curation. **Miran Mozetič:** Writing – original draft, Funding acquisition. **Alenka Vesel:** Supervision, Formal analysis, Project administration, Writing – review & editing.

Declaration of Competing Interest

The authors declare that they have no known competing financial interests or personal relationships that could have appeared to influence the work reported in this paper.

Acknowledgment

The authors acknowledge the financial support from the Slovenian Research Agency (research core funding No. P2-0082), and project L2-2616 “Selected area functionalization of polymeric components by gaseous plasma”. D.L. also acknowledges the grant for a young researcher.

References

[1] M. Okazaki, K. Yamashita, M. Okazaki, Comparison of hexagonal crystal structures between fluorapatite and polytetrafluoroethylene, BME. 28 (1) (2017) 3–8.
[2] K.-S. Kwon, M.K. Rahman, T.H. Phung, S. Hoath, S. Jeong, J.S. Kim, Review of digital printing technologies for electronic materials, Flex. Print. Electron. (2020), https://doi.org/10.1088/2058-8585/abc8ca.
[3] R. Takata, T. Iwao, M. Yumoto, Surface Modification of PTFE Using Low-Energy Nitrogen Ion Irradiation: Improvement in Adhesive Strength on Modification of Deep Modifying Layer, Electron Comm Jpn. 99 (2016) 93–99, https://doi.org/10.1002/ecj.11844.
[4] L. Ma, X. Li, X. Guo, Y. Jiang, X. Li, H. Guo, B. Zhang, Y. Xu, X. Wang, Q. Li, Promotion of Endothelial Cell Adhesion and Antithrombogenicity of Polytetrafluoroethylene by Chemical Grafting of Chondroitin Sulfate, ACS Appl. Bio Mater. 3 (2020) 891–901, https://doi.org/10.1021/acsabm.9b00970.
[5] J.J. Bikerman, CAUSES OF POOR ADHESION: WEAK BOUNDARY LAYERS, Ind. Eng. Chem. 59 (1967) 40–44, https://doi.org/10.1021/ie51403a010.
[6] H. Schonhorn, R.H. Hansen, Surface treatment of polymers for adhesive bonding, J. Appl. Polym. Sci. 11 (1967) 1461–1474, https://doi.org/10.1002/app.1967.070110809.
[7] M. Gabriel, M. Dahm, C.-F. Vahl, Wet-chemical approach for the cell-adhesive modification of polytetrafluoroethylene, Biomed. Mater. 6 (2011) 035007. https://doi.org/10.1088/1748-6041/6/3/035007.
[8] J.T. Marchesi, K. Ha, A. Garton, G.S. Swei, K.W. Kristal, Adhesion to Sodium Naphthalenide Treated Fluoropolymers. Part II. Effects of Treatment Conditions and Fluoropolymer Structure, The Journal of Adhesion. 36 (1991) 55–69, https://doi.org/10.1080/00218469108026523.

[9] S. Ebnesajjad, Fluoroplastics, Volume 1: Non-Melt Processible Fluoroplastics, William Andrew, 2000.

[10] I. Mathieson, D.M. Brewis, I. Sutherland, R.A. Cayless, Pretreatments of Fluoropolymers, The Journal of Adhesion. 46 (1994) 49–56, https://doi.org/10.1080/00218469408026648.

[11] Y. Ohkubo, K. Endo, K. Yamamura, Adhesive-free adhesion between heat-assisted plasma-treated fluoropolymers (PTFE, PFA) and plasma-jet-treated polydimethylsiloxane (PDMS) and its application, Sci Rep. 8 (2018) 18058, https://doi.org/10.1038/s41598-018-36469-y.

[12] Y. Ohkubo, K. Ishihara, M. Shibahara, A. Nagatani, K. Honda, K. Endo, K. Yamamura, Drastic Improvement in Adhesion Property of Polytetrafluoroethylene (PTFE) via Heat-Assisted Plasma Treatment Using a Heater, Sci Rep. 7 (2017) 9476, https://doi.org/10.1038/s41598-017-09901-y.

[13] S. Ebnesajjad, in: Handbook of Adhesives and Surface Preparation, Elsevier, 2011, pp. 49–81.

[14] N.T. Klokkou, D.J. Rowe, B.M. Bowden, N.P. Sessions, J.J. West, J.S. Wilkinson, V. Apostolopoulos, Structured surface wetting of a PTFE flow-cell for terahertz spectroscopy of proteins, Sensors and Actuators B: Chemical. 352 (2022), 131003, https://doi.org/10.1016/j.snb.2021.131003.

[15] U. Fantz, S. Briefi, D. Rauner, D. Wünderlich, Quantification of the VUV radiation in low pressure hydrogen and nitrogen plasmas, Plasma Sources Sci. Technol. 25 (2016) 045006. https://doi.org/10.1088/0963-0252/25/4/045006.

[16] A. Fridman, Plasma Chemistry (2008) 1022.

[17] H. Tanaka, M. Inokuti, Plasma Processing of Materials and Atomic, Molecular, and Optical Physics. An Introduction, in: Advances In Atomic, Molecular, and Optical Physics, Elsevier, 2000, pp. 1–17.

[18] D. Popović, M. Mozetič, A. Vesel, G. Primc, R. Zaplotnik, Review on vacuum ultraviolet generation in low-pressure plasmas, Plasma Processes and Polymers. 18 (2021) 2100061, https://doi.org/10.1002/ppap.202100061.

[19] D. Lojen, R. Zaplotnik, G. Primc, M. Mozetič, A. Vesel, Effect of VUV radiation and reactive hydrogen atoms on depletion of fluorine from polytetrafluoroethylene surface, Applied Surface Science. 533 (2020), 147356, https://doi.org/10.1016/j.apsusc.2020.147356.

[20] G. Primc, Recent Advances in Surface Activation of Polytetrafluoroethylene (PTFE) by Gaseous Plasma Treatments, Polymers. 12 (2020) 2295, https://doi.org/10.3390/polym12102295.

[21] S.-H. Hong, T.-H. Kim, S. Choi, Hydrophilic Surface Modification of Polytetrafluoroethylene Film with Gliding Arc Plasma, Applied Science and Convergence, Technology. 28 (4) (2019) 101–106.

[22] D.J. Wilson, R.L. Williams, R.C. Pond, Plasma modification of PTFE surfaces. Part I: Surfaces immediately following plasma treatment, Surf. Interface Anal. 31 (2001) 385–396, https://doi.org/10.1002/sia.1065.

[23] J.P. Badey, E. Espuche, D. Sage, B. Chabert, Y. Jugnet, C. Batier, T.M. Duc, A comparative study of the effects of ammonia and hydrogen plasma downstream treatment on the surface modification of polytetrafluoroethylene, Polymer. 37 (1996) 1377–1386, https://doi.org/10.1016/0032-3861(96)81135-9.

[24] N. Inagaki, S. Tasaka, T. Umehara, Effects of surface modification by remote hydrogen plasma on adhesion in poly(tetrafluoroethylene)/copper composites, (n. d.) 10.

[25] M.E. Ryan, J.P.S. Badyal, Surface Texturing of PTFE Film Using Nonequilibrium Plasmas, Macromolecules. 28 (1995) 1377–1382, https://doi.org/10.1021/ma00109a008.

[26] Y. Yamada, T. Yamada, S. Tasaka, N. Inagaki, Surface Modification of Poly (tetrafluoroethylene) by Remote Hydrogen Plasma, Macromolecules. 29 (1996) 4331–4339, https://doi.org/10.1021/ma951072r.

[27] N. Vandencasteele, B. Nisol, P. Viville, R. Lazzaroni, D.G. Castner, F. Reniers, Plasma-Modified PTFE for Biological Applications: Correlation between Protein-Resistant Properties and Surface Characteristics, Plasma Process. Polym. 5 (2008) 661–671, https://doi.org/10.1002/ppap.200700143.

[28] L.F. Dumée, H. Alglave, T. Chaffraix, B. Lin, K. Magniez, J. Schütz, Morphology-properties relationship of gas plasma treated hydrophobic meso-porous membranes and their improved performance for desalination by membrane distillation, Applied Surface Science. 363 (2016) 273–285, https://doi.org/10.1016/j.apsusc.2015.12.034.

[29] C. Jie-Rong, T. Wakida, Studies on the surface free energy and surface structure of PTFE film treated with low temperature plasma, Journal of Applied Polymer Science. 63 (1997) 1733–1739, https://doi.org/10.1002/(SICI)1097-4628(19970328)63:13<1733::AID-APP4>3.0.CO;2-H.

[30] Z. Kolská, A. Řezníčková, V. Hnatowicz, V. Švorčík, PTFE surface modification by Ar plasma and its characterization, Vacuum. 86 (2012) 643–647, https://doi.org/10.1016/j.vacuum.2011.07.015.

[31] E.A.D. Carbone, M.W.G.M. Verhoeven, W. Keuning, J.J.A.M. van der Mullen, PTFE treatment by remote atmospheric Ar/O_2 plasmas: a simple reaction scheme model proposal, J. Phys.: Conf. Ser. 715 (2016), 012011, https://doi.org/10.1088/1742-6596/715/1/012011.

[32] K. Ishikawa, N. Sumi, A. Kono, H. Horibe, K. Takeda, H. Kondo, M. Sekine, M. Hori, Synergistic Formation of Radicals by Irradiation with Both Vacuum Ultraviolet and Atomic Hydrogen: A Real Time In Situ Electron Spin Resonance Study, J. Phys. Chem. Lett. 2 (2011) 1278–1281, https://doi.org/10.1021/jz2002937.

[33] K. Gotoh, Y. Nakata, M. Tagawa, M. Tagawa, Wettability of ultraviolet excimer-exposed PE, PI and PTFE films determined by the contact angle measurements, Colloids and Surfaces A: Physicochemical and Engineering Aspects. 224 (2003) 165–173, https://doi.org/10.1016/S0927-7757(03)00263-2.

[34] P. Slepička, O. Neděla, P. Sajdl, Z. Kolská, V. Švorčík, Polyethylene naphthalate as an excellent candidate for ripple nanopatterning, Applied Surface Science. 285 (2013) 885–892, https://doi.org/10.1016/j.apsusc.2013.09.007.

[35] K. Gotoh, Y. Nagai, Y. Yonehara, Y. Kobayashi, Surface hydrophilization of two polyester films by atmospheric-pressure plasma and ultraviolet excimer light exposures, Journal of Adhesion Science and Technology. 29 (2015) 473–486, https://doi.org/10.1080/01694243.2014.995342.

[36] A. Hozumi, H. Inagaki, T. Kameyama, The hydrophilization of polystyrene substrates by 172-nm vacuum ultraviolet light, Journal of Colloid and Interface Science. 278 (2004) 383–392, https://doi.org/10.1016/j.jcis.2004.06.005.

[37] A. Vesel, D. Lojen, R. Zaplotnik, G. Primc, M. Mozetič, J. Ekar, J. Kovač, M. Gorjanc, M. Kurečič, K. Stana-Kleinschek, Defluorination of Polytetrafluoroethylene Surface by Hydrogen Plasma, Polymers. 12 (2020) 2855, https://doi.org/10.3390/polym12122855.

[38] K. Kutasi, R. Zaplotnik, G. Primc, M. Mozetic, Controlling the oxygen species density distributions in the flowing afterglow of O_2/Ar–O_2 surface-wave microwave discharges, J. Phys. D: Appl. Phys. 47 (2014) 025203. https://doi.org/10.1088/0022-3727/47/2/025203.

[39] I. Šorli, R. Ročak, Determination of atomic oxygen density with a nickel catalytic probe, Journal of Vacuum Science & Technology A: Vacuum, Surfaces, and Films. 18 (2000) 338–342, https://doi.org/10.1116/1.582189.

[40] J.C. Greaves, J.W. Linnett, The recombination of oxygen atoms at surfaces, Trans. Faraday Soc. 54 (1958) 1323, https://doi.org/10.1039/tf9585401323.

[41] K.J. Taylor, G.R. Tynan, Control of dissociation by varying oxygen pressure in noble gas admixtures for plasma processing, Journal of Vacuum Science & Technology A: Vacuum, Surfaces, and Films. 23 (2005) 643–650, https://doi.org/10.1116/1.1931682.

[42] Y. Fukunaga, R.C. Longo, P.L.G. Ventzek, B. Lane, A. Ranjan, G.S. Hwang, G. Hartmann, T. Tsutsumi, K. Ishikawa, H. Kondo, M. Sekine, M. Hori, Interaction of oxygen with polystyrene and polyethylene polymer films: A mechanistic study, Journal of Applied Physics. 127 (2020) 023303. https://doi.org/10.1063/1.5127863.

[43] L.J. Gerenser, XPS studies of in situ plasma-modified polymer surfaces, Journal of Adhesion Science and Technology. 7 (1993) 1019–1040, https://doi.org/10.1163/156856193X00556.

[44] M. Morra, E. Occhiello, F. Garbassi, Chemical reactions on plasma-treated polyethylene surfaces, Journal of Adhesion Science and Technology. 7 (1993) 1051–1063, https://doi.org/10.1163/156856193X00574.

[45] S.A. Rich, T. Dufour, P. Leroy, L. Nittler, J.J. Pireaux, F. Reniers, Low-density polyethylene films treated by an atmospheric Ar–O_2 post-discharge: functionalization, etching, degradation and partial recovery of the native wettability state, J. Phys. D: Appl. Phys. 47 (2014) 065203. https://doi.org/10.1088/0022-3727/47/6/065203.

[46] T. Shikata, M. Okuzono, Are All Polar Molecules Hydrophilic? Hydration Numbers of Ketones and Esters in Aqueous Solution, J. Phys. Chem. B. 117 (2013) 7718–7723, https://doi.org/10.1021/jp4029968.

[47] T. Dufour, J. Minnebo, S. Abou Rich, E.C. Neyts, A. Bogaerts, F. Reniers, Understanding polyethylene surface functionalization by an atmospheric He/O_2 plasma through combined experiments and simulations, J. Phys. D: Appl. Phys. 47 (2014) 224007. https://doi.org/10.1088/0022-3727/47/22/224007.

[48] P. Slepicka, N. Slepickova Kasalkova, E. Stranska, L. Bacakova, V. Svorcik, Surface characterization of plasma treated polymers for applications as biocompatible carriers, Express Polym. Lett. 7 (2013) 535–545, https://doi.org/10.3144/expresspolymlett.2013.50.

[49] P. Slepička, L. Peterková, S. Rimpelová, A. Pinkner, N. Slepičková Kasálková, Z. Kolská, T. Ruml, V. Švorčík, Plasma activated perfluoroethylenepropylene for cytocompatibility enhancement, Polymer Degradation and Stability. 130 (2016) 277–287, https://doi.org/10.1016/j.polymdegradstab.2016.06.017.

[50] P. Slepička, N. Slepičková Kasálková, A. Pinkner, P. Sajdl, Z. Kolská, V. Švorčík, Plasma induced cytocompatibility of stabilized poly-L-lactic acid doped with graphene nanoplatelets, Reactive and Functional Polymers. 131 (2018) 266–275, https://doi.org/10.1016/j.reactfunctpolym.2018.08.006.

[51] M. Travnickova, N.S. Kasalkova, A. Sedlar, M. Molitor, J. Musilkova, P. Slepicka, V. Svorcik, L. Bacakova, Differentiation of adipose tissue-derived stem cells towards vascular smooth muscle cells on modified poly(L-lactide) foils, Biomed. Mater. 16 (2021) 025016. https://doi.org/10.1088/1748-605X/abaf97.

Chapter 5

Power Characteristics of Multiple Inductively Coupled RF Discharges Inside a Metallic Chamber

Gaseous non-equilibrium inductively coupled low-pressure cold plasmas can be effectively coupled at high power densities and moderately high pressures only in relatively small volumes. This represents an obstacle to their use in industrial applications where there is a need for treatment of various dimensions and large atom densities, as well as high radiation intensities at moderate gas pressures.

Several solutions have been developed, including stainless steel reactors with multiple coils mounted on the top flange connected in parallel, low-impedance antennas mounted inside the stainless-steel reactor, and helicons mounted on dielectric covers of the stainless steel reactors.

However, there are certain drawbacks of the developed solutions. For example, systems with multiple coils connected in parallel mounted on the top flange of the reactor have typical problems regarding power distribution between the coils, which can be substantially improved by the use of a power distributor consisting of symmetrical hot wire connectors with equal impedances and grounding connections connected to the shielding of coaxial wire that are also symmetrical to provide equal impedances (coil geometry must also be the same). Additionally to the power distribution problem, there is a problem regarding ions, atoms, and radiation density because the coils are typically mounted onto dielectric cups above the reactor flange, resulting in a loss of charged particles and neutrals due to their recombination on the surface of the glass cup and stainless steel flange.

Because our goal is upscaling the PTFE hydrophilisation process explained in chapters 2, 3 and 4, we had to solve the problems regarding ICP plasma in industrial-scale systems.

We designed a new innovative industrial-scale stainless-steel plasma system with four inductors mounted in parallel. The innovative power distributor for the parallel connections of coils with a single RF generator via a matching network was developed. The power distributor was designed based on the perfect symmetry of electrical leads of hot wire connectors and the ground connectors of individual coils while enabling precise impedance adjustments by use of sliders for each individual lead of each hot wire and the ground connector of each coil. Additionally, a new type of dielectric cup was invented and engineered. The dielectric cup consists of two glass tubes fused at the bottom. The inner tube is longer and the outer is shorter, having a flange for vacuum sealing. The coil is inserted into the slit between the two fused tubes. The new design of the cup shortened the path of the plasma into the volume of the stainless-steel reactor and therefore reduced the recombination, thus enabling higher densities of neutral atoms and ions. Furthermore,

in the new type of dielectric cup, plasma is generated in the middle of the coil within the volume of the discharge tube. This is superior to the design presented in the literature.

The diameter of the reactor is 0.6 m, and the height is 0.5 m. Four coils are centrally mounted onto the flange and sunk under the lower level of the flange within the specially designed dielectric cups with an internal diameter of discharge tubes of 36 mm. The coils are water-cooled and have 6 and ¾ turns. The dielectric cups are forced air-cooled.
The coils are connected to a custom-made matching network consisting of two Commet Maxi-Con variable capacitors (capacitances between 20 and 250 pF) connected into a gamma circuit. The power distributor was made of three 10 mm thick Vitroplast (FR4) layers, and the electrical leads were made of copper and brass (star-like shapes of distribution leads). The power distributor was connected to the matching network via a short coaxial wire. The matching network was connected to a 5 kW Advanced Energy Cesar 1350 RF generator with another coaxial wire. The chamber was pumped with a two-stage rotary pump with a nominal pumping speed of 40 m^3/h. Gas was leaked into the system through all four dielectric cups equipped with small diameter nozzles that were connected to a single tube leading to a needle valve that was connected to an oxygen bottle. The pressure in the reactor was measured with an absolute capacitive gauge. The new innovative plasma system is shown in Figure 9.

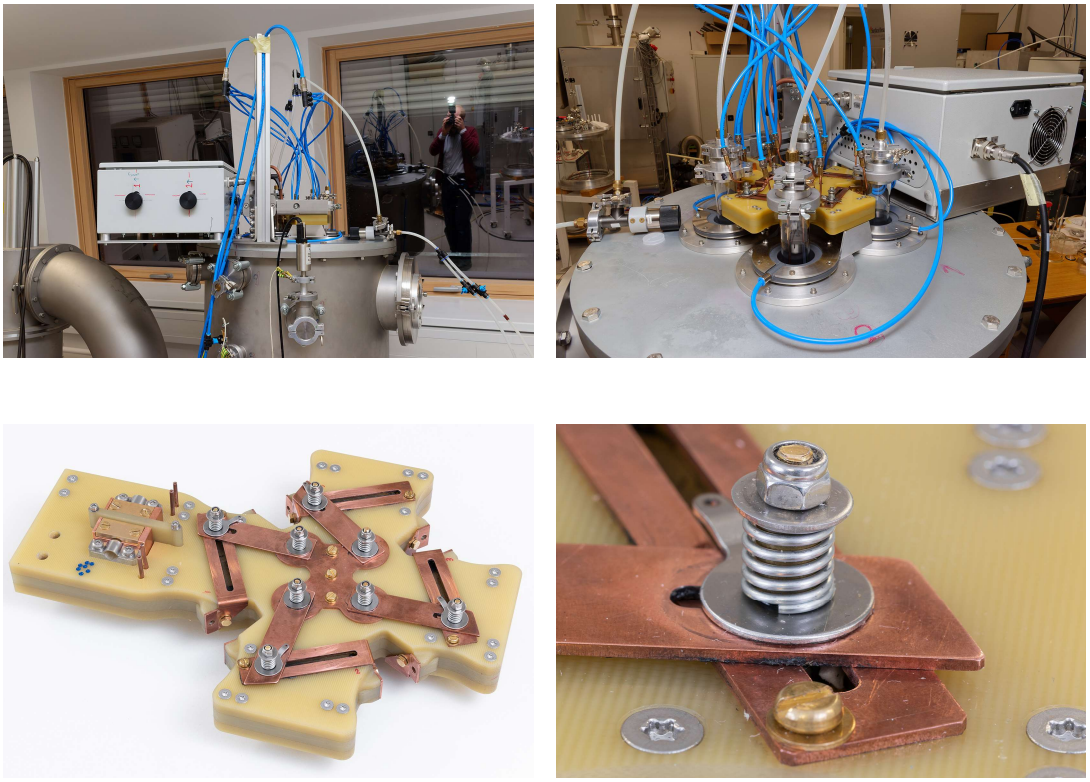

Figure 9: The innovative plasma reactor (upper left), the flange of the reactor (upper right), the power divider (lower left), and a detail of the impedance regulation slider (lower right).

After assembly, the plasma system was tested to confirm that oxygen plasma was sustained. The impedances of individual coils were adjusted based on the powers required for E- to H-mode plasma transitions in each coil. E-mode plasma differs from H-mode

plasma by its luminosity, which is about two orders of magnitude greater in H-mode plasma (as measured by OES) than in E-mode plasma, so the transitions can be easily recognised by the naked eye. Besides that, H-mode plasma has a much higher density of ions than E-mode plasma. Initially, the sliders of the power divider were carefully aligned. Alignment of the sliders was done by igniting plasma in E-mode in all four coils, increasing the RF power very slowly, identifying the order of the E- to H-mode transitions for each coil, decreasing the impedances of coils with transitions at higher power, and increasing the impedances of coils with transitions at lower power. Additional impedance adjustments were made by aligning the spacings between the loops of the coils. After several iterations, the power increases between the E- to H-modes of individual coils became more even, and the power required to sustain H-mode plasma in all four coils was substantially decreased.

After the impedances were aligned, the powers required for the transitions of plasma in each coil from E- to H-mode and from H- to E-mode in the dependence on the oxygen pressure in the reactor were systematically characterised. At each selected pressure between 5 and 25 Pa, at the required forward power of the generator for the sustaining of H-mode plasma, the matching network was optimised for the minimisation of reflected power. If the forward powers of transitions from E- to H-mode are plotted versus the oxygen pressure by the number of coils in H-mode (the order of coils in which plasma mode transitions occur is not taken into account), it can be seen that the increases in forwarding powers for each subsequent transition become almost perfectly linear.

To eliminate the effects of the matching network optimisation for H-mode plasma sustained in all four coils at specific pressures on the forward powers required for plasma mode transitions, the real powers of E- to H-mode transitions were calculated by subtraction of the reflected powers. Plotting the real powers of subsequent coils transitions from E- to H-mode versus pressure revealed that the curves are somewhat lower. It is worth highlighting that each subsequent transition of the coil from E- to H- mode requires approximately the same increase in real power as the previous transition. Theoretically, this means that several coils could be efficiently coupled in parallel in the manner demonstrated here.

If the forward powers of subsequent transitions from H- to E-mode are plotted by the number of coils in H-mode versus pressure, it becomes apparent that the transitions from H- to E-mode occur at much lower powers than transitions from E- to H-mode. The differences in forward powers between transitions of different coils from H- to E-mode appear because of uneven power distribution due to the matching network optimisation for the H-mode, which means that after one coil changes its mode to E, the energy absorption becomes less efficient and the remaining power is redistributed to other coils in H-mode. If the real powers of subsequent transitions from H- to E-mode are plotted by the number of coils in H-mode versus pressure, it can be seen that the power of transitions increases linearly with pressure.

Plotting the real power of subsequential transitions from E- to H-mode after subtracting the real powers of subsequential H- to E-mode transitions revealed the hysteresis, which increased with pressure in an almost linear manner, and equally for all four coils.

The sequential transition of coils from E-to H-modes are the consequence of plasma peculiarities, plasma impedances, and imperfection in the equalisation of coil impedances. The power is equally distributed when all four coils are sustaining the H-mode plasma. The power absorbed in E- mode is also marginal compared to the power absorbed in H-mode. Because the hysteresis is already high at moderate pressures, it is possible to ignite plasma at high power and then reduce the power for treatment to save energy. The minimum discharge power per coil in H-mode was approximately 300 W, which is comparable with simple single-coil plasma systems.

Plasma Science and Technology

PAPER

Power characteristics of multiple inductively coupled RF discharges inside a metallic chamber

To cite this article: Dane LOJEN *et al* 2022 *Plasma Sci. Technol.* **24** 015403

 Plasma Science and Technology

Plasma Sci. Technol. **24** (2022) 015403 (7pp) https://doi.org/10.1088/2058-6272/ac363f

Power characteristics of multiple inductively coupled RF discharges inside a metallic chamber

Dane LOJEN[1,2], Rok ZAPLOTNIK[1,3], Miran MOZETIČ[1,3], Alenka VESEL[1,3] and Gregor PRIMC[1,3]

[1] Department of Surface Engineering, Jozef Stefan Institute, Jamova cesta 39, 1000 Ljubljana, Slovenia
[2] Jozef Stefan International Postgraduate School, Jamova cesta 39, 1000 Ljubljana, Slovenia
[3] Plasmadis Ltd, Teslova ulica 30, 1000 Ljubljana, Slovenia

E-mail: rok.zaplotnik@ijs.si

Received 27 August 2021, revised 3 November 2021
Accepted for publication 3 November 2021
Published 25 November 2021

Abstract

The characteristics of an innovative configuration of multiple radiofrequency (RF) coils immersed in a large metallic chamber are presented. Water-cooled copper coils were mounted within the slits of double-walled glass tubes, which were immersed into a stainless-steel chamber. The coils were connected in parallel to a gamma-type matching network, powered by an RF generator operating at industrial frequency. Adjustable leads enabled optimisation of the line impedances and thus uniformly distributed RF power across the four coils. Transitions from E- to H-mode and vice versa were measured for all coils at various oxygen pressures between 5 and 25 Pa. A uniform plasma was sustained in H-mode at the absorbed power threshold, which increased monotonously with increasing pressure in the metallic chamber. All coils exhibit the same E- to H-mode transition hysteresis and need the same amount of power for transitioning from E- to H-mode. The setup enables maintaining uniform plasma in virtually any number of coils at high power without the risk of arcing and without the dead volume typical for a classical configuration with coils mounted outside the metallic chamber.

Keywords: inductively coupled plasma, large-area plasma, E- to H-mode transition, high power

1. Introduction

Inductively coupled radio-frequency (RF) plasmas are widely used for tailoring the surface properties of solid samples, such as cleaning, functionalisation, nanostructuring, etching and deposition of various coatings. The key advantage of such plasmas over those sustained by other types of discharges arises from the fact that inductively coupled plasma (ICP) is often only in contact with dielectric materials; thus, the risk for unwanted effects such as the sputtering of electrodes or electrode coating and heterogeneous surface recombination of plasma radicals is suppressed. ICPs in H-mode can be sustained at a relatively high power density (power absorbed by a unit volume) in a limited range of plasma volumes and pressures. Such plasmas cannot be sustained in large volumes at moderate pressures, which are usually needed in industrial applications. The solution to this natural limitation is to apply several coils mounted on a large vacuum chamber; however, sustaining uniform plasma in numerous coils still represents a technological challenge.

Inductively coupled RF discharges have been popular for sustaining gaseous plasma for decades. The discharges are self-sustained in such a configuration up to the atmospheric pressure and beyond of noble gas, providing that the electromagnetic field is large enough [1]. Sustaining such discharges in molecular gases at atmospheric pressure is more challenging, but specific solutions enable even such devices to be useful for gas-phase chemistry [2]. The majority of applications, however, employ low-pressure devices for sustaining stable and uniform ICPs. Two types of ICPs are most often used: cylindrical- and planar-type [3]. A classical cylindrical-type ICP configuration employs a coil wrapped around a cylindrical dielectric tube connected to an RF generator via a matching network [4]. Although the theoretical

background was elaborated decades ago [5], the theory of such discharges is still a subject of scientific interest [6].

ICP at low pressure can be sustained in two distinctive modes: the E- and H-mode [7]. The difference between modes is significant and visible with the naked eye because the H-mode is much more luminous than the E-mode. In E-mode, the primary coupling is capacitive, i.e. the discharge is governed by the capacitive character of the plasma impedance. In H-mode, however, the electrons are coupled with the induced electric field in the volume inside the coil rather than accelerated in the sheath next to the powered segment of the coil. This feature enables the ICP to be sustained at a large power density without the danger of melting the dielectric walls of the plasma reactor due to extensive ion bombardment. An excellent introduction to capacitive and inductive modes was published recently [8]. The transition between modes is indistinct at low pressures, below a few 0.1 Pa [9], but becomes abrupt at higher pressures. The plasma luminosity may rise by 3 orders of magnitude upon transition from E- to H-mode at the pressure of several tens of Pa [10–13]. Some authors also mention W-mode, characterised by the 'wave heating' of the electrons, resulting in efficient RF power absorption in the bulk of the plasma [9]. The W-mode is found in ICPs with magnetic field presence above a certain threshold value due to the helicon mode.

Initially, the ICP is always ignited in E-mode. The plasma transforms to H-mode under favourable conditions. The transformation occurs at a suitable forward RF power. The discharge impedance drops instantly at the transition, and the absorbed power increases instantly. Further increase of the available power causes the plasma density to increase. In the opposite direction, i.e. upon reducing the discharge power, plasma remains in H-mode (i.e. high plasma density and high luminosity) until a critical power is achieved. As soon as the power is lower than the critical value, the abrupt transition to E-mode occurs. The transition from E- to H-mode always occurs at lower forward power than the transition from the E-to-H-mode. The ICP is either in E-mode (low absorbed power) or H-mode (high absorbed power). In between, there is a so-called inaccessible region of absorbed powers [14]. With a fixed chamber geometry and coupling peculiarities, the width of the inaccessible region depends on the type of gas and increases with increasing pressure; it may be several 100 W. Details about the transition from E-to-H-mode in molecular gases at higher pressures have been published recently [15]. Discharge instabilities have been reported for ICPs sustained at a relatively low power densities in electronegative gases [16].

While the classical configuration with a coil wrapped around a dielectric tube is acceptable for treating various samples in small experimental plasma reactors, upscaling of the ICP sustained in H-mode to large systems is not trivial. One solution is the application of numerous coils mounted outside a large metallic chamber. Chang's group published an excellent paper revealing 16 coils on a single metallic chamber [17, 18]. The key technological challenge was the adjustment of line impedances. A direct connection from the coil's ground to the shield of the coaxial transmission line was vital to obtain H-mode plasmas within all coils. Namely, only equal ground paths for each coil enabled a relatively uniform distribution of available RF power to the plasmas in all coils. The authors [18] proved the principle for argon at a rather low pressure of 1.3 Pa. The operation of such devices with molecular gases at elevated pressures remains a technological challenge, despite recent achievements. For example, another group [19] reported a relatively uniform nitrogen plasma in a system almost identical to [18].

An alternative to a multi-coil system is to apply a spiral instead of a coil [20]. In such a case, the metallic flange is substituted with a dielectric one, and a spiral is mounted on the flange. Theoretical simulations show that the inductive component might be larger than the capacitive at RF power as low as 5 W [21]. The transitions between E- and H-mode in such systems were studied in detail for plasmas sustained in argon, nitrogen, oxygen and mixtures of these gases [22, 23]. Interestingly, they found a minimum power of solely 20 W for E- to H-mode transition in argon with a pressure of about 3 Pa. In mixtures of oxygen and nitrogen at the same pressure, transition occurred at about 5 times greater power. At a moderate pressure of 13 Pa, the transition occurred at about 200 W for molecular gases. Interestingly enough, theoretical predictions forecast the highest electron density in the middle of the plasma reactor, instead of at the spiral's proximity [24].

Another alternative is the application of low-impedance antennas. In this case, numerous loops are mounted inside a metallic chamber and coupled in parallel to an RF generator. One of the first reports was provided by Kim and Yeon [25]. They sustained plasma in argon at 2 Pa using an RF power of up to 5 kW. No apparent transition between the discharge modes was reported in this configuration. Simultaneously, Setsuhara *et al* [26] reported a similar device operating in argon at 1.5 Pa and found gradients in plasma parameters when a single RF generator was used to power multiple loops coupled in parallel. A more complex configuration of low-impedance antennas was published recently [27].

The preferred gas in the literature survey above is argon and the preferred pressure range is between 1 and 10 Pa. Multiple coils, however, may also be installed inside the chamber and operate at pressures as high as 300 Pa, as reported by Liang *et al* [28]. The arcing, which should appear at this pressure under ordinary conditions, was avoided by placing each coil in a tube kept at atmospheric pressure because the tubes were open to the outer environment through the hollow sustaining pole. With this innovative design, the authors [28] managed to sustain dense uniform plasma within the coils in a range of pressures between 10 and 300 Pa. The electron temperature was close to 1.5 eV and the density exceeded $10^{19}\,\mathrm{m}^{-3}$ at elevated pressures. However, these coils had a central magnetic core and were only used as an antenna, forming plasma outside the coil.

In the present paper, we present the innovative configuration of multiple RF coils immersed in a large metallic chamber in such a way that ICP is excited inside the coil where the magnetic field is largest. With this configuration, one can ignite an H-mode ICP over a large area inside the metallic chamber at pressures up to few tens of Pa. The

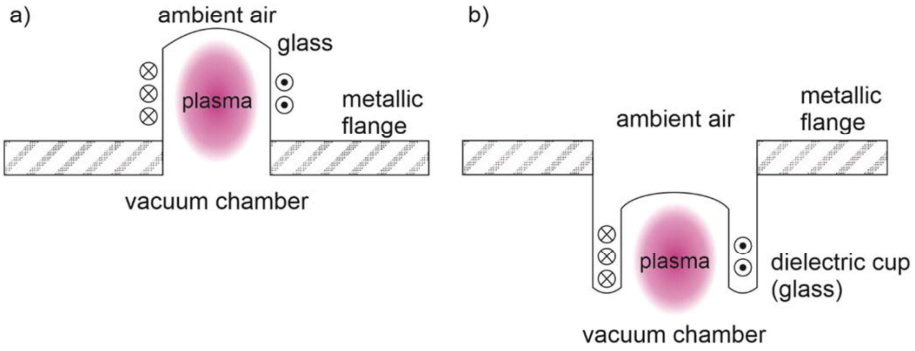

Figure 1. (a) A classical and (b) our positioning of the RF coil.

transitions from E- to H-mode were investigated in oxygen plasma generated in the experimental system with 4 such coils.

2. Experimental details

The classical configuration and our positioning of RF coils inside a metallic chamber are shown in figure 1. In the classical configuration adopted by numerous authors [3, 14–17, 26], the RF coil is positioned outside the metallic flange (figure 1(a)), so the dense plasma in H-mode is limited to the space outside of the chamber. Therefore, this plasma is not in contact with samples placed inside the chamber. In the configuration proposed in this paper, the dense plasma also stretches into the main chamber (figure 1(b)).

More details of our positioning of the coil within a slit of a double-walled glass tube, i.e. dielectric cup are shown in figure 2. The dielectric cup was made of borosilicate glass. The outer and inner diameters of the slit between the cup's walls were 55 and 40 mm, respectively. The thickness of the outer wall of the cup was 4 mm, and of the inner wall was 2.5 mm. The coil was made of a copper tube with outer and inner diameters of 3 and 1 mm, respectively. It was connected to a cooling water system maintained at a pressure of 5 bar. Although placed inside the metallic chamber, the coil was in ambient air due to the special construction peculiarities of the dielectric cup. A Teflon spacer was placed between the powered and grounded segments of the copper tube, as shown in figure 2. Such conditions prevented arcing between the coil's powered and grounded sides even at the highest discharge powers.

The coils of our configuration were mounted onto a metallic flange of the vacuum chamber with a height of 0.5 m and a diameter of 0.6 m. All connections between the matching network, the coils and the ground were adjustable in length to enable fine adjustment according to suggestions published in [17, 18]. Four coils were connected in parallel to the matching network, which was in turn connected to an RF generator. The matching network was gamma-type, i.e. consisting of two variable capacitors (Commet Maxi-Con), each with a capacitance between 20 and 250 pF. The RF generator was an Advanced Energy Cesar 1350, with an adjustable

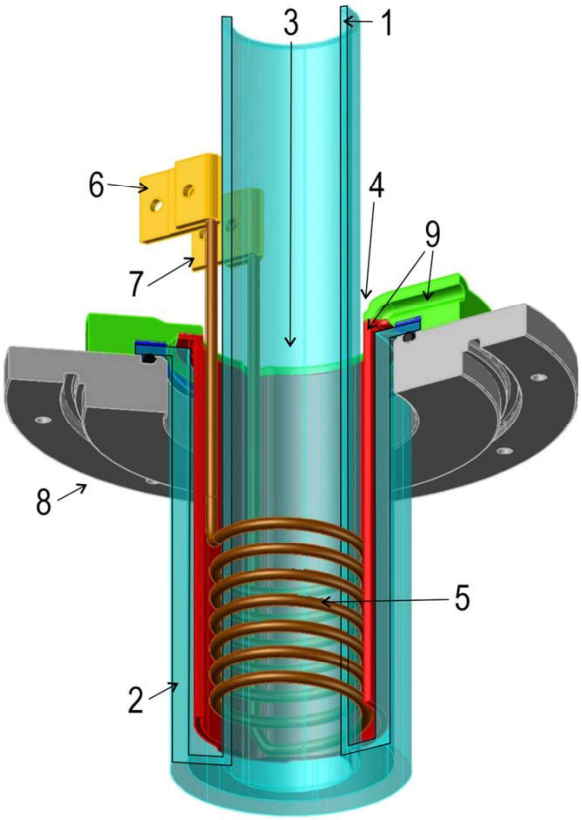

Figure 2. A dielectric cup with the RF coil. 1—inner wall, 2—outer wall, 3—vacuum side, 4—atmospheric pressure side, 5—coil, 6—connection to the power supply, 7—ground, 8—fixation ring, 9—forced air cooling air lead and upper glass fixation ring.

forward power of up to 5 kW at the maximum voltage of 795 V. A photograph of the outer side of the anodised aluminium flange with all four cups and electrical leads is shown in figure 3.

The chamber was pumped with a two-stage rotary pump with a nominal pumping speed of 40 $m^3\ h^{-1}$, and an ultimate pressure below 0.1 Pa. Oxygen gas of commercial purity was leaked into the metallic chamber during continuous pumping. The pressure in the chamber was measured with an absolute

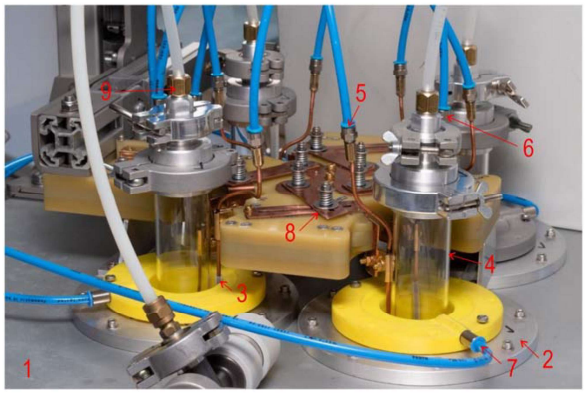

Figure 3. A photo of the 4 coils mounted on the flange. 1—anodised aluminium flange, 2—fixation flange, 3—Teflon spacer, 4—inner wall, 5—water inlet, 6—water outlet, 7—compressed air inlet, 8 – hot-wire length regulation slider, 9—gas inlet.

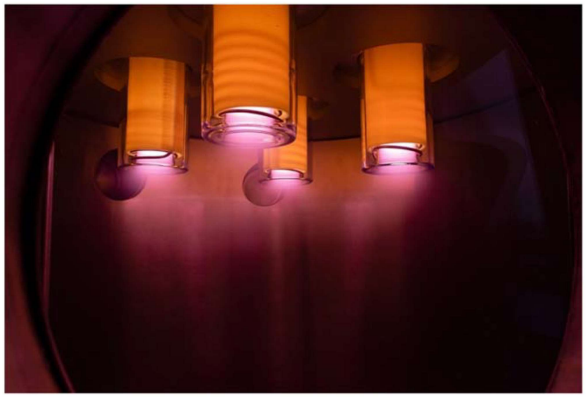

Figure 4. Plasma in the reactor with an oxygen pressure of 20 Pa and total forward power of 1500 W.

capacitive gauge (MKS pressure transducer 722B) and was adjusted between 5 and 25 Pa. Plasma was ignited at low forward power (i.e. in E-mode). The forward power was increased gradually to detect the transition from E- to H-mode. A photograph of the inner side of the chamber with four plasmas in H-mode is shown in figure 4.

3. Results and discussion

As already mentioned, the transition between E- and H-mode is clearly visible with the naked eye because H-mode is much more luminous than E-mode. The emission intensity of H-mode plasma is more than two orders of magnitude larger than the emission intensity of E-mode plasma. This can be measured by optical emission spectroscopy (OES). In figure 5 optical emission spectra of E- and H-mode plasma are presented. It can be seen that the intensities of oxygen lines in H-mode plasma (figure 5(b)) are more than 200 times higher than the intensities of oxygen lines in E-mode plasma (figure 5(a)).

The transitions between E- and H-mode were measured systematically at different oxygen pressures. First, a pressure was fixed to a selected value, and the RF generator was switched on at low forward power. The forward power was increased, and both forward, as well as reflected power were monitored. The transition from E- to H-mode was observed as a sudden increase of plasma luminosity. The forward power was increased up to approximately 3000 W. The plasma was sustained at this power for a few minutes, and then the forward power was gradually decreased. The transitions from H- to E-mode were measured at different pressures when decreasing the forward power from maximum to minimum power value.

Figure 6 represents the forward powers at which transitions from E- to H-mode were observed versus the pressure for all four coils. The transitions occur at the relatively low forward power of approximately 400 W at the lowest pressure of 5 Pa. The transition shifts to higher powers at higher pressures. In the first approximation, the forward power required for transitions from E- to H-mode increases quite linearly with increasing pressure. At the maximum experimental pressure, i.e. 25 Pa, the required forward power was approximately 1700 W. The transition never occurred in all coils simultaneously. With increasing power, E- to H-mode transitions occurred in coils one by one. The sequence of the coils for these transitions is not always the same, nevertheless, the differences between coils are not dramatic, as revealed in figure 6. Such deviations between coils are a consequence of the peculiarities of plasma impedances. Despite all precautions taken when constructing the electrical circuit, minor impedance differences cause sequential transitions. Incidentally, the lowest power needed for the transition from E-to-H-mode at 5 Pa was observed for coil #1, followed by #2, #3 and #4. At 10, 15 and 25 Pa, coil #3 required the highest forward power for the transition indicating minute details that govern the E-H transitions.

The curves in figure 6 are not perfectly linear because of the peculiarities described above. However, if points in figure 6 are connected not by the E- to H-mode transition of the particular individual coils but by the number of coils that underwent transition, the curves become totally linear. In this case, it is not important in which coil sequence the transitions occurred. This is presented in figure 7, where also linear fits are plotted. From here on all the curves will be plotted in the same manner, with number of coils connected. Now, the linearity is more obvious. The RF generator power needed for a certain number of coils to be ignited in H-mode at a certain pressure can simply be calculated using linear fits.

The RF generator was also equipped with a reflected power meter. The real power dissipated on the coils is the difference between the forward and reflected power. The real power needed for the transition of plasma from E-to-H-mode versus pressure is shown in figure 8. Results for the transitions of all four coils are not much different from the results in figure 7 because of the almost optimal coupling. Specifically, the matching network has been optimised in the state where all four coils were in H-mode, i.e. reflected power was almost zero for all four coils at the transition from E- to H-mode.

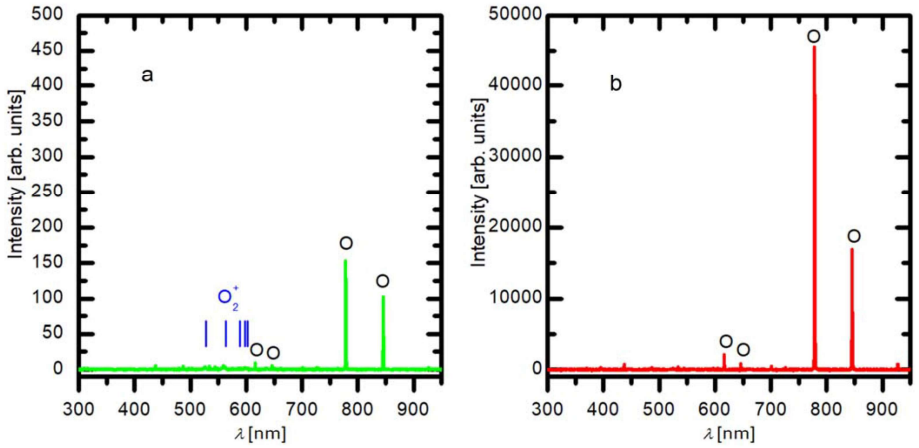

Figure 5. OES spectra of E-mode plasma (a) and H-mode plasma (b).

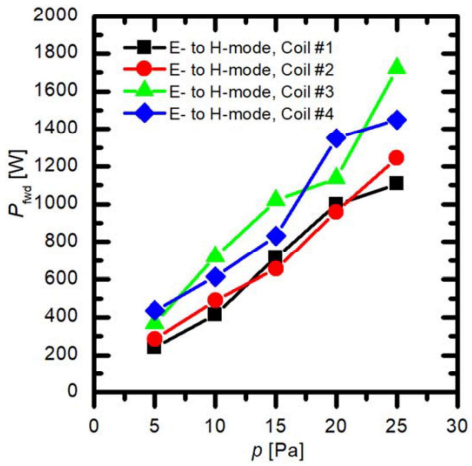

Figure 6. Forward powers at transitions from the E- to H-mode for different coils versus pressure.

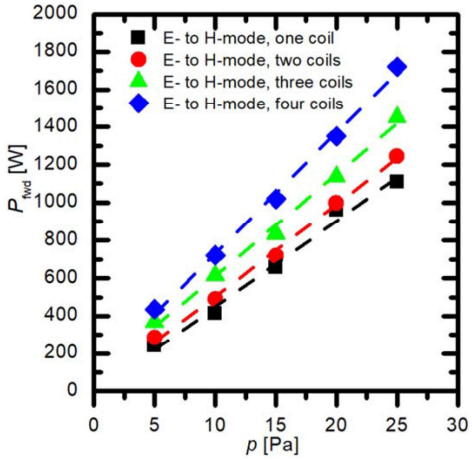

Figure 7. Forward powers at transitions from E- to H-mode for different numbers of coils versus pressure.

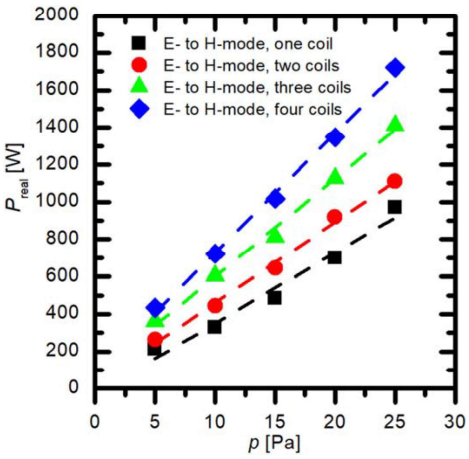

Figure 8. Difference between forward and reflected powers (real power) at transitions from E- to H-mode versus pressure.

This optimisation was performed before measurements at every oxygen pressure. However, because of the optimization method of the matching network, the curves, for the case where one or more coils are in E-mode, are lower than the curves in figure 7.

The transitions between the discharge modes exhibit hysteresis, i.e. the transition from E- to the H-mode always appears at a larger power than the transition from H- to E-mode [29]. The hysteresis is the consequence of the fact that H-mode will persist at moderate power if the plasma density is large enough to assure absorption of energy from the electric field by plasma electrons. The transition from H- to E-mode will occur once the electron density drops below the critical value. The transitions were measured at different pressures, and the results are summarised in figure 9. The first observation is that lower forward powers are needed for H- to E-mode transitions (figure 9) than when measuring the E-to-H transitions (figure 7). For example, at 25 Pa, where the differences are most striking, the H- to E-mode transition for the first coil occurs at a forward power of 1200 W, while the last

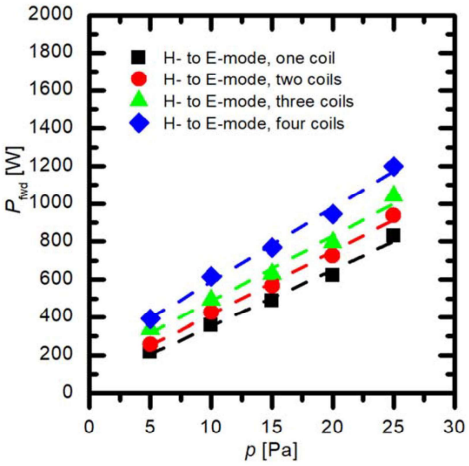

Figure 9. Forward powers at transitions from H- to E-mode for different coils versus pressure.

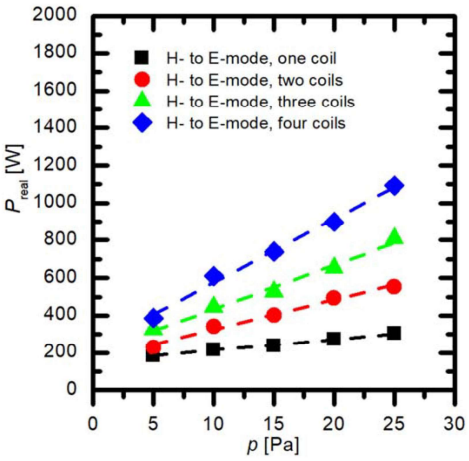

Figure 10. Difference between forward and reflected powers (real power) at transitions from H- to E-mode versus pressure.

transition from E- to H-mode is observed at power as large as 1722 W. The H- to E-mode transition for the last coil occurs at a forward power of 830 W, while the first transition from E- to H-mode is observed at 1108 W.

The real (forward minus reflected) powers where transitions from the H- to E-modes occur are plotted in figure 10. The values at 25 Pa are similar as in figure 9 for the first coil, where the H-mode is lost (approximately 1100 W) but much different for the last coil (approximately 300 W). The large difference is a consequence of the matching network optimisation method described above. That is why a small amount of power is absorbed in coils when they are in E-mode. As long as all coils are in H-mode, the real power is fairly equally distributed among all four coils. Once one coil transitions to E-mode, the available power is shared among the three coils which still persist in H-mode. As revealed from figure 10, the differences between the real powers absorbed in separate coils are nearly equal. For example, at 25 Pa, the critical powers needed to sustain the plasma in H-mode are 304, 554, 807 and

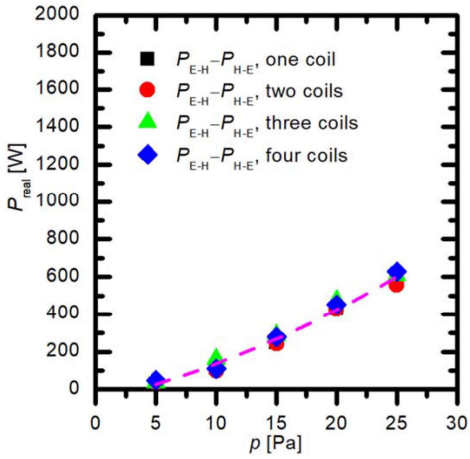

Figure 11. The width of hysteresis versus pressure.

1093 W for one, two, three and all four coils in H-mode, respectively. Such a linear increase of the real power with the increasing number of coils in H-mode reflects that the absorbed power is marginal in E-mode compared to H-mode. This means that each additional coil needs the same amount of real power in order to sustain H-mode.

In figures 9 and 10, a linear increase of power versus pressure can be seen. A few authors reported the pressure dependence of the critical power needed to sustain plasma in H-mode [27, 28], but most are limited to experiments at low pressure (preferably argon) plasma, where plasma can be sustained in H-mode at reasonably low power. Due to the technological applications, however, higher pressures are preferred because the density of electrons [27, 28], the radiation in the VUV range [30], and the density of neutral radicals [8] are larger than those at very low pressures. At the lowest pressure used in this study, i.e. 5 Pa, all of four coils were sustained in the H-mode at the absorbed power of only 386 W (figure 10). Furthermore, the same applies also for the forward power (figure 9) because the discharge coupling for all of four coils in H-mode at low powers and low pressure is near the optimum value of the matching, which was set as described above. However, with increasing pressure, the real power needed to sustain all four coils in H-mode increases and reaches 1093 W at 25 Pa. For the ignition of H-mode from E-mode of course even more power is needed, i.e. in the case of 25 Pa more than 1700 W. Sustaining H-mode and especially igniting the H-mode in several coils at larger pressures, therefore, requires a rather powerful RF generator.

As mentioned earlier, there is a hysteresis behaviour between the transition from E- to H-mode and back H- to E-mode in ICPs. Because we have here four ICPs there are four hystereses stacked one after another. The width of these hystereses, i.e. the difference between the real power of the E- to H-mode transition (figure 8) and the H- to E-mode transition (figure 10) versus pressure, is shown in figure 11. It can be clearly seen that the width of hysteresis at a certain pressure is almost the same for one, two, three or all four coils. This means that each additional coil will behave the same.

In figure 11 it can also be seen that the hysteresis energy width increases with pressure. The marginal energy width of solely 35 W is observed at the lowest pressure of 5 Pa. As mentioned earlier, the width becomes immeasurable at very low pressures [8]. Figure 11 reveals a dramatic increase of the hysteresis width with increasing oxygen pressure. At the highest pressure used in these experiments (25 Pa), the energy width was greater than 600 W. Therefore, one can save a lot of energy if plasma is ignited at the power needed for the E- to H-mode transition and then the power is lowered near the power of the H- to E-mode transition, while maintaining all of the coils in H-mode.

4. Conclusions

An innovative discharge system consisting of four ICPs coupled inside a metallic chamber was constructed and transitions from E- to H-modes and vice versa were measured at different oxygen pressures. Oxygen is a molecular gas of numerous excitation levels, so the electron energy is predominantly lost for molecule dissociation and excitation of various molecular and atomic states. Consequently, the discharge power needed to sustain ICP in oxygen gas in H-mode is much larger than in noble gases. We have shown that careful alignment of the electrical leads enables sustaining H-mode in all of four coils coupled in parallel to the RF power source. The transitions from E- to H-mode exhibited hysteresis. The width of hysteresis increased with increasing pressure. At the highest oxygen pressure in these experiments (25 Pa), the minimum discharge power still enabling operation in H-mode was approximately 300 W per coil. This is about the same power as observed for a simple one-coil discharge [8, 13]. The results presented in this paper clearly show that oxygen plasma can be sustained in H-mode at an optimal discharge power, even for multiple coils mounted inside a large metallic chamber. Possible applications include both etching and plasma-assisted deposition of various coatings where a rather large power density at a minimum interaction between positive ions and the walls of the discharge chambers is preferred.

Acknowledgments

This research was funded by the Slovenian Research Agency, project No. L2-9235 (Innovative configuration of inductively coupled gaseous plasma sources for up-scaling to industrial-size reactors) and core funding P2-0082 (thin-film structures and plasma surface engineering).

References

[1] Yu M H, Ma L B and Liu K 2019 *J. Korean Phys. Soc.* **75** 131
[2] Song H *et al* 2020 *Curr. Appl. Phys.* **20** 196
[3] Lee H C 2018 *Appl. Phys. Rev.* **5** 011108
[4] Hua Y *et al* 2018 *Plasma Sci. Technol.* **20** 065402
[5] You K I and Yoon N S 1999 *Phys. Rev.* E **59** 7074
[6] Kropotkin A N and Voloshin D G 2020 *Phys. Plasmas* **27** 053507
[7] Moon J H *et al* 2020 *Phys. Plasmas* **27** 033511
[8] Chabert P, Tsankov T V and Czarnetzki U 2021 *Plasma Sources Sci. Technol.* **30** 024001
[9] Zhang T L *et al* 2020 *Plasma Sci. Technol.* **22** 085405
[10] Zaplotnik R, Vesel A and Mozetic M 2011 *Europhys. Lett.* **95** 55001
[11] Zaplotnik R 2014 *IEEE Trans. Plasma Sci.* **42** 2532
[12] Draškovič-Bračun A, Mozetič M and Zaplotnik R 2018 *Plasma Process. Polym.* **15** 1700105
[13] Kang N *et al* 2011 *Plasma Sources Sci. Technol.* **20** 045015
[14] Kang N and Gaboriau F 2011 *J. Phys. D: Appl. Phys.* **44** 442001
[15] Zaplotnik R *et al* 2021 Generation of atomic species by RF plasmas and applications ed F L Tabarés *Plasma Applications for Material Modification* (Singapore: Jenny Stanford Publishing) p 350
[16] Marakhtanov A M *et al* 2003 *J. Vac. Sci. Technol.* A **21** 1849
[17] Lee J W *et al* 2014 *Phys. Plasmas* **21** 083502
[18] Lee J W *et al* 2016 *Curr. Appl. Phys.* **16** 415
[19] Song H, Seo S and Chang H 2018 *Curr. Appl. Phys.* **18** 1436
[20] Godyak V A, Piejak R B and Alexandrovich B M 2002 *Plasma Sources Sci. Technol.* **11** 525
[21] Zhao S X *et al* 2009 *J. Appl. Phys.* **105** 083306
[22] Lee J K, Lee H C and Chung C W 2011 *Curr. Appl. Phys.* **11** S149
[23] Gao F *et al* 2012 *Chin. Phys.* B **21** 075203
[24] Kim D G *et al* 2019 *Appl. Sci. Converg. Technol.* **28** 221
[25] Kim K N and Yeom G Y 2006 *J. Korean Phys. Soc.* **48** 256
[26] Setsuhara Y *et al* 2007 *Plasma Process. Polym.* **4** S628
[27] Takenaka K *et al* 2015 *Japan. J. Appl. Phys.* **54** 06GC02
[28] Liang O Y *et al* 2007 *Plasma Sci. Technol.* **9** 265
[29] Gao F *et al* 2010 *Phys. Plasmas* **17** 103507
[30] Fantz U *et al* 2016 *Plasma Sources Sci. Technol.* **25** 045006

Chapter 6

Oxygen Atom Density in a Large Reactor Powered by Four Inductively Coupled Plasma Sources

As the efficiency of the coupling of four coils in parallel was proved as described in chapter 5, the gradient of O-atoms within the chamber was evaluated by use of a catalytic probe. Please refer to chapter 5 for a description of the system. The difference was that the pumping speed was increased by the consecutive coupling of roots (Busch vacuum Wv 0500 B OHI KAFA) and two-stage rotary pump (Trivac DB 40). The nominal pumping speed of the roots pump is 600 m^3/h and of the rotary pump 40 m^3/h. Within a few minutes, the reactor was evacuated to a pressure of less than 1 Pa (below the quantification limit of the absolute capacitive gauge). The inner walls of the reactor were covered with an aluminium mantle (with holes where the ports for equipment and measurements are TIG welded).

Prior to measurement of neutral O-atom densities, the catalytic probe was mounted and the reactor evacuated to the ultimate pressure. For each measurement, oxygen plasma was sustained at the real power of 1800 W and oxygen pressure of 20 Pa (oxygen flow of 420 sccm) during continuous pumping to provide efficient transport from the discharge tubes into the reactor's chamber. The O-atom density was measured with the catalytic probe (calibrated for oxygen) at distances of 0.5, 21 and 43 cm below the lower level of the dielectric cups. The probe was moved in increments of 2.5 or 5 cm depending on the gradients found and the scientific relevance of the specific location within the reactor.

In the measurement line of 0.5 mm under the level of the dielectric cups, O-atom density in the centre between the cups was around 2×10^{21} m^{-3}. There were two distinctive peaks under the exhausts from the dielectric cups where the O-atom density was about 4×10^{21} m^{-3}. Toward the walls of the reactor, with a distance of approximately 10 cm from the inner aluminium mantle, the O-atom densities decreased to the value of 1×10^{20} m^{-3}.

A smooth curve free of maxima was obtained 21 cm below the lower level of the dielectric cups' exhausts. In the middle of the reactor, O-atom density was about 1.2×10^{21} m^{-3}, and the values were approximately the same over the whole diameter of the reactor, except within a distance of approximately 10 cm from the walls. That plasma density decreased in the proximity of the walls can be explained by the recombination of O-atoms on the aluminium surface. The coefficient is low but not negligible, which becomes obvious when O-atom densities at the lowest level of the reactor are taken into account.

The O-atom density decreased to approximately 4×10^{20} m^{-3} 43 cm under the lower level of the dielectric cups, and some gradients appeared that are hard to explain but might be a consequence of the proximity of gas exit from the reactor.

To demonstrate the importance of the reactor's aluminium mantle for supressing the recombination of O-atoms, the O-atom density was measured in stainless steel side tubes with a diameter of 4 cm. Within the side tube at the top of the reactor, the O-atom density decreased from 1×10^{21} to 1×10^{20} m^{-3} within the distance of 8 cm. This demonstrates high recombination of O-atoms on the surface of the stainless steel.

Figure 10 shows a photograph of the reactor with oxygen plasma. The catalytic probe is a small bright disc.

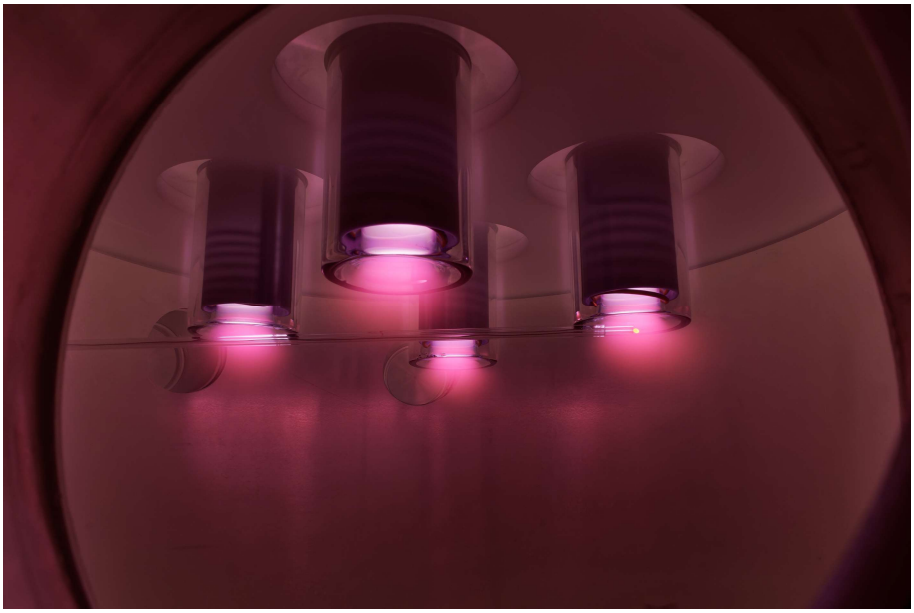

Figure 10: Catalytic probe at the exhaust of the discharge tube. The probe is visible as a bright disc just below the rightmost discharge tube.

Vacuum 199 (2022) 110964

Contents lists available at ScienceDirect

Vacuum

journal homepage: www.elsevier.com/locate/vacuum

Oxygen atom density in a large reactor powered by four inductively coupled plasma sources

Gregor Primc [a,*], Dane Lojen [a,b], Alenka Vesel [a], Miran Mozetič [a], Rok Zaplotnik [a]

[a] Department of Surface Engineering, Jozef Stefan Institute, Jamova cesta 39, 1000, Ljubljana, Slovenia
[b] Jozef Stefan International Postgraduate School, Jamova cesta 39, 1000, Ljubljana, Slovenia

ARTICLE INFO

Keywords:
Inductively coupled plasma
Catalytic probe
Oxygen atoms
Industrial-size
Polymer

ABSTRACT

Gradients in O-atom density in metallic plasma reactor useful for rapid surface activation of 3D polymer products have been measured. The reactor of a volume of 150 l was equipped with four inductively coupled plasma sources (ICPS) of (predominantly) oxygen atoms, parallelly coupled with a radio-frequency generator of adjustable power up to 5 kW at 13.56 MHz. Molecular oxygen was continuously introduced into the ICP sources, where it was dissociated upon plasma conditions. The constant pumping of the plasma reactor enabled the effective transfer of O-atoms from the ICP sources, so that their density remained high in the entire chamber even far from plasma sources. The O-atom density was measured across the reactor with a movable catalytic probe calibrated for oxygen. The sophisticated immersible design enabled the O-atom density to exceed 10^{21} m^{-3} in the major chamber volume at the pressure of 20 Pa. At this pressure, a uniform plasma in the H-mode was sustained at the total real RF power of 1800 W. Significant gradients in the O-atom density were only detected next to ICP sources' exhausts and in the main chamber's metallic side tubes. Such uniform distribution of O-atoms in a large reactor is advantageous for rapid surface activation of 3D polymer products.

1. Introduction

Oxygen-plasma treatment of polymers has been a subject of numerous scientific studies due to its applicability on an industrial scale [1,2]. Such plasma is a source of charged particles, neutral reactive species, and vacuum ultraviolet (VUV) radiation [3,4]. Non-equilibrium oxygen plasma can be sustained at low pressures (often between 10 and 100 Pa) or atmospheric pressure [5,6]. Atmospheric-pressure plasmas are characterized by extensive gradients in reactive species [7,8], so they are not very useful for treating 3D objects but perform well in cases of 1D or 2D objects such as wires, foils of fabrics. Such atmospheric-pressure plasmas indeed enable treatment in continuous mode [9,10], which is preferred in the industry [10,11]. However, large gradients in plasma parameters remain an obstacle for extensive application of these plasmas for treating 3D objects, where a robot is necessary to move a plasma jet over the surface.

On the other hand, low-pressure plasmas are convenient low power density sources (power per unit volume) of neutral reactive species and thus suitable for treating objects of almost arbitrary shape [12,13]. An appropriate gaseous discharge sustains plasma, and the neutral reactive species diffuse inside the reactor, so their density may be significant even far away from plasma sources [1]. Still, gradients in O-atom density are likely to occur even in low-pressure oxygen reactors [14].

A polymer material's surface finish depends on the type of polymer and fluxes of different reactive species onto the polymer surface. The oxygen-plasma treatment usually leads to two effects: surface functionalization with polar functional groups and etching. An appropriate surface finish is achieved by optimizing fluences of different plasma species onto a polymer surface. Functionalization and etching kinetics are still a subject of extensive research. According to a recent theory [15], which has been confirmed by carefully designed experiments [16], surface functionalization with oxygen functional groups occurs in several steps. First, the hydrogen atoms on the polymer surface are substituted with hydroxyl radicals. The surface saturation with the hydroxyl groups is accomplished at the O-atom fluence as low as about 10^{19} m^{-2}. Second, epoxy bonds are formed, followed by breaking bonds between the carbon atoms in the polymer chain. Such effects have been observed at the O-atom fluence of several 10^{20} m^{-2}. The bond scission enables the formation of various functional groups and oxygen atoms' diffusion into the sub-surface film. The surface is finally saturated with polar functional groups after being treated with an O-atom fluence of about 10^{23} m^{-2}. Etching is observed simultaneously with

* Corresponding author.
E-mail address: gregor.primc@ijs.si (G. Primc).

https://doi.org/10.1016/j.vacuum.2022.110964
Received 8 December 2021; Received in revised form 11 February 2022; Accepted 17 February 2022
Available online 22 February 2022

functionalization with carboxyl or ester groups [16]. The polymers' etching rate upon treatment with oxygen atoms only may be lower than 0.1 nm/s [17]. The etching rate is usually between 1 and 10 nm/s for many polymers when exposed to weakly ionized oxygen plasma rich in oxygen atoms at room temperature [18,19]. Highly ionized oxygen plasma is not very appropriate for surface functionalization since the etching prevails and the surface wettability remains inadequate even at prolonged treatment times [20,21]. Therefore, the best conditions for surface activation of polymers are at relatively high O-atom density and low density of charged particles. The requirements are contradictory, so the careful design of a plasma reactor is necessary to meet these criteria.

The O-atom density in a plasma reactor depends on the dissociation and recombination rates. The most intensive production of oxygen atoms is in moderately ionized gaseous plasma, in particular oxygen plasma sustained by electrodeless discharges, for example, inductively coupled RF plasma [22] and microwave plasma [23]. Gas-phase recombination is unlikely to occur at pressures below about 100 Pa since a three-body collision is required. The primary loss mechanism at low pressures is heterogeneous surface recombination. The probability depends on the recombination coefficient, which depends on the type of material facing plasma and its morphology. For example, at room temperature, the recombination coefficient for oxygen atoms on stainless steel is 0.07 [24]; on glass surfaces, it is as low as 10^{-3} [25], while on extremely porous nanostructured materials, it may come close to 1 [26]. Values of O-atom loss coefficients on many polymers are a few 10^{-3}, so the polymer products inside a metallic vacuum chamber do not present a significant drain of O-atoms [27].

Stainless steel is the material of choice for the inside part of an industrial-scale low-pressure plasma reactor. However, in such reactors, it is difficult to obtain a large density of O-atoms, which is required for rapid treatment of polymeric products. Hence, using an electrodeless discharge atom source in metallic chambers is impractical. Further, a moderately large coefficient for heterogeneous surface recombination of O-atoms to parent molecules on stainless steel surfaces prevents large O-atom density at reasonable discharge power. High-power reactors are not suitable for surface activation of polymers with oxygen plasma since the surface functional groups are unstable at elevated temperatures.

The limitations of the stainless-steel reactors may be avoided by immersing electrodeless plasma sources inside the vacuum chamber, as explained in this paper.

2. Experimental details

A high-vacuum compatible stainless-steel reactor was constructed. The reactor was a cylindrical stainless-steel tube with an inner diameter of 60 cm and an inner height of 50 cm. The inner wall of the stainless-steel cylinder was overlaid with an aluminium sheet of a cylindrical shape. This sheet also had holes on the side that were aligned with side-flanges of the chamber. Aluminium is regarded as an inert material and should not represent a significant drain for oxygen atoms by heterogeneous surface recombination. The upper and bottom part of the reactor tube were terminated with 2-cm thick aluminium flanges and sealed with Viton O-rings in between. Several tubes, perpendicular to the main stainless-steel cylinder wall, were TIG-welded according to high-vacuum standards. These side-tubes served for the mounting of gauges, probes and windows. On one side, the reactor also has a door equipped with a window to reach into the chamber and get an overview of the inside. Four specifically designed dielectric tubes (or cups) were mounted onto the upper flange of the reactor as shown in Fig. 1. The dielectric tubes were placed through holes drilled into the upper flange; the vacuum-sealing was achieved with O-rings, which act as gaskets between a dielectric tube and an aluminium flange. Details of dielectric tubes can be seen on Fig. 2. In each dielectric tube there is a 3D-printed insert made of acrylonitrile butadiene styrene (ABS) that is reinforced with stainless steel rings. These 3D-printed covers serve for guidance of compressed air used for cooling of the coils and is guided from the bottom of the dielectric tube towards the top of the coils. A single RF coaxial cable from the generator (Advanced Energy, Cesar 1350) was connected to a matching network made of two vacuum capacitors, each with a capacitance between 20 and 250 pF (Commet Maxi-Con), in a gamma configuration. Forward and reflected powers were measured by the RF generator reflected power measurement functionality. Reflected

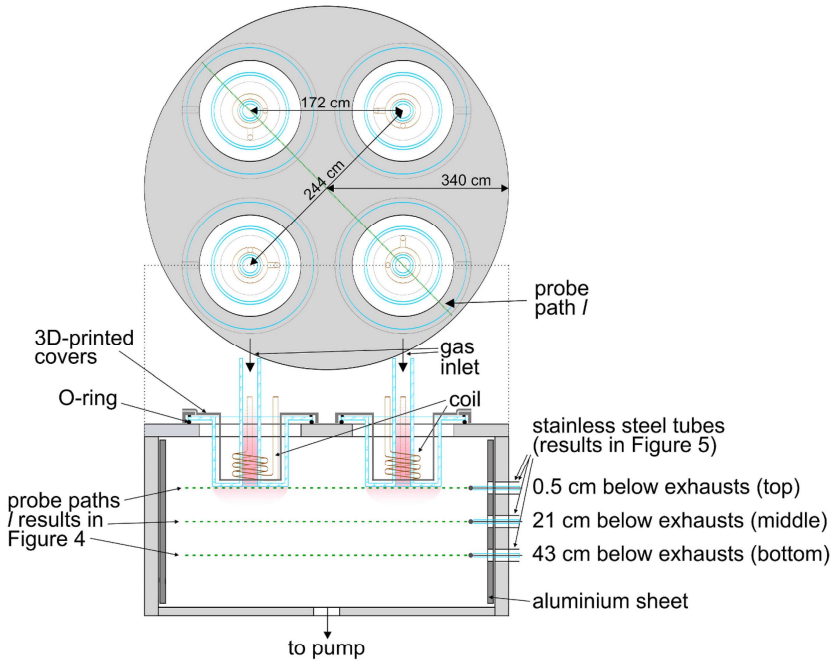

Fig. 1. Schematic of the plasma reactor (below) and the position of the four dielectric tubes for RF coils on the upper flange (above).

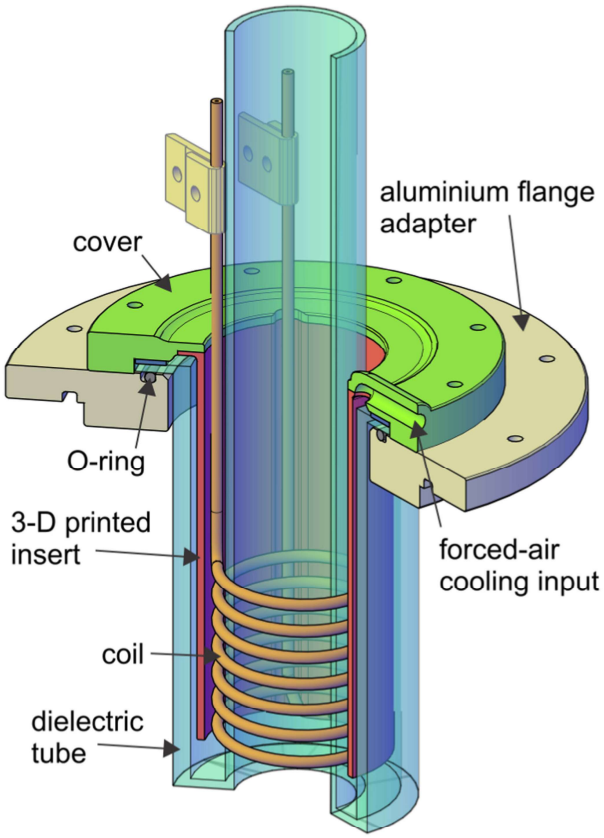

Fig. 2. Detailed schematic of a single ICP source.

power was in the range between 15 and 55 W, depending on the reactor temperature, which was gradually increasing during prolonged measurements, and daily conditions. Capacitors were always set to provide the real power of 1800 W at the start of each series of measurements. Copper coils were immersed into the dielectric tubes and connected to the matching network in parallel to ensure appropriate RF voltages on all four coils. Each coil is made from a copper tube with an outer diameter of 3 mm and inner diameter of 1 mm and has 6 and ¾ turns. Internal diameter of the coil is 42 mm. The coils were mounted on the atmospheric-pressure side, while plasma was ignited in the inner sides of dielectric tubes under vacuum conditions. The cable from the matching network was mounted on a special holder made of three 10-mm thick FR4 layers. The middle layer serves as insulation between both electrodes. The holder serves as power distributor and is made in a star-like distribution. This means that conducting paths from the RF cable to each coil are exactly the same. Moreover, between the main RF cables' hot wire and each coil (also RF cables' ground and each coil) there are sliders that are used to match any differences in the impedance for each coil. Top and bottom layers are symmetric in respect of both electrodes and can be interchangeable, meaning that the powered electrode can be on the top or bottom layer.

The reactor in Fig. 1 was pumped by a combination of roots (Busch Vacuum, Wv 0500 B OHI KAFA) and rotary (Trivac, D40B) vacuum pumps. Nominal pumping speed of the roots pump was 600 m^3/h, and the nominal ultimate pressure was about 10^{-2} Pa. The two-stage rotary pump had a nominal pumping speed of 40 m^3/h and an ultimate pressure of about 0.1 Pa. With the combination of both pumps, the plasma reactor was pumped within a few minutes down to a pressure below the detection limit of the capacitive vacuum gauge (Baratron, MKS), i.e., 1 Pa.

A catalytic probe for measuring the O-atom density was mounted on three different side tubes, as shown in Fig. 1; the distances between the end of the dielectric tubes and centers of each side tubes were 0.5, 21 and 43 cm, respectively. We used a standard probe configuration as disclosed in Ref. [28]. As depicted in Fig. 2, the thermocouple wires were embedded into a glass tube and vacuum-sealed at the end with both wires sticking outside of the glass tube. The probe was mounted to a special feedthrough that enabled continuous horizontal movement through the chamber almost without friction that would cause the outside air to protrude into the evacuated chamber. The O-ring sealing was lubricated with a high vacuum grease to assure for smooth movement of the glass tube. In short, a catalytic probe determines the O-atom density in its vicinity by measuring the heat dissipated on the surface of a small catalytic disc immersed into a gas rich in O-atoms. The oxygen atoms recombine to parent molecules on the catalytic disc's surface. The disc is thus heated well above the ambient gas temperature. The power dissipated on the disc's surface is proportional to the flux of oxygen atoms, considering the value of the recombination coefficient of the catalytic material. Cobalt was used as catalytic material since it exhibits a constant and high recombination coefficient in a broad range of temperatures and O-atom fluxes. The probe gives accurate and reliable results as long as heterogeneous surface recombination is the predominant

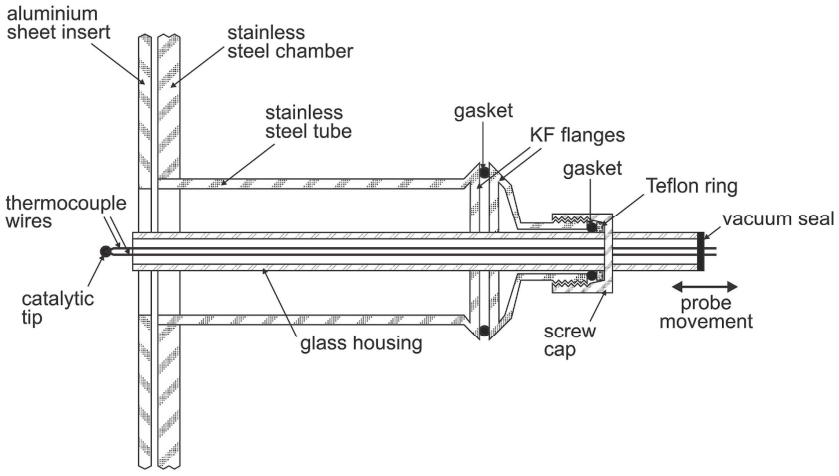

Fig. 3. Detail of the stainless-steel chamber sidewall with a movable probe.

heating mechanism, i.e., in highly dissociated weakly ionized oxygen plasmas.

The probe measurements under different conditions were compared to Ref. [29] and we found very good agreement, so the probes are regarded as a reliable tool for measuring the density of atoms in weakly ionized plasmas of molecular gases such as oxygen, nitrogen or hydrogen.

3. Results and discussion

The chamber in Fig. 1 was first evacuated to the ultimate pressure, which was below the detection limit of the capacitive vacuum gauge (1 Pa). Commercially available oxygen of purity 99.99% was leaked through a needle valve into ICP sources, as marked in Fig. 1. The plasma reactor was pumped continuously during oxygen leakage to reach the pressure of 20 Pa. Oxygen flow was 420 sccm. This pressure assured for sustaining stable plasma in the H-mode in all four ICP sources. A photo of the plasma reactor with four ICP sources at 20 Pa and the real ($P_{\text{forward}} - P_{\text{reflected}}$) RF power of 1800 W is shown in Fig. 4. The luminous plasma was concentrated within the dielectric tubes. About a centimeter below the edges of dielectric tubes, the electromagnetic field becomes too low to sustain plasma in the H-mode leading to a steep decrease in plasma emission intensity. The major volume of the plasma reactor away from the four ICP sources is therefore filled with diffusing plasma of a very weak luminosity. Such a low luminosity indicates low electron temperature and/or density in the majority of the plasma reactor. Production of oxygen atoms by dissociative collisions between plasma electrons and oxygen molecules in the plasma reactor's major volume is therefore marginal compared to the production of oxygen atoms within the ICP sources. As mentioned earlier, the gas is leaked at the top of ICP sources flowing through them into the main chamber.

The O-atom density was measured by positioning the catalytic probe through the three side tubes. The probe was movable, making it possible to determine the O-atom density along its path. The paths are indicated in Fig. 1. One port for the catalytic probe was placed just below the ICP sources, 0.5 cm below the exhausts from the dielectric tubes, as shown in Fig. 1. The second port was located in the middle of the stainless-steel cylinder and the third at the lowest position, i.e., about 3 cm from the pump duct.

The results of systematic measurements are shown in Figs. 5 and 6. In Fig. 5, the three curves represent the O-atom density at the top position (0.5 cm below dielectric tubes with RF coils), in the middle of the reactor, and at the bottom. The upper curve exhibits two maxima, while the other two curves are somewhat monotonous.

The upper curve in Fig. 5 shows an interesting probe signal along the diameter of the plasma reactor. The two maxima in the curve correspond to the position of the ICP sources. The O-atom density right below an ICP source is higher than away from the source. The effect may be explained by a higher flux of oxygen atoms at the exhaust from the ICP source. As mentioned above, the O-atom density is determined from the flux of O-atoms onto the catalytic disc surface. The flux is a product of the O-atom density (n) and the average random velocity ($\langle v \rangle$), i.e., $j = ¼\, n \langle v \rangle$. The random velocity increases as the square root of the gas kinetic temperature. Therefore, the maxima in the upper curve in Fig. 5 can be explained by a higher kinetic temperature of oxygen atoms next to the ICP source. The gas temperature in plasma in the H-mode is elevated due to the high density of electrons and also the super-elastic nature of the

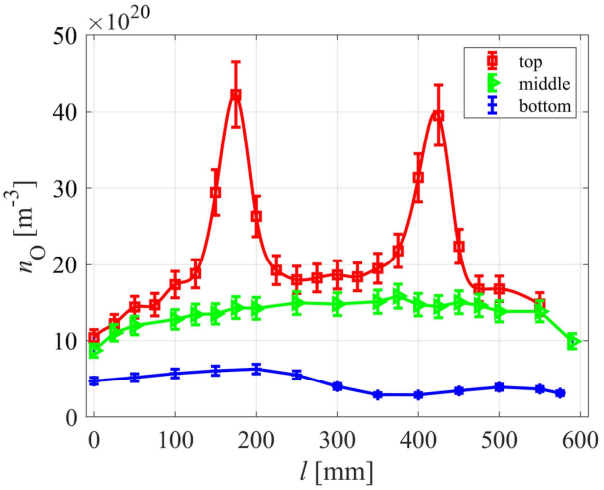

Fig. 5. The O-atom density in the plasma reactor at positions just below the ICP sources (upper curve), in the middle (middle curve), and at the bottom (lower curve) of the metallic reactor.

Fig. 4. A photograph of the four ICPs in the plasma reactor at 20 Pa and real power of 1800 W.

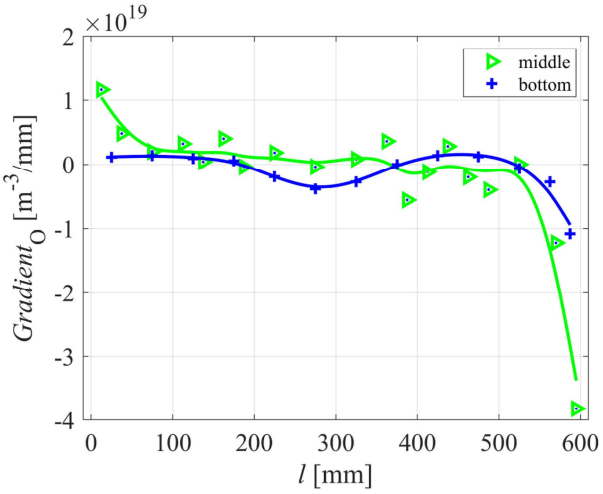

Fig. 6. Gradients of O-atom density in the middle section (21 cm from the exhausts) and at the bottom (43 cm from the exhausts).

dissociative collisions [25]. Hence these two effects may contribute to the increased probe signal when positioned just below an ICP source. Another reason for the maxima may be additional heating of the catalyst surface due to the absorption of light quanta from the ICP source. Namely, ICP plasma in the H-mode is a significant radiation source, especially in the VUV range of wavelengths [4]. The primary radiation from oxygen plasma arises from resonant transitions of oxygen atoms with peak intensity at 130.4 nm [30,31]. Whatever the reason, the O-atom density determined by the catalytic probe exhibits maxima below the ICP sources. In between ICP sources, the O-atom density is relatively constant at a value of about 2×10^{21} m^{-3}. This indicates a high dissociation fraction of O_2 molecules. Specifically, the density of oxygen molecules is $n_{O2} = p/k_B T$, where p is gas pressure, k_B Boltzmann constant, and T the neutral gas kinetic temperature. Considering the pressure is 20 Pa and temperature 300 K, the density of O_2 molecules at the selected experimental conditions with the absence of plasma is 4.8×10^{21} m^{-3}. A significant dissociation fraction of oxygen molecules (about a fifth, considering that a molecule consists of two atoms) is obtained right below ICP sources in the volume between them. The O-atom density at the exhaust of an ICP source (maxima of the upper curve in Fig. 5) is almost as high as the theoretical density of molecules at 20 Pa. However, such a high value is probably an artifact in light of the upper discussion.

The middle curve in Fig. 5 is smooth and free from maxima. The probe was moved 21 cm below the exhausts of the ICP sources when acquiring the measured points of the middle curve. The O-atom density in the middle of the reactor is almost gradient-free. The O-atom density of approx. 1.2×10^{21} m^{-3} prevails in almost the entire range of probe positions except near the reactor wall (a few centimeters away). Close to the chamber walls, gradients of O-atom density appear, which can be explained by the higher heterogeneous surface recombination value. The gradients, however, are not significant since the O-atom density at the position just next to the wall is still about 1×10^{21} m^{-3}. These small gradients appeared because the inner side of the reactor cylinder was wrapped with a thin aluminum sheet, as depicted in Figs. 1 and 3. The coefficient for heterogeneous O-atom recombination on aluminum is much smaller than on stainless steel [32].

Fig. 6 depicts spatial gradients of O-atom density in the middle (21 cm from the exhausts) and bottom section (43 cm from the exhausts). Their values were calculated as $(y_2 - y_1)/(x_2 - x_1)$, where y_1 and y_2 are the oxygen atom densities at positions x_1 and x_2. These gradients were drawn between x_1 and x_2, what basically means that each gradient point is the inclination of the line between two points between two points on the x-axis. Small gradients were also measured at the bottom of the stainless-steel reactor, where the probe was positioned 43 cm below the exhausts of ICP sources. The O-atom density versus probe position is presented as the lower curve in Fig. 5. Somehow lower O-atom density in the segment 300–600 mm compared to the segment 0–300 mm is difficult to explain. An important feature is that the density remains at around 4×10^{20} m^{-3}, although the probe was more than 40 cm away from ICP sources. The reason was already explained: selecting appropriate materials with low recombination coefficient.

As mentioned earlier, the coefficient for heterogeneous surface recombination of oxygen atoms on stainless steel surfaces is moderately high at the value of 0.07 [24]. The O-atom density within side tubes made from this material and not wrapped into an aluminum sheet should be much lower than within the main chamber. To prove this, we also performed some measurements inside a stainless-steel side tube attached to the side of the main chamber, as shown schematically in Fig. 3. A probe was moved from the main reactor wall into the stainless-steel tube. The O-atom density versus the probe's tip position in the stainless-steel side tube is presented in Fig. 7. The value $l = 0$ mm corresponds to the position of the cylindrical reactor wall and the negative values to the depth inside the stainless-steel tube. The inner diameter of the stainless-steel tube was 4 cm.

Fig. 7 reveals a strong gradient in the O-atom density inside the stainless-steel tube. The density drops for an order of magnitude in a few centimeters. The gradient is explained by heterogeneous surface recombination of the oxygen atoms on the surface of the stainless-steel tube. The tube is terminated with a KF flange which holds the catalytic probe, so any gas movement is diffusion-dependent. There is a continuous supply of oxygen atoms from the main chamber at the entrance to the stainless-steel side tube and a gradual sink on the side walls and on the flange at the end of the stainless-steel side tube. The gradient as observed in Fig. 7 is therefore expected.

The O-atom density throughout the chamber was close to 1×10^{21} m^{-3}; thus, the flux of oxygen atoms on any object placed into the reactor was a few 10^{23} m^{-2}s^{-1}. Such a large flux should ensure complete surface functionalization of commonly used polymer materials in a time below a second, making the plasma reactor effective for rapid activation of any polymer products in the continuous mode.

4. Conclusions

A high and relatively constant density of oxygen atoms can be

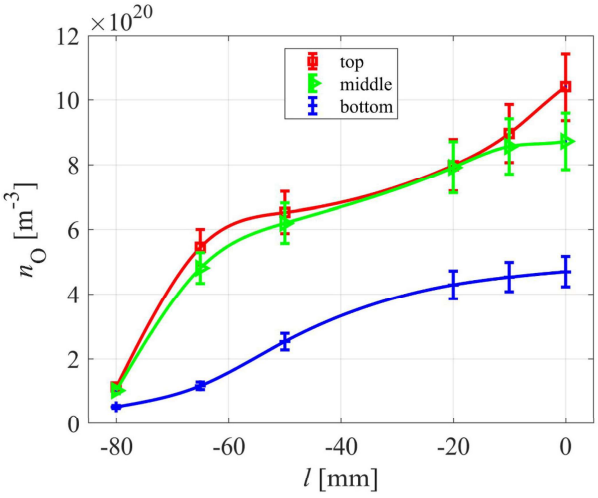

Fig. 7. The O-atom density within the side stainless steel tubes.

sustained in a large metallic plasma reactor by immersing several inductively coupled plasma sources into the reactor. The dissociation fraction of oxygen atoms in such sources is at least 40%. Continuous supply of molecular oxygen to the ICP sources and pumping the chamber enables the dissociation fraction of about 10% in the entire chamber. At our particular conditions, the dissociation fraction at the position 21 cm from the exhaust (middle) was about 25%, while at the position 43 cm from the exhaust (bottom) it was about 12%. The technique was elaborated for a cylindrical stainless-steel chamber of a diameter of 60 cm and a volume of about 150 l but is scalable to larger systems providing plasmas in the H-mode are sustained in multiple ICP sources. The experiments were performed at the oxygen pressure of 20 Pa because such a moderately low pressure ensures a relatively large gas density on the one hand and the ability to ignite the H-mode in all four ICP sources at a reasonable RF power on the other hand. Sustaining such conditions at lower pressure is trivial, but higher pressures require much higher RF power, which is not convenient for an industrial application of such sources. Both radial and longitudinal gradients of O-atom density were marginal. However, gradients in any stainless-steel side tube are relatively large due to extensive loss of atoms by heterogeneous recombination on stainless-steel surfaces. The flux of oxygen atoms on any object that might be placed in the plasma reactor is as high as a few 10^{23} $m^{-2}s^{-1}$, and it does not depend much on the position of an object. Such fluxes are suitable for processing polymers in terms of rapid functionalization, which can be achieved in under a second of plasma treatment.

CRediT authorship contribution statement

Gregor Primc: Writing – review & editing, Writing – original draft, Validation, Methodology. **Dane Lojen:** Visualization, Data curation, Formal analysis. **Alenka Vesel:** Writing – review & editing, Visualization, Investigation, Formal analysis. **Miran Mozetič:** Conceptualization, Funding acquisition, Methodology, Project administration, Writing – review & editing. **Rok Zaplotnik:** Writing – review & editing, Software, Methodology, Investigation.

Declaration of competing interest

The authors declare that they have no known competing financial interests or personal relationships that could have appeared to influence the work reported in this paper.

Acknowledgment

This research was funded by the Slovenian Research Agency, project No. L2-9235 (Innovative configuration of inductively coupled gaseous plasma sources for up-scaling to industrial-size reactors) and core funding P2-0082 (Thin-film structures and plasma surface engineering).

References

[1] F.F. Chen, Helicon discharges and sources: a review, Plasma Sources Sci. Technol. 24 (2015), 014001, https://doi.org/10.1088/0963-0252/24/1/014001.
[2] C. Arpagaus, G. Oberbossel, P. Rudolf von Rohr, Plasma treatment of polymer powders - from laboratory research to industrial application, Plasma Process. Polym. 15 (2018) 1800133, https://doi.org/10.1002/ppap.201800133.
[3] K. Niemi, D. O'Connell, N. de Oliveira, D. Joyeux, L. Nahon, J.P. Booth, T. Gans, Absolute atomic oxygen and nitrogen densities in radio-frequency driven atmospheric pressure cold plasmas: synchrotron vacuum ultra-violet high-resolution Fourier-transform absorption measurements, Appl. Phys. Lett. 103 (2013), 034102, https://doi.org/10.1063/1.4813817.
[4] U. Fantz, S. Briefi, D. Rauner, D. Wünderlich, Quantification of the VUV radiation in low pressure hydrogen and nitrogen plasmas, Plasma Sources Sci. Technol. 25 (2016), 045006, https://doi.org/10.1088/0963-0252/25/4/045006.
[5] A. Kuwabara, S. Kuroda, H. Kubota, Polymer surface treatment by atmospheric pressure low temperature surface discharge plasma: its characteristics and comparison with low pressure oxygen plasma treatment, Plasma Sci. Technol. 9 (2007) 181–189, https://doi.org/10.1088/1009-0630/9/2/14.
[6] X. Lu, D. Liu, Y. Xian, L. Nie, Y. Cao, G. He, Cold atmospheric-pressure air plasma jet: physics and opportunities, Phys. Plasmas 28 (2021) 100501, https://doi.org/10.1063/5.0067478.
[7] J. Dedrick, S. Schröter, K. Niemi, A. Wijaikhum, E. Wagenaars, N. de Oliveira, L. Nahon, J.P. Booth, D. O'Connell, T. Gans, Controlled production of atomic oxygen and nitrogen in a pulsed radio-frequency atmospheric-pressure plasma, J. Phys. D Appl. Phys. 50 (2017) 455204, https://doi.org/10.1088/1361-6463/aa8da2.
[8] A. Mai-Prochnow, R. Zhou, T. Zhang, K. (Ken) Ostrikov, S. Mugunthan, S.A. Rice, P. J. Cullen, Interactions of plasma-activated water with biofilms: inactivation, dispersal effects and mechanisms of action, Npj Biofilm. Microb. 7 (2021) 11, https://doi.org/10.1038/s41522-020-00180-6.
[9] K. O'Flynn, V. Milosavljević, P. Dobbyn, D.P. Dowling, Evaluation of a reel-to-reel atmospheric plasma system for the treatment of polymers, Surface. Interfac. 6 (2017) 162–169, https://doi.org/10.1016/j.surfin.2017.01.005.
[10] X. Yu, W. Chao-Liang, Q. Si-Cheng, Z. Yu, H. Tao, G. Ying, D. Ke, Z. Yu-Ru, Y. Wei, S. Jian-Jun, D. Cheng-Ran, Z. Jing, Treatment uniformity of atmospheric pressure plasma on flexible and porous material surface: a critical review, Acta Phys. Sin. 70 (2021), https://doi.org/10.7498/aps.70.20210077, 099401–099401.
[11] J. Heine, R. Damm, C. Gerhard, S. Wieneke, W. Viöl, Surface activation of plane and curved automotive polymer surfaces by using a fittable multi-pin DBD plasma source, Plasma Sci. Technol. 16 (2014) 593–597, https://doi.org/10.1088/1009-0630/16/6/10.
[12] P. Ahr, T. V Tsankov, J. Kuhfeld, U. Czarnetzki, Inductively coupled array (INCA) discharge, Plasma Sources Sci. Technol. 27 (2018) 105010, https://doi.org/10.1088/1361-6595/aadb69.
[13] M. Evrard, A. Besnard, S. Lucas, Study of the influence of the pressure and rotational motion of 3D substrates processed by magnetron sputtering: a comparative study between Monte Carlo modelling and experiments, Surf. Coating. Technol. 378 (2019) 125070, https://doi.org/10.1016/j.surfcoat.2019.125070.
[14] K. Kutasi, V. Guerra, P.A. Sá, Active species downstream of an Ar–O 2 surface-wave microwave discharge for biomedicine, surface treatment and nanostructuring, Plasma Sources Sci. Technol. 20 (2011), 035006, https://doi.org/10.1088/0963-0252/20/3/035006.
[15] R.C. Longo, A. Ranjan, P.L.G. Ventzek, Density functional theory study of oxygen adsorption on polymer surfaces for atomic-layer etching: implications for semiconductor device fabrication, ACS Appl. Nano Mater. 3 (2020) 5189–5202, https://doi.org/10.1021/acsanm.0c00618.
[16] A. Vesel, R. Zaplotnik, M. Mozetič, G. Primc, Surface modification of PS polymer by oxygen-atom treatment from remote plasma: initial kinetics of functional groups formation, Appl. Surf. Sci. 561 (2021) 150058, https://doi.org/10.1016/j.apsusc.2021.150058.
[17] A. Vesel, M. Kolar, A. Doliska, K. Stana-Kleinschek, M. Mozetic, Etching of polyethylene terephthalate thin films by neutral oxygen atoms in the late flowing afterglow of oxygen plasma, Surf. Interface Anal. 44 (2012) 1565–1571, https://doi.org/10.1002/sia.5064.
[18] L.P.T. Schepers, W.L. IJzerman, J. Beckers, Oxygen content dependent etch rate of single polymer microparticles confined in the sheath region of a low pressure radiofrequency argon/oxygen plasma, J. Phys. D Appl. Phys. 51 (2018) 375203, https://doi.org/10.1088/1361-6463/aad5b4.
[19] S. Saloum, S. Abou Shaker, M. Alwazzeh, R. Hussin, Polymer surface modification using He/O 2 RF remote low-pressure plasma, Surf. Interface Anal. 53 (2021) 754–761, https://doi.org/10.1002/sia.6976.
[20] Y. Setsuhara, K. Cho, K. Takenaka, A. Ebe, M. Shiratani, M. Sekine, M. Hori, E. Ikenaga, H. Kondo, O. Nakatsuka, S. Zaima, Plasma surface treatment of polymers with inductivity-coupled RF plasmas driven by low-inductance antenna units, Thin Solid Films 518 (2009) 1006–1011, https://doi.org/10.1016/j.tsf.2009.07.161.
[21] T. Shinozuka, T. Kawakami, H. Okamura, M. Tsunooka, M. Shirai, Methacrylonitrile based Si-containing polymers for 157-nm positive resist, J. Photopolym. Sci. Technol. 15 (2002) 629–636, https://doi.org/10.2494/photopolymer.15.629.
[22] A. Annušová, D. Marinov, J.-P. Booth, N. Sirse, M.L. da Silva, B. Lopez, V. Guerra, Kinetics of highly vibrationally excited O 2 (X) molecules in inductively-coupled oxygen plasmas, Plasma Sources Sci. Technol. 27 (2018), 045006, https://doi.org/10.1088/1361-6595/aab47d.
[23] P. Vašina, V. Kudrle, A. Tálský, P. Boto, M. Mrázková, M. Meško, Simultaneous measurement of N and O densities in plasma afterglow by means of NO titration, Plasma Sources Sci. Technol. 13 (2004) 668–674, https://doi.org/10.1088/0963-0252/13/4/016.
[24] M. Mozetič, A. Zalar, Recombination of neutral oxygen atoms on stainless steel surface, Appl. Surf. Sci. 158 (2000) 263–267, https://doi.org/10.1016/S0169-4332(00)00007-6.
[25] J.P. Booth, O. Guaitella, A. Chatterjee, C. Drag, V. Guerra, D. Lopaev, S. Zyryanov, T. Rakhimova, D. Voloshin, Y. Mankelevich, Oxygen (3 P) atom recombination on a Pyrex surface in an O 2 plasma, Plasma Sources Sci. Technol. 28 (2019), 055005, https://doi.org/10.1088/1361-6595/ab13e8.
[26] M. Mozetic, A. Vesel, S.D. Stoica, S. Vizireanu, G. Dinescu, R. Zaplotnik, Oxygen atom loss coefficient of carbon nanowalls, Appl. Surf. Sci. 333 (2015) 207–213, https://doi.org/10.1016/j.apsusc.2015.02.020.
[27] J. Krištof, P. Macko, P. Veis, Surface loss probability of atomic oxygen, Vacuum 86 (2012) 614–619, https://doi.org/10.1016/j.vacuum.2011.07.041.
[28] I. Šorli, R. Ročak, Determination of atomic oxygen density with a nickel catalytic probe, J. Vac. Sci. Technol. A Vac. Surf. Film 18 (2000) 338, https://doi.org/10.1116/1.582189.

[29] F. Gaboriau, U. Cvelbar, M. Mozetic, A. Erradi, B. Rouffet, Comparison of TALIF and catalytic probes for the determination of nitrogen atom density in a nitrogen plasma afterglow, J. Phys. D Appl. Phys. 42 (2009), 055204, https://doi.org/10.1088/0022-3727/42/5/055204.
[30] J. Lee, D.B. Graves, The effect of VUV radiation from Ar/O2 plasmas on low-k SiOCH films, J. Phys. D Appl. Phys. 44 (2011) 325203.
[31] J.R. Woodworth, M.E. Riley, V.A. Amatucci, T.W. Hamilton, B.P. Aragon, Absolute intensities of the vacuum ultraviolet spectra in oxide etch plasma processing discharges, J. Vac. Sci. Technol. A Vac. Surf. Film 19 (2001) 45–55, https://doi.org/10.1116/1.1335685.
[32] S. Wickramanayaka, S. Meikle, T. Kobayashi, N. Hosokawa, Y. Hatanaka, Measurements of catalytic efficiency of surfaces for the removal of atomic oxygen using NO * 2 continuum, J. Vac. Sci. Technol. A Vac. Surf. Film 9 (1991) 2999–3002, https://doi.org/10.1116/1.577163.

Chapter 7

Conclusions

We studied the mechanisms of PTFE defluorination in E- and H-mode hydrogen plasmas. We explained the mechanisms of superhydrophilisation of hydrogen plasma pre-treated PTFE samples with oxygen plasma and clarified the role of O-atom fluences on the functionalisation of the PTFE surface. We also designed, engineered, manufactured, and tested an innovative industrial size reactor using four inductors coupled in parallel to generate large volume plasmas featuring homogeneous atom densities. The conclusions are summarised as follows:

- Low-pressure hydrogen plasma in both H- and E-modes is capable of defluorinating the PTFE surface by breaking C—F bonds.
- In the E-mode of hydrogen plasma, the defluorination process is much slower than in H- mode because radiation is several orders weaker. The functionalised layer is thinner, and less fluorine is removed in the E-mode, which is consistent with the F/C ratio of 0.6 determined by XPS after several seconds of treatment.
- An F/C ratio of 0.4 was obtained after 1 s of hydrogen plasma treatment in H-mode. By XPS analysis performed at several photoelectron take-off angles (TOA) and extrapolation of TOA to zero TOA, an F/C ratio of practically zero was observed, indicating the formation of a polyolefin-like film on the PTFE surface. This was confirmed by the SIMS analysis, where the amount of C_xF_y ions was barely detectable, and the C_xH_y ions signals prevailed in SIMS spectra.
- By selective exposure of PTFE to only VUV radiation, we found that the VUV radiation alone is very effective in breaking C—F bonds. As the decrease in F/C ratio was somewhat faster during combined exposure to VUV and H-atoms, we concluded that H-atoms play an important role in the termination of dangling bonds (H-atom covalent bonding in accordance with SIMS results) and in binding the released fluorine atoms. The optimal VUV fluence for the depletion of F-atoms in the PTFE surface film during hydrogen plasma treatment was found to be about 10^{17} cm^{-2}.
- Afterglow oxygen plasma with a prevailing content of O-atoms was found to be optimal for rendering superhydrophilic PTFE with a polyolefin-like layer of a few nm thickness, formed by previous treatment with H-mode glow hydrogen plasma. The competitive processes of functionalisation and etching were found occurring on the surface. The water contact angle of 5° was achieved on the PTFE surface after a very short treatment time of 0.2 s with

oxygen plasma. We discovered that the initial functionalisation resulting in the decrease of water contact angle to about 20° occurred within 0.03 s of oxygen plasma treatment. It is of special interest that the elemental composition of the sample monitored by XPS remained constant with an O-concentration of 20 at.% during the oxygen plasma treatment from 0.03 s to 0.2 s when the WCA minimum was achieved. This leads to the conclusion that the WCA is not solely dependent on the chemical composition but also depends on the surface roughness. Within several seconds after reaching the minimum, the WCA increased. The oxygen concentration in the PTFE surface decreased close to zero, and the F/C ratio increased to the value of untreated material after prolonged treatment with oxygen plasma. Complete hydrophobic recovery occurred, meaning that oxygen bound in hydrophilic and hydroneutral functional groups (hydroxylic, carboxylic and carbonyl groups formed on the surface) was completely etched, and so was the polyolefin-like film.

- The functionalisation required for superhydrophilicity of the pre-treated PTFE surface depends primarily on O-atom fluence (in the range of 1×10^{23} m^{-2} to 3×10^{23} m^{-2}). However, it is apparent that a higher abundance of charged particles in plasma causes minimal changes in superhydrophilisation time, but importantly accelerates the etching process leading to quicker hydrophobic recovery.

- Power distribution in the innovative plasma system was proved to be efficiently equalised, so that each coil receives almost exactly the same power (minor differences in power distribution cause successive transitions of coils from E- to H-mode). It was found that the real powers required for subsequential transitions of coils from E- to H-mode during increasing power were almost exactly the same for each subsequent coil, and their sum rose almost linearly with the oxygen pressure within the reactor. The transitions from H- to E-mode during the decrease of real power were also consequential. At all transitions, almost the same power decreases were found and occurred at much lower powers than E- to H-mode transitions. The absolute values of real powers of H- to E-mode transitions also rose linearly with increased pressure. Hysteresis between real powers of E- to H-mode transitions and H- to E-mode transitions were found to increase linearly with increasing pressure and were approximately the same for each coil at a given pressure. At an oxygen pressure of 5 Pa, hysteresis was negligible but increased to 600 W at an oxygen pressure of 25 Pa. We found that power can be saved if plasma is ignited in H-mode at the required power, and then the working power is decreased just to above the limit of the first H- to E-mode transition.

- The innovative industrial scale plasma system with four inductors efficiently generates a large volume of plasma with homogeneous neutral atom densities within the area starting about 20 cm below the plasma exhaust from the dielectric cups and at least 10 cm away from the walls of the inner aluminium mantle. In this volume, at the real power of 1800 W, and oxygen pressure of 20 Pa, the O-atom density of 1.2×10^{21} m^{-3} was measured.

To conclude, an environmentally friendly method for the functionalisation of PTFE to the superhydrophilic state (water contact angle of 5° was obtained), using only low-pressure nonequilibrium hydrogen and oxygen plasmas was discovered, developed, and explained in

detail. An industrial plasma system based on the newest scientific discoveries, able to sustain a high volume of plasma featuring homogeneous neutral atom densities was engineered, developed and successfully tested. The presented research is highly relevant because the innovative method has not been previously published in the scientific literature. In the end, it can be noted that further research work is needed to achieve a deeper understanding of the effects of morphology (etching of the surface by O-atoms and ions) on the WCA of PTFE rendered superhydrophilic by the presented method. Further research in upscaling the presented process to take place in an industrial size plasma reactor would also be beneficial to protect the environment by providing a real option for substituting the use of environmentally harmful chemicals with ecologically friendly plasma technologies in industry.

References

Badey, J. P., Espuche, E., Sage, D., Chabert, B., Jugnet, Y., Batier, C., & Duc, T. M. (1996). A comparative study of the effects of ammonia and hydrogen plasma downstream treatment on the surface modification of polytetrafluoroethylene. Polymer, 37(8), 1377–1386. https://doi.org/10.1016/0032-3861(96)81135-9

Behera, S. N., Sharma, M., Aneja, V. P., & Balasubramanian, R. (2013). Ammonia in the atmosphere: A review on emission sources, atmospheric chemistry and deposition on terrestrial bodies. Environmental Science and Pollution Research, 20(11), 8092–8131. https://doi.org/10.1007/s11356-013-2051-9

Bico, J., Thiele, U., & Quéré, D. (2002). Wetting of textured surfaces. Colloids and Surfaces A: Physicochemical and Engineering Aspects, 206(1–3), 41–46. https://doi.org/10.1016/S0927-7757(02)00061-4

Bikerman, J. J. (1967). CAUSES OF POOR ADHESION: WEAK BOUNDARY LAYERS. Industrial & Engineering Chemistry, 59(9), 40–44. https://doi.org/10.1021/ie51403a010

Calleja, G., Jourdan, A., Ameduri, B., & Habas, J.-P. (2013). Where is the glass transition temperature of poly(tetrafluoroethylene)? A new approach by dynamic rheometry and mechanical tests. European Polymer Journal, 49(8), 2214–2222. https://doi.org/10.1016/j.eurpolymj.2013.04.028

Carbone, E. A. D., Verhoeven, M. W. G. M., Keuning, W., & van der Mullen, J. J. A. M. (2016). PTFE treatment by remote atmospheric Ar/O 2 plasmas: A simple reaction scheme model proposal. Journal of Physics: Conference Series, 715, 012011. https://doi.org/10.1088/1742-6596/715/1/012011

Clark, E. S. (1999). The molecular conformations of polytetrafluoroethylene: Forms II and IV. Polymer, 40(16), 4659–4665. https://doi.org/10.1016/S0032-3861(99)00109-3

Drobny, J. G. (2009). Technology of fluoropolymers (2nd ed). Boca Raton: CRC Press.

Dumée, L. F., Alglave, H., Chaffraix, T., Lin, B., Magniez, K., & Schütz, J. (2016). Morphology-properties relationship of gas plasma treated hydrophobic meso-porous membranes and their improved performance for desalination by membrane distillation. Applied Surface Science, 363, 273–285. https://doi.org/10.1016/j.apsusc.2015.12.034

Ebnesajjad, S. (2000). Fluoroplastics, Volume 1: Non-Melt Processible Fluoroplastics. William Andrew.

Ebnesajjad, S. (2011). Material Surface Preparation Techniques. In Handbook of Adhesives and Surface Preparation (pp. 49–81). Elsevier. https://doi.org/10.1016/B978-1-4377-4461-3.10005-7

Fantz, U., Briefi, S., Rauner, D., & Wünderlich, D. (2016). Quantification of the VUV radiation in low pressure hydrogen and nitrogen plasmas. Plasma Sources Science and Technology, 25(4), 045006. https://doi.org/10.1088/0963-0252/25/4/045006

Gabriel, M., Dahm, M., & Vahl, C.-F. (2011). Wet-chemical approach for the cell-adhesive modification of polytetrafluoroethylene. Biomedical Materials, 6(3), 035007. https://doi.org/10.1088/1748-6041/6/3/035007

Hai, W., Hi, T., Shimizu, K., & Yajima, T. (2015a). Preparation of a Super Hydrophilic Polytetrafluoroethylene Surface Using a Gaseous Ammonia-Water Low-Temperature Plasma. Journal of Photopolymer Science and Technology, 28(3), 479–483. https://doi.org/10.2494/photopolymer.28.479

Hai, W., Hi, T., Shimizu, K., & Yajima, T. (2015b). Preparation of a Super Hydrophilic Polytetrafluoroethylene Surface Using a Gaseous Ammonia-Water Low-Temperature Plasma. Journal of Photopolymer Science and Technology, 28(3), 479–483. https://doi.org/10.2494/photopolymer.28.479

Hong, S.-H., Kim, T.-H., & Choi, S. (2019). Hydrophilic Surface Modification of Polytetrafluoroethylene Film with Gliding Arc Plasma. Applied Science and Convergence Technology, 28, 101–106. https://doi.org/10.5757/ASCT.2019.28.4.101

Huang, C., Ma, W. C., Tsai, C.-Y., Hou, W.-T., & Juang, R.-S. (2013). Surface modification of polytetrafluoroethylene membranes by radio frequency methane/nitrogen mixture plasma polymerization. Surface and Coatings Technology, 231, 42–46. https://doi.org/10.1016/j.surfcoat.2012.03.005

Inagaki, N., Tasaka, S., & Umehara, T. (1999). Effects of surface modification by remote hydrogen plasma on adhesion in poly(tetrafluoroethylene)/copper composites. Journal of Applied Polymer Science, 71(13), 2191–2200. https://doi.org/10.1002/(SICI)1097-4628(19990328)71:13<2191::AID-APP9>3.0.CO;2-3

Ishikawa, K., Sumi, N., Kono, A., Horibe, H., Takeda, K., Kondo, H., … Hori, M. (2011). Synergistic Formation of Radicals by Irradiation with Both Vacuum Ultraviolet and Atomic Hydrogen: A Real-Time In Situ Electron Spin Resonance Study. The Journal of Physical Chemistry Letters, 2(11), 1278–1281. https://doi.org/10.1021/jz2002937

Jie-Rong, C., & Wakida, T. (1997). Studies on the surface free energy and surface structure of PTFE film treated with low temperature plasma. Journal of Applied Polymer Science, 63(13), 1733–1739. https://doi.org/10.1002/(SICI)1097-4628(19970328)63:13<1733::AID-APP4>3.0.CO;2-H

Kwon, K.-S., Rahman, Md. K., Phung, T. H., Hoath, S., Jeong, S., & Kim, J. S. (2020). Review of digital printing technologies for electronic materials. Flexible and Printed Electronics. https://doi.org/10.1088/2058-8585/abc8ca

Lee, J.-W., Lee, Y.-S., Chang, H.-Y., & An, S.-H. (2014). On the possibility of the multiple inductively coupled plasma and helicon plasma sources for large-area processes. Physics of Plasmas, 21(8), 083502. https://doi.org/10.1063/1.4892170

Liu, C. Z., Wu, J. Q., Ren, L. Q., Tong, J., Li, J. Q., Cui, N., … Meenan, B. J. (2004). Comparative study on the effect of RF and DBD plasma treatment on PTFE surface modification. Materials Chemistry and Physics, 85(2–3), 340–346. https://doi.org/10.1016/j.matchemphys.2004.01.026

Ma, L., Li, X., Guo, X., Jiang, Y., Li, X., Guo, H., … Li, Q. (2020). Promotion of Endothelial Cell Adhesion and Antithrombogenicity of Polytetrafluoroethylene by Chemical Grafting of Chondroitin Sulfate. ACS Applied Bio Materials, 3(2), 891–901. https://doi.org/10.1021/acsabm.9b00970

Marchesi, J. T., Ha, K., Garton, A., Swei, G. S., & Kristal, K. W. (1991). Adhesion to Sodium Naphthalenide Treated Fluoropolymers. Part II. Effects of Treatment Conditions and Fluoropolymer Structure. The Journal of Adhesion, 36(1), 55–69. https://doi.org/10.1080/00218469108026523

Mathieson, I., Brewis, D. M., Sutherland, I., & Cayless, R. A. (1994). Pretreatments of Fluoropolymers. The Journal of Adhesion, 46(1–4), 49–56. https://doi.org/10.1080/00218469408026648

Nguyen, H. D., & Yajima, T. (2017). A Spectroscopic Study on Argon-Ammonia Water Gaseous Plasma Super-hydrophilizing Polytetrafluoroethylene. Journal of

Photopolymer Science and Technology, 30(3), 325–330. https://doi.org/10.2494/photopolymer.30.325

Nunes, L. C. S., Dias, F. W. R., & da Costa Mattos, H. S. (2011). Mechanical behavior of polytetrafluoroethylene in tensile loading under different strain rates. Polymer Testing, 30(7), 791–796. https://doi.org/10.1016/j.polymertesting.2011.07.004

Ohkubo, Y., Endo, K., & Yamamura, K. (2018). Adhesive-free adhesion between heat-assisted plasma-treated fluoropolymers (PTFE, PFA) and plasma-jet-treated polydimethylsiloxane (PDMS) and its application. Scientific Reports, 8(1), 18058. https://doi.org/10.1038/s41598-018-36469-y

Ohkubo, Y., Ishihara, K., Shibahara, M., Nagatani, A., Honda, K., Endo, K., & Yamamura, K. (2017). Drastic Improvement in Adhesion Property of Polytetrafluoroethylene (PTFE) via Heat-Assisted Plasma Treatment Using a Heater. Scientific Reports, 7(1), 9476. https://doi.org/10.1038/s41598-017-09901-y

Okazaki, M. (2017). Comparison of hexagonal crystal structures between fluorapatite and polytetrafluoroethylene. Bio-Medical Materials and Engineering, 28(1), 3–8. https://doi.org/10.3233/BME-171650

Olabisi, O., & Adewale, K. (2015). Handbook of Thermoplastics, Second Edition. https://doi.org/10.13140/RG.2.1.2068.4881

Owens, D. K., & Wendt, R. C. (1969). Estimation of the surface free energy of polymers. Journal of Applied Polymer Science, 13(8), 1741–1747. https://doi.org/10.1002/app.1969.070130815

Primc, G. (2020). Recent Advances in Surface Activation of Polytetrafluoroethylene (PTFE) by Gaseous Plasma Treatments. Polymers, 12(10), 2295. https://doi.org/10.3390/polym12102295

Ryan, M. E., & Badyal, J. P. S. (1995). Surface Texturing of PTFE Film Using Nonequilibrium Plasmas. Macromolecules, 28(5), 1377–1382. https://doi.org/10.1021/ma00109a008

Schonhorn, H., & Hansen, R. H. (1967). Surface treatment of polymers for adhesive bonding. Journal of Applied Polymer Science, 11(8), 1461–1474. https://doi.org/10.1002/app.1967.070110809

Shikata, T., & Okuzono, M. (2013). Are All Polar Molecules Hydrophilic? Hydration Numbers of Ketones and Esters in Aqueous Solution. The Journal of Physical Chemistry B, 117(25), 7718–7723. https://doi.org/10.1021/jp4029968

Takata, R., Iwao, T., & Yumoto, M. (2016). Surface Modification of PTFE Using Low-Energy Nitrogen Ion Irradiation: Improvement in Adhesive Strength on Modification of Deep Modifying Layer. Electronics and Communications in Japan, 99(8), 93–99. https://doi.org/10.1002/ecj.11844

Vandencasteele, N., Nisol, B., Viville, P., Lazzaroni, R., Castner, D. G., & Reniers, F. (2008). Plasma-Modified PTFE for Biological Applications: Correlation between Protein-Resistant Properties and Surface Characteristics. Plasma Processes and Polymers, 5(7), 661–671. https://doi.org/10.1002/ppap.200700143

Wilson, D. J., Williams, R. L., & Pond, R. C. (2001). Plasma modification of PTFE surfaces. Part I: Surfaces immediately following plasma treatment. Surface and Interface Analysis, 31(5), 385–396. https://doi.org/10.1002/sia.1065

Wypych, G. (2018). 4—SUBSTRATES – SURFACE CONDITION AND TREATMENT. In G. Wypych (Ed.), Handbook of Adhesion Promoters (pp. 55–76). ChemTec Publishing. https://doi.org/10.1016/B978-1-927885-29-1.50006-7

Xu, H., Hu, Z., Wu, S., & Chen, Y. (2003). Surface modification of polytetrafluoroethylene by microwave plasma treatment of H2O/Ar mixture at low pressure. Materials Chemistry and Physics, 80(1), 278–282. https://doi.org/10.1016/S0254-0584(02)00490-X

Yamada, Y., Yamada, T., Tasaka, S., & Inagaki, N. (1996). Surface Modification of Poly(tetrafluoroethylene) by Remote Hydrogen Plasma. Macromolecules, 29(12), 4331–4339. https://doi.org/10.1021/ma951072r

Yuan, Y., & Lee, T. R. (2013). Contact Angle and Wetting Properties. In G. Bracco & B. Holst (Eds.), Surface Science Techniques (Vol. 51, pp. 3–34). Berlin, Heidelberg: Springer Berlin Heidelberg. https://doi.org/10.1007/978-3-642-34243-1_1

Bibliography

Publications Related to the Thesis

Journal Articles

Lojen, D., Zaplotnik, R., Mozetič, M., Vesel, A., & Primc, G. (2022). *Power characteristics of multiple inductively coupled RF discharges inside a metallic chamber*. *24*(1), 015403-1-015403–015407.

Lojen, D., Zaplotnik, R., Primc, G., Mozetič, M., & Vesel, A. (2020). Effect of VUV radiation and reactive hydrogen atoms on depletion of fluorine from polytetrafluoroethylene surface. *Applied Surface Science*, *533*, 147356. https://doi.org/10.1016/j.apsusc.2020.147356

Lojen, D., Zaplotnik, R., Primc, G., Mozetič, M., & Vesel, A. (2022). Optimization of surface wettability of polytetrafluoroethylene (PTFE) by precise dosing of oxygen atoms. *Applied Surface Science*, *598*, 153817. https://doi.org/10.1016/j.apsusc.2022.153817

Primc, G., Lojen, D., Vesel, A., Mozetič, M., & Zaplotnik, R. (2022). Oxygen atom density in a large reactor powered by four inductively coupled plasma sources. 199, 110964-1-110964–110967.

Vesel, A., Lojen, D., Zaplotnik, R., Primc, G., Mozetič, M., Ekar, J., … Stana-Kleinschek, K. (2020). Defluorination of Polytetrafluoroethylene Surface by Hydrogen Plasma. *Polymers*, *12*(12), 2855. https://doi.org/10.3390/polym12122855

Conference Paper

Lojen D., Vesel. A., Primc.G, Mozetič. M., Zaplotnik R., “PTFE hydrophylization in inductively coupled RF plasma,” in the Programme and book of abstracts 27th International Conference on Materials and Technology, Portorož, Slovenija: Ljubljana: Inštitut za kovinske materiale in tehnologije, 2019.

Lojen D, Zaplotnik R., Primc. G., Mozetič M., Vesel. A., “Effect of VUV radiation and reactive hydrogen atoms on depletion of fluorine from polytetrafluoroethylene surface,” in the Programme and book of abstracts 27th International Scientific Meeting on Vacuum Science and Techniques, Gozd Martuljek, Slovenija: Ljubljana: Slovenian Society for Vacuum Technique, 2021.

Lojen D., Zaplotnik R., Vesel A., Ekar J., Primc G., Mozetič M., “Low pressure plasma functionalIsation of fluoropolymers,” in the Programme and book of abstracts 28th International Scientific Meeting on Vacuum Science and Technique, Crikvenica, Croatia: Zagreb: Croatian Vacuum Society, 2022.

Other Publications

Paul D., Zaplotnik R., Primc G., Vesel A., Lojen D., Mozetič M., Hančič A., "Comparison measument with different catalytic probes in RF and MV plasma," in the Programme and book of abstracts 8th Central European Symposium on Plasma Chemistry, Gozd Martuljek, Slovenija: Ljubljana: Plasmadis, 2019.

Biography

The author of this thesis was born in Maribor in 1991. He attended the Škofijska Gimnazija Antona Martina Slomška in Maribor, and obtained his high school diploma in 2010. In 2014, the author graduated in environmental science from the Faculty of Environmental Science at the University of Nova Gorica. During research for the Diploma thesis, the author became acquainted with the techniques of epifluorescence microscopy and calcium dies that he used to research the impacts of a neonicotinoid insecticide (Imidacloprid) on the calcium signalling in rat hippocampal cells. In 2017 the author finished his master's studies at the Faculty of Mechanical Engineering, University of Maribor, in the field of Environmental Engineering. During the research for his Master thesis, the author was familiarised with the techniques of Fourier-transform infrared spectroscopy and Raman spectroscopy during his work on separation techniques of elastane from the textiles containing elastane and polyacrylonitrile and elastane and polyamide or polyethylene terephthalate for further chemical recycling. In 2018 the author was employed at the Jožef Stefan Institute at the Department of Surface Engineering and started his doctoral degree in Ecotechnology at Jožef Stefan International Postgraduate School. During his work, the author gained extensive knowledge about the low-pressure non-equilibrium plasmas of various gasses and methods of plasma functionalisation of polymers and also plasma treatments of other materials. The author designed (using 3D CAD modelling), engineered and manufactured an innovative low-pressure plasma system sustaining plasma by four inductors coupled in parallel to the same RF generator, with the specialty of accurate impedance regulation for each inductor. The author gained experience in the measurement of concentrations of neutral atoms in low-pressure plasmas by using catalytic probes and measurements of plasma radiation due to electronic transitions using optical emission spectroscopy. The author also gained experience in goniometry (contact angle measurement and determination of surface energies) and surface analysis using atomic force microscopy. Furthermore, the author learnt about the interpretations of X-ray photoelectron and Time-of-Flight Secondary Ion Mass spectra. The author conducted guided tours for visitors at the Department and gained experience in explaining science to the laic public, whereby special attention was given to the importance of plasma science toward the technics used in everyday life. For his doctoral dissertation, the author dedicated his research to the low-pressure plasma functionalisation of polytetrafluoroethylene (PTFE) and presented his results during research at several conferences. In 2019, the author presented a lecture at the 27th International Conference on Materials and Technology in Portorož (*PTFE hydrophilisation in inductively coupled RF plasma*). In 2021, he presented a lecture at the 56th International Conference on Microelectronics, Devices and Materials (*Polytetrafluoroethylene functionalisation by subsequent treatment with hydrogen and oxygen radiofrequency low-pressure plasmas*) and a poster at the 27th International Scientific Meeting on Vacuum Science and Techniques (*The role of VUV radiation and H-atoms on F depletion from polytetrafluoroethylene (PTFE) surface*). In 2022, the author was invited to present a lecture at the 28th International Scientific Meeting on Vacuum Science and Technique (*Low-Pressure Plasma Functionalisation of Fluoropolymers*).

The author is a keen amateur cyclist, mountaineer (completed a beginner's alpinist course in 2021), sport climber, skier and amateur photographer.